

6. Fields in Cylindrical and Spherical Regions

6.1 DISTINCTIVE FIELD CHARACTERISTICS

In contrast to the unbounded cross sections in Chapter 5, this chapter is concerned with partially bounded waveguide cross sections. In particular, we investigate in detail the effect of waveguide walls whose location is describable simply in terms of a circular-cylindrical or spherical coordinate system; included therein are the important configurations of the circular cylinder, the wedge, the sphere and the cone. Fields in cylindrical configurations are analyzed in detail (Secs. 6.1–6.7), but only a brief summary of the analogous spherical configurations is given in Sec. 6.8. The generic waveguide boundary in cylindrical coordinates is the tipped wedge configuration in Fig. 6.1.1, comprising a cylinder

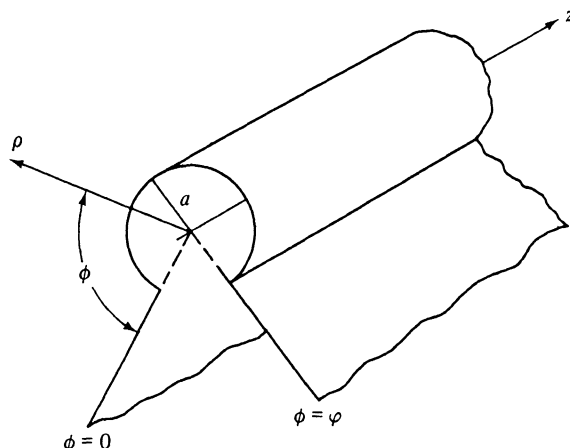


FIG. 6.1.1 Tipped wedge configuration.

with radius a superposed upon a wedge formed by two intersecting half-planes; the axis of the cylinder coincides with the wedge apex (z axis), and the sides of the wedge are defined by the angular locations $\phi = 0$ and $\phi = \varphi$ in a cylindrical coordinate system. We shall be concerned with the exterior region $0 \leq \phi \leq \varphi$, $a \leq \rho < \infty$. When $a = 0$, one recovers the wedge, and for the special case $a = 0$, $\varphi = 2\pi$, one obtains the configuration of a half-plane. The case of a cylinder with radius a cannot be obtained directly from the structure in Fig 6.1.1 since even for $\varphi = 2\pi$, the two wedge faces coalesce into a single septum. However, the difficulty may be easily circumvented by a modification of the angular boundary conditions to furnish the required 2π periodicity of the fields. In spherical coordinates, analogous considerations apply to the generic region depicted in Fig. 6.8.1.

Formal solutions for radiation problems in the region of Fig. 6.1.1 can be written down from the formulas in Sec. 5.2, provided only that one inserts the mode functions or characteristic Green's functions appropriate to the new waveguide cross section (see Sec. 2.2). The real task, as in Chapter 5, is the reduction of these formal representations to obtain the approximate evaluation of radiated fields. The presence of waveguide boundaries gives rise to effects not encountered in the study of totally unbounded cross sections. For example, because of the presence of the waveguide walls, there may exist one or more geometrical regions from which the source configuration is not visible. In the terminology of geometrical optics, these are the "shadow" or "dark" regions; at high frequencies (i.e., in the quasi-optic range) the fields in these dark regions are weak compared to those in the "illuminated" regions, from which the source configuration can be seen directly. The evaluation and ray-optical interpretation of the time-harmonic high-frequency fields in the illuminated and shadow regions, and in the transition regions surrounding the light-shadow boundaries (particularly for the wedge), is of major concern in this chapter. Field solutions in the spherical region depicted in Fig. 6.8.1 can be constructed from the modal representations in Sec. 2.6, with the eigenfunctions taken from the appropriate sections of Chapter 3. The presence of these boundaries gives rise to quasi-optic phenomena analogous to those described for cylindrical regions.

Examination of Fig. 6.1.1 shows that when a source is located at the point $\mathbf{r}' = (\rho', \phi', z')$, the regions of illumination and shadow are separated by a plane boundary which is tangent to the obstacle and passing through \mathbf{r}' ; see Figs. 6.3.1 and 6.7.1 for the special cases of the wedge and cylinder and note that the latter configuration admits two boundary planes. Evidently, the description of shadow boundary planes does not involve the axial (z) coordinate. It may be anticipated that similar quasi-optic phenomena are associated with a point source at \mathbf{r}' , a line source at $\mathbf{p}' = (\rho', \phi')$, and a plane wave whose propagation vector lies in the boundary plane. This aspect is exploited in the analysis where field solutions for the plane wave or the point source are derived from two-dimensional line-source results. It is also suggestive, in view of the dominant role played by the angular coordinates in specifying the shadow boundary, that field

penetration by diffraction into the shadow region is described best in terms of angularly propagating waves. The validity of this conjecture is confirmed by the analysis in Secs. 6.3–6.7, which shows that an angular transmission representation for the fields yields a solution wherein the quasi-optic (geometric-optical and diffracted) constituents appear explicitly and can be approximated readily in the limit of high frequencies. Alternatively, no well-defined illuminated and shadow regions may be distinguished in the low-frequency regime, and for approximate evaluation of the field in this parameter range, a radial transmission representation is found to be the more rapidly convergent. Although the z -transmission formulation is not especially useful for field calculations in the presence of an obstacle as in Fig. 6.1.1, it forms a convenient starting point for deriving alternative representations for the scalar functions $\mathcal{S}'(\mathbf{r}, \mathbf{r}')$ and $\mathcal{S}''(\mathbf{r}, \mathbf{r}')$, and thence for the general vector electromagnetic field. These general considerations are pursued in Sec. 6.2 for the cylindrical geometry and in Sec. 6.8b for the spherical geometry.

In the high-frequency range, the fields in the illuminated and shadow regions may be described almost everywhere in terms of rays that propagate locally like plane waves and are capable of accounting for the effects of diffraction as well as those of geometrical optics. This description fails in the vicinity of boundaries that delimit the domain of existence of a particular ray species. Examples are provided by the light-shadow boundary which confines the incident ray species, and by an analogous boundary for the geometrically reflected rays. In these transition regions, the field changes so rapidly as to invalidate a local plane-wave characterization which, in the equiphase plane, requires slow variation over a wavelength interval. Although these regions are of narrow angular extent (see Figs. 6.4.4 and 6.7.1 for cylindrical regions), they play an important role since they must provide a smooth transformation from one ray-optical field type to another. Transition functions for the wedge configuration are studied in detail in the following sections. Because of the observations made previously concerning the similarity of shadow formation for point-source, line-source, or plane-wave excitation, the transition functions exhibit a corresponding behavior.

The preceding ray and wavefront considerations apply also to excitation by impulsive sources since there exists an intimate connection between the time-harmonic high-frequency field and the transient field near the time of arrival of the various wavefronts (see Sec. 1.6c). For various wedge configurations, it is found, however, that the transient response at *all* observation times can be evaluated in closed form, thereby providing an insight into the field behavior at observation times immediately and long after the passage of a wavefront. Special attention is given to the perfectly conducting half-plane, which constitutes one of the classical diffraction problems both for impulsive and time-harmonic excitation.

Since the angular transmission approach is fundamental for the quasi-optic formulation of the fields, it is natural to explore initially those configurations analyzed most simply in terms of angularly propagating waves. As in regions

describable in terms of propagation along a rectilinear coordinate, bilaterally matched (reflectionless) structures fall into this category. In angular coordinates, this condition is satisfied by “perfectly absorbing” boundaries at $\phi = 0, \varphi$ and $\theta = \theta_{1,2}$ in cylindrical and spherical regions, respectively (see Fig. 3.4.11). The matched boundary condition is equivalent to regarding the angular space as being infinitely extended so that a traveling wave experiences no reflection. This concept of an infinite angular space, introduced in Sec. 3.4b, is exploited in the analysis. From the resulting solutions for the perfectly absorbing case, one may synthesize by an image construction effects either of reflecting boundaries at $\phi = 0, \varphi$ or $\theta = \theta_{1,2}$, or of periodicity when no physical boundaries are present in the angular domain (see Sec. 3.4b). The image procedure grants insight into the different phenomena encountered in regions with rectilinear and curved transmission coordinates. In the former, all images are visible from the source point and therefore contribute to the geometric-optical field, whereas in the latter, the more distant images are obscured by space curvature and contribute only to diffraction.

6.2 GREEN'S FUNCTION REPRESENTATIONS IN CYLINDRICAL REGIONS

6.2a Derivation of the Field from Scalar Potentials

The electromagnetic fields radiated by an arbitrarily oriented time-harmonic electric or magnetic current element in the presence of the perfectly conducting configuration in Fig. 6.1.1 can be derived as in Sec. 5.2a from the vector Hertz potentials $\mathbf{z}_0\Pi'(\mathbf{r}, \mathbf{r}')$ and $\mathbf{z}_0\Pi''(\mathbf{r}, \mathbf{r}')$ expressive, respectively, of the *E*-mode and *H*-mode contributions with respect to the axial coordinate *z*. When the source direction is parallel to *z*, the Hertz potentials are proportional to the scalar Green's functions $G'(\mathbf{r}, \mathbf{r}')$ or $G''(\mathbf{r}, \mathbf{r}')$ [Eqs. (5.2.4c)], whereas the response to sources directed transverse to *z* requires a knowledge of the potential functions $\mathcal{S}'(\mathbf{r}, \mathbf{r}')$ and $\mathcal{S}''(\mathbf{r}, \mathbf{r}')$ [Eqs. (5.2.4a) and (5.2.4b)]. The functions $\mathcal{S}', \mathcal{S}''$ and G', G'' satisfy the differential equations (5.2.2) and (5.2.3), respectively; in a *z*-transmission representation, their solutions are given by Eqs. (5.2.5), with the scalar-mode functions $\Phi_i(\rho)$ and $\psi_i(\rho)$ chosen to satisfy the required boundary conditions on the waveguide boundary sketched in Fig. 6.1.1. When the source behavior is impulsive in time, these considerations are modified as in Sec. 5.2c (see also Sec. 1.6).

While the separability of the vector electric and magnetic fields into *E* and *H* modes requires the choice of the preferred axial coordinate *z*, the scalar Green's functions G', G'' and the potential functions $\mathcal{S}', \mathcal{S}''$ may be represented in any convenient alternative form corresponding to transmission along one of the transverse coordinates. As mentioned in Sec. 6.1, the class of problems involving a boundary of the type shown in Fig. 6.1.1 is analyzed most conveniently in terms of angular transmission. This applies to the three-dimensional fields resulting from point-source excitation as well as to the two-dimensional

fields excited by a line source extending parallel to the z axis; since the physical configuration has z -invariant properties (see Fig. 6.1.1), an axial line source of constant strength will excite z -independent fields. The two-dimensional z -independent Green's function $\bar{G}(\rho, \rho')$ may be synthesized from the three-dimensional function $G(\mathbf{r}, \mathbf{r}')$ by integrating over z' between $-\infty$ and $+\infty$. When this operation is performed on Eqs. (5.2.3), the resulting function satisfies the two-dimensional wave equation (3) below, so $\bar{G}(\rho, \rho')$ may also be derived directly from this equation.

It may be noted from Eqs. (5.2.1) and (5.2.4c) (see also Sec. 5.4c) that a line source of electric current

$$\hat{\mathbf{J}}(\mathbf{r}, t) = z_0 I \delta(\rho - \rho') e^{-i\omega t}, \quad \rho = (\rho, \phi), \quad (1a)$$

generates an electromagnetic field whose components are given by

$$E_z = \frac{I}{i\omega\epsilon} [\nabla_t^2 \bar{G}' + \delta(\rho - \rho')] = i\omega\mu I \bar{G}', \quad H_\rho = I \frac{\partial \bar{G}'}{\rho \partial \phi}, \quad H_\phi = -I \frac{\partial \bar{G}'}{\partial \rho}, \quad (1b)$$

$$E_\rho = E_\phi = H_z = 0,$$

whereas a line source of magnetic current,

$$\hat{\mathbf{M}}(\mathbf{r}, t) = z_0 V \delta(\rho - \rho') e^{-i\omega t} \quad (2a)$$

generates an electromagnetic field whose components are given by

$$H_z = i\omega\epsilon V \bar{G}'', \quad E_\rho = -V \frac{\partial \bar{G}''}{\rho \partial \phi}, \quad E_\phi = V \frac{\partial \bar{G}''}{\partial \rho}, \quad H_\rho = H_\phi = E_z = 0. \quad (2b)$$

In these equations, \bar{G}' and \bar{G}'' still denote E - and H -mode solutions with respect to the z axis which satisfy the equations

$$\begin{aligned} (\nabla_t^2 + k^2) \frac{\bar{G}'(\rho, \rho')}{\bar{G}''(\rho, \rho')} &= -\delta(\rho - \rho') = -\frac{\delta(\rho - \rho')}{\rho'} \delta(\phi - \phi'), \\ \nabla_t^2 &= \frac{1}{\rho} \frac{\partial}{\partial \rho} \rho \frac{\partial}{\partial \rho} + \frac{1}{\rho^2} \frac{\partial^2}{\partial \phi^2}, \end{aligned} \quad (3)$$

subject to the following conditions on the perfectly conducting boundary s in Fig. 6.1.1:

$$\bar{G}' = 0, \quad \frac{\partial \bar{G}''}{\partial n} = 0 \quad \text{on } s, \quad (3a)$$

where $k = \omega\sqrt{\mu\epsilon}$ is the (constant) wavenumber in the medium and n is in the direction normal to s . While the two-dimensional Green's function $\bar{G}(\rho, \rho')$ may be constructed from the three-dimensional Green's function $G(\mathbf{r}, \mathbf{r}')$ by integration over z' as noted above, it is important to recognize that the converse is also true. To demonstrate this fact, we note that from Eq. (5.4.52), the two-dimensional Green's function $\bar{G}(\mathbf{r}, \rho')$ corresponding to a z -directed line source with linearly progressing phase $\exp(i\zeta z')$ is given by

$$\bar{G}(\mathbf{r}, \rho') = \int_{-\infty}^{\infty} e^{i\zeta z'} G(\mathbf{r}, \mathbf{r}') dz' = e^{i\zeta z} \bar{G}_\zeta(\rho, \rho'), \quad (3b)$$

where $\bar{G}_\zeta(\rho, \rho')$ satisfies Eq.(3) with k^2 replaced by $k^2 - \zeta^2$ [see also Eqs.(5.4.46)]. By Fourier inversion of Eq. (3b),

$$G(\mathbf{r}, \mathbf{r}') = \frac{1}{2\pi} \int_{-\infty}^{\infty} e^{-i\zeta z'} \bar{G}(\mathbf{r}, \rho') d\zeta = \frac{1}{2\pi} \int_{-\infty}^{\infty} e^{i\zeta(z-z')} \bar{G}_\zeta(\rho, \rho') d\zeta, \quad (3c)$$

whence the three-dimensional Green's function $G(\mathbf{r}, \mathbf{r}')$ can be recovered from the two-dimensional Green's function $\bar{G}(\rho, \rho')$ on replacing k by $(k^2 - \zeta^2)^{1/2}$ and performing the operation $(1/2\pi) \int_{-\infty}^{\infty} d\zeta \exp[i\zeta(z - z')]$.

It is of interest to observe that no field components in addition to those in Eqs. (1b) or (2b) are required even for other z -invariant boundary shapes, or for penetrable boundaries. Regions interior to s filled with a z -independent but otherwise arbitrary dielectric material are also included herein provided that the boundary conditions are modified accordingly. The reader may verify that the components in Eqs. (1b) or (2b) suffice for enforcement of the continuity of tangential electric and magnetic fields.

6.2b Angular Transmission Representation

In an angular transmission formulation, the scalar Green's functions G' , G'' or \bar{G}' , \bar{G}'' are represented in terms of eigenfunctions in the (ρ, z) domain and one-dimensional Green's functions along the angular coordinate ϕ . In view of the translational invariance of the configuration in Fig. 6.1.1 with respect to z , the three-dimensional solutions G' , G'' are related to the two-dimensional solutions \bar{G}' , \bar{G}'' by the transformation noted in Eq. (3c). Owing to greater simplicity, the analysis of various diffraction problems will be carried out primarily for two-dimensional cases, and three-dimensional results pertaining to point-source excitation will be deduced therefrom.

For two-dimensional (z -independent), time-harmonic source arrangements, the completeness relation for eigenfunctions that algebraize the radial operator

$$\frac{1}{\rho} \frac{\partial}{\partial \rho} \rho \frac{\partial}{\partial \rho} + k^2$$

in Eq. (3) is given in the generic form [see Eqs. (3.4.91) and (3.4.94e)]

$$\rho' \delta(\rho - \rho') = \sum_p \Phi_p(k\rho) \bar{\Phi}_p(k\rho'), \quad (4)$$

where $\Phi_p(k\rho)$, the eigenfunction for the radial domain, and $\bar{\Phi}_p(k\rho)$, the adjoint eigenfunction, are listed in Sec. 3.4c for various boundary conditions. With z in the interval $-\infty < z < \infty$ for the three-dimensional time-harmonic case, the algebraization of the (ρ, z) dependent part of the $\nabla^2 + k^2$ operator,

$$\frac{1}{\rho} \frac{\partial}{\partial \rho} \rho \frac{\partial}{\partial \rho} + \frac{\partial^2}{\partial z^2} + k^2,$$

is achieved by the two-dimensional eigenfunctions characterized by the completeness relation

$$\rho' \delta(\rho - \rho') \delta(z - z') = \frac{1}{2\pi} \int_{-\infty}^{\infty} d\zeta \sum_p e^{i\zeta(z-z')} \Phi_p(\sqrt{k^2 - \zeta^2}\rho) \bar{\Phi}_p(\sqrt{k^2 - \zeta^2}\rho'), \quad (5)$$

which is obtained from the two-dimensional result in Eq. (4) by the rule stated in Eq. (3c): k in the former is replaced by $\sqrt{k^2 - \zeta^2}$ and the operation

$$\frac{1}{2\pi} \int_{-\infty}^{\infty} d\zeta \exp [i\zeta(z - z')]$$

is performed subsequently. For impulsive excitation, k^2 on the left-hand side of Eq. (3) or its three-dimensional counterpart is replaced by the temporal operator $-\partial^2/\tilde{c}^2\partial t^2$, whose algebraization is achieved by eigenfunctions satisfying the completeness relation

$$\delta(t - t') = \frac{1}{2\pi} \int_{-\infty}^{\infty} e^{-i\omega(t-t')} d\omega, \quad \omega = k\tilde{c}. \quad (6)$$

The relevant representation theorem (completeness relation) for

$$\rho' \delta(\rho - \rho') \delta(t - t') \quad \text{and} \quad \rho' \delta(\rho - \rho') \delta(z - z') \delta(t - t')$$

is then obtained by applying the integral operator in Eq. (6) to the time-harmonic formulation on the right-hand sides of Eqs. (4) and (5), respectively (see also Sec. 5.2c).

In the angular transmission representation, the dependence on the ϕ coordinate is given in terms of the angular Green's function $g_{\phi\rho}(\phi, \phi')$, which satisfies the differential equation

$$\left(\frac{d^2}{d\phi^2} + p^2 \right) g_{\phi\rho}(\phi, \phi') = -\delta(\phi - \phi'), \quad (7)$$

subject to appropriate boundary conditions at the endpoints of the ϕ domain. Various solutions are given in Sec. 3.4b, and their availability permits direct construction of formal solutions for scalar Green's functions by the method described in Sec. 3.3c.

Time-harmonic line source

The two-dimensional Green's functions \bar{G}' and \bar{G}'' satisfy Eq. (3) and, via Eqs. (4) and (7), have the formal solution

$$\bar{G}(\rho, \rho') = \sum_p \Phi_p(k\rho) \bar{\Phi}_p(k\rho') g_{\phi\rho}(\phi, \phi'). \quad (8)$$

The appropriate form of the functions Φ_p and $g_{\phi\rho}$ for the E - or H -mode cases depends on the specific boundary shapes comprised under the wedge or cylinder configurations sketched in Fig. 6.1.1.

Time-harmonic point source

The three-dimensional Green's functions satisfy the differential equations†

†The separable cylindrical coordinate representation of the delta function follows from the requirement that $\int_V dV \delta(\mathbf{r} - \mathbf{r}') = 1$, \mathbf{r}' in V , with the volume element represented as $dV = \rho d\rho d\phi dz$.

$$\begin{aligned} & \left(\frac{1}{\rho} \frac{\partial}{\partial \rho} \rho \frac{\partial}{\partial \rho} + \frac{1}{\rho^2} \frac{\partial^2}{\partial \phi^2} + \frac{\partial^2}{\partial z^2} + k^2 \right) G'(\mathbf{r}, \mathbf{r}') \\ &= -\frac{\delta(\rho - \rho')}{\rho'} \delta(\phi - \phi') \delta(z - z'), \end{aligned} \quad (9)$$

subject to the boundary conditions [see Eq. (3a)]

$$G' = 0, \quad \frac{\partial G'}{\partial n} = 0 \text{ on } s. \quad (9a)$$

The formal solution is given by

$$G(\mathbf{r}, \mathbf{r}') = \frac{1}{2\pi} \int_{-\infty}^{\infty} d\zeta \sum_p e^{i\zeta(z-z')} \Phi_p(\sqrt{k^2 - \zeta^2}\rho) \bar{\Phi}_p(\sqrt{k^2 - \zeta^2}\rho') g_{\phi p}(\phi, \phi'). \quad (10)$$

Impulsive line source

The two-dimensional time-dependent Green's functions $\hat{G}'(\mathbf{p}, \mathbf{p}'; t, t')$ and $\hat{G}''(\mathbf{p}, \mathbf{p}'; t, t')$ satisfy the wave equation

$$\left(\frac{1}{\rho} \frac{\partial}{\partial \rho} \rho \frac{\partial}{\partial \rho} + \frac{1}{\rho^2} \frac{\partial^2}{\partial \phi^2} - \frac{1}{c^2} \frac{\partial^2}{\partial t^2} \right) \hat{G} = -\frac{\delta(\rho - \rho')}{\rho'} \delta(\phi - \phi') \delta(t - t'), \quad (11)$$

subject to appropriate spatial boundary conditions and to quiescence for $t < t'$. The formal solution is given by

$$\hat{G} = \frac{1}{2\pi} \int_{-\infty}^{\infty} d\omega e^{-i\omega(t-t')} \sum_p \Phi_p(k\rho) \bar{\Phi}_p(k\rho') g_{\phi p}(\phi, \phi'), \quad \omega = kc. \quad (12)$$

Impulsive point source

The three-dimensional time-dependent Green's functions $\hat{G}'(\mathbf{r}, \mathbf{r}'; t, t')$ and $\hat{G}''(\mathbf{r}, \mathbf{r}'; t, t')$ satisfy the wave equation

$$\begin{aligned} & \left(\frac{1}{\rho} \frac{\partial}{\partial \rho} \rho \frac{\partial}{\partial \rho} + \frac{1}{\rho^2} \frac{\partial^2}{\partial \phi^2} + \frac{\partial^2}{\partial z^2} - \frac{1}{c^2} \frac{\partial^2}{\partial t^2} \right) \hat{G} \\ &= -\frac{\delta(\rho - \rho')}{\rho'} \delta(\phi - \phi') \delta(z - z') \delta(t - t'), \end{aligned} \quad (13)$$

subject to appropriate spatial boundary conditions and to quiescence for $t < t'$. The formal solution is given by

$$\begin{aligned} \hat{G} &= \frac{1}{(2\pi)^2} \int_{-\infty}^{\infty} d\omega e^{-i\omega(t-t')} \\ & \times \int_{-\infty}^{\infty} d\zeta \sum_p e^{i\zeta(z-z')} \Phi_p(\sqrt{k^2 - \zeta^2}\rho) \bar{\Phi}_p(\sqrt{k^2 - \zeta^2}\rho') g_{\phi p}(\phi, \phi'). \end{aligned} \quad (14)$$

Plane-wave incidence

By letting ρ' and z' tend to infinity in the preceding results and employing the normalizations in Eqs. (5.4.6c) or (5.4.30b) (with $\hat{\rho}' \rightarrow \rho'$), one may derive the wavefunctions corresponding to plane-wave incidence. These wavefunctions satisfy in the finite domain the homogeneous wave equations obtained by equating to zero the right-hand sides in Eqs. (3), (9), (11), and (13).

The rule for deducing three-dimensional from two-dimensional solutions, stated in connection with Eq. (5), may also be employed in the present case. Let $\bar{u}(\rho, \phi'; k)$ denote the two-dimensional wave function derived from $\bar{G}(\rho, \phi'; k)$ in Eq. (3) by letting $\rho' \rightarrow \infty$ along the angular direction ϕ' . For reasons to become evident, the dependence on k has been shown explicitly. The function \bar{u} satisfies the source-free equation (3) subject to appropriate boundary conditions and corresponds to an incident plane wave

$$\bar{u}_{\text{inc}}(\rho, \phi'; k) = \exp[-ik\rho \cos(\phi - \phi')]$$

propagating perpendicular to the z axis. The three-dimensional wavefunction $u(\mathbf{r}; \theta', \phi'; k)$ corresponding to a plane wave

$$u_{\text{inc}}(\mathbf{r}; \theta', \phi'; k) = \exp[-ik\rho \sin \theta' \cos(\phi - \phi') - ikz \cos \theta'], \quad (15)$$

incident obliquely along the direction θ', ϕ' , where $\theta' = \tan^{-1}(\rho'/z')$, satisfies the wave equation

$$\left(\frac{1}{\rho} \frac{\partial}{\partial \rho} \rho \frac{\partial}{\partial \rho} + \frac{1}{\rho^2} \frac{\partial^2}{\partial \phi'^2} + \frac{\partial^2}{\partial z^2} + k^2 \right) u(\mathbf{r}; \theta', \phi'; k) = 0, \quad (16)$$

subject to appropriate boundary conditions. Evidently,

$$u_{\text{inc}}(\mathbf{r}; \theta', \phi'; k) = \bar{u}_{\text{inc}}(\rho, \phi'; k \sin \theta') e^{-ikz \cos \theta'}, \quad (17)$$

and since the obstacle configuration in Fig. 6.1.1 is invariant with respect to z , the wavefunction u has the same z dependence. Thus, the z -independent part of u satisfies the two-dimensional wave equation with k replaced by $k \sin \theta'$, so

$$u(\mathbf{r}; \theta', \phi'; k) = \bar{u}(\rho, \phi'; k \sin \theta') e^{-ikz \cos \theta'}. \quad (18)$$

In connection with the remarks following Eq. (5), ζ takes on the fixed value $k \cos \theta'$, thereby making the ζ integration unnecessary, and $\sqrt{k^2 - \zeta^2} \rightarrow k \sin \theta'$.

The preceding considerations cannot be applied directly to the scalar functions \mathcal{S}' and \mathcal{S}'' since the transverse part of the differential operator $(\nabla_i^2 + \partial^2/\partial z^2 + k^2)\nabla_i^2$ in Eq. (5.2.2) is algebraized readily in a z -transmission, but not in a ϕ -transmission, representation [see Eqs. (5.2.5) and note that $\nabla_i^2 = -k_i^2$]. It is then best to proceed via the contour-integral representation deduced from Eqs. (5.2.5) (Sec. 3.3c) and to derive the angular transmission formulation from the z transmission formulation by deformation of contours in the complex k_i plane. The results resemble those obtained for G' and G'' except for the presence of a factor corresponding to $1/k_i^2$ in Eqs. (5.2.5a) and (5.2.5b), and also for a possible residue contribution arising from the additional pole at $k_i = 0$ in the complex k_i plane.

Before proceeding to the application of these results, it is well to recall that the eigenfunction expansions in Eqs. (8), (10), (12), and (14) are to be considered as formal and that they may be employed only for a class of "representable" functions (i.e., functions for which the representations are convergent). In view of the somewhat anomalous behavior of the radial eigenfunctions $\Phi_p(k\rho)$ [see remarks following Eqs. (6.3.1)], the expansions are found to converge only for restricted locations of source and observation points. A modified procedure [see Eq. (6.3.8)] must be employed to make arbitrary locations accessible.

6.3 WEDGE-TYPE PROBLEMS—INTEGRATION TECHNIQUES

The first class of problems to be discussed involves geometries that result from Fig. 6.1.1 when the cylinder radius $a \rightarrow 0$. The boundary conditions in the radial domain $0 < \rho < \infty$ require a radiation condition at $\rho \rightarrow \infty$, and boundedness at $\rho = 0$ to satisfy the “edge condition,” which delimits the permissible growth of the fields near the wedge apex (see Sec. 1.5b). The relevant completeness relation is given by the Lebedev–Kontorovitch transform theorem [see Eq. (3.4.94b)]:

$$\rho' \delta(\rho - \rho') = \frac{1}{2} \int_{-i\infty}^{i\infty} \mu J_\mu(k\rho) H_\mu^{(1)}(k\rho') d\mu = \frac{1}{4} \int_{-i\infty}^{i\infty} \mu H_\mu^{(1)}(k\rho) H_\mu^{(1)}(k\rho') d\mu, \quad (1a)$$

$$= \frac{1}{4} \int_0^{i\infty} \mu (1 - e^{i2\mu\pi}) H_\mu^{(1)}(k\rho) H_\mu^{(1)}(k\rho') d\mu. \quad (1b)$$

Comparison with the generic form in Eq. (6.2.4) permits identification of the eigenfunctions $\Phi_p(k\rho)$ and $\bar{\Phi}_p(k\rho)$, with the continuous mode index p denoted by μ .[†] Substitution of Eqs. (1) into Eqs. (6.2.8), (6.2.10), (6.2.12), or (6.2.14) yields the modal representation of the two- or three-dimensional Green’s functions in terms of a modal Green’s function $g_{\phi,p}(\phi, \phi') \rightarrow g(\phi, \phi'; \mu)$ whose explicit form depends on the assumed boundary conditions on the wedge faces at $\phi = 0$ and $\phi = \varphi$ (the subscript ϕ on g_ϕ will be suppressed for convenience). From Eq. (6.A19a) it is found that since $H_\mu^{(1)}(k\rho)$ grows like $\exp(|\mu|\pi/2)$ as $\mu \rightarrow i\infty$, the radial eigenfunction (angular transmission) representation can be employed only when $g(\phi, \phi'; \mu)$ decays sufficiently rapidly to overcome the $\exp(|\mu|\pi)$ behavior arising from the integrand in Eq. (1b). Since g exhibits the exponential behavior [see Eqs. (6.4.1) and (6.5.2)]

$$g(\phi, \phi'; \mu) \propto \exp(-|\mu| |\phi - \phi'|), \quad \text{as } \mu \rightarrow i\infty, \quad (2)$$

the representation applies only when $|\phi - \phi'| > \pi$ (i.e., in the geometric-optical shadow region).

The consequences of these anomalous convergence characteristics are illustrated in detail for the two-dimensional Green’s function descriptive of excitation by a time-harmonic line source.

6.3a Time-harmonic Line-source Excitation

Solution in integral form

From Eqs. (6.2.8) and (1), one obtains the representation for the two-dimensional time-harmonic Green’s function

$$\tilde{G} = \frac{1}{4} \int_0^{i\infty} \mu (1 - e^{i2\mu\pi}) H_\mu^{(1)}(k\rho) H_\mu^{(1)}(k\rho') g(\phi, \phi'; \mu) d\mu, \quad (3)$$

which, as noted above, converges only in the angular domain $|\phi - \phi'| > \pi$ coincident with the geometric-optical shadow (Fig. 6.3.1). In the shadow region,

[†]In the remainder of this chapter, μ denotes a separation parameter and is not to be confused with the same symbol used elsewhere for the permeability.

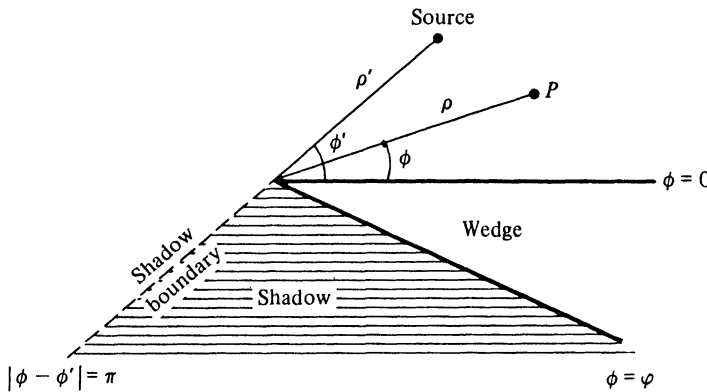


FIG. 6.3.1 Illuminated and shadow regions in a wedge diffraction problem.

the field comprises only outgoing waves, whereas in the illuminated region, incoming waves exist as well. Since the radial dependence in Eq. (3) involves only outgoing-wave Hankel functions [the time dependence is $\exp(-i\omega t)$], the incoming field is not directly expressible in this form. This deficiency is repaired below by an alternative representation valid for all $|\phi - \phi'|$. Because the shadow boundary $|\phi - \phi'| = \pi$ delimits the domain of Eq. (3), this representation is expected to be appropriate to a study of the quasi-optic properties of the diffraction field.

To obtain a formulation valid for all $|\phi - \phi'|$, we replace the Hankel functions of imaginary order μ by the expression [see Eq. (6.B3)]

$$H_{\mu}^{(1)}(k\rho)H_{\mu}^{(1)}(k\rho') = \frac{1}{\pi} \int_{-\infty}^{+\infty} H_0^{(1)}(k\sqrt{\rho^2 + \rho'^2 + 2\rho\rho' \cos w}) e^{i\mu(w-\pi)} dw, \quad (4)$$

and invert the orders of integration (permissible for $|\phi - \phi'| > \pi$) to obtain

$$\bar{G}(\rho, \rho') = \frac{1}{8\pi} \int_{-\infty}^{+\infty} H_0^{(1)}(k\chi) A(\phi, \phi'; w) dw, \quad \chi = \sqrt{\rho^2 + \rho'^2 + 2\rho\rho' \cos w}, \quad (5)$$

where

$$A(\phi, \phi'; w) = 2 \int_0^{i\infty} \mu(1 - e^{i2\mu\pi}) e^{i\mu(w-\pi)} g(\phi, \phi'; \mu) d\mu, \quad |\phi - \phi'| > \pi. \quad (6)$$

While the integral representation on the right-hand side of Eq. (6) converges only when $|\phi - \phi'| > \pi$ [see Eq. (2)], it will be found possible to evaluate the integral in closed form so that the resulting function $A(\phi, \phi'; w)$ is defined even when $|\phi - \phi'| < \pi$. To proceed further, the integrand in Eq. (5) must be examined in the entire complex w plane. The analytic properties of the Hankel function are discussed in connection with Fig. 6.3.2; for the type of problem considered, $A(\phi, \phi'; w)$ will generally have pole singularities in the complex w plane. In particular, one pole, located at $w_p = \pi - |\phi - \phi'|$, moves across the

integration path in Eq. (5) as $|\phi - \phi'|$ decreases through π , and near this pole, A behaves like

$$A(\phi, \phi'; w) = \frac{-1}{w - w_p} + D(w), \quad w_p = \pi - |\phi - \phi'|, \quad (7)$$

where $D(w)$ is regular near w_p . Hence, when $|\phi - \phi'| < \pi$, the value of \bar{G} differs from the expression in Eq. (5) by the residue at w_p , and one obtains, for all $|\phi - \phi'|$,

$$\begin{aligned} \bar{G}(\rho, \rho') &= \frac{i}{4} H_0^{(1)}(k|\rho - \rho'|)U(\pi - |\phi - \phi'|) + \frac{1}{8\pi} \int_{i\infty}^{-i\infty} H_0^{(1)}(k\chi) A(\phi, \phi'; w) dw, \\ |\rho - \rho'| &= \sqrt{\rho^2 + \rho'^2 - 2\rho\rho' \cos(\phi - \phi')}, \end{aligned} \quad (8)$$

where $U(x) = 1$ when $x > 0$, $U(x) = 0$ when $x < 0$, and the closed-form result is employed for A . The first term on the right-hand side of Eq. (8), the free-space Green's function [see Eq. (5.4.25)], exists only in the “illuminated” region $|\phi - \phi'| < \pi$ in Fig. 6.3.1, from which the source is visible. The integral represents a correction to the free-space field, and therefore displays directly the diffraction effects introduced by the wedge. It is noted that the functional form of the diffraction field in its dependence on (ρ, ρ') is the same in the illuminated and shadow regions. When $A(\phi, \phi'; w)$ has other pole singularities, which also move across the integration path for certain ranges of ϕ, ϕ' , their residue contributions must be included in a similar manner. Such additional poles furnish the reflected field of geometrical optics (see Sec. 6.5).

Asymptotic approximation

To effect an asymptotic evaluation of the diffraction integral in Eq. (8) via the steepest-descent method, it is necessary to investigate the analytic properties of the square-root function χ in Eq. (5) throughout the complex w plane. χ has first-order branch points at

$$w = w_b = \pm \left[n\pi \pm i \cosh^{-1}\left(\frac{a^2}{2\rho\rho'}\right) \right], \quad n = 1, 3, 5, \dots, \quad (9)$$

where $a^2 = \rho^2 + \rho'^2 > 2\rho\rho'$. If branch cuts are drawn along the curves $\text{Re } \chi = 0$ as in Fig. 6.3.2, the algebraic sign of $\text{Re } \chi$ can change only upon passing through a cut. On the top sheet of the Riemann surface, we define

$$\chi = (\rho + \rho') > 0 \text{ when } w = 0, \quad (10)$$

whence $\text{Re } \chi > 0$ on the entire top sheet. $\text{Im } \chi$ changes sign upon crossing the curves $\text{Im } \chi = 0$, shown dashed in Fig. 6.3.2. To determine the algebraic sign of $\text{Im } \chi$ in the various regions, note that near a branch point

$$\frac{\chi}{\sqrt{2\rho\rho'}} \approx \sqrt{i(w - w_b) \sinh w_{bi}}, \quad w \approx w_b, \quad (11)$$

with $\sqrt{w - w_b}$ defined so as to yield $\text{Re } \chi > 0$. For $w_b = \pi + i|w_{bi}|$, for example, one has $\sqrt{w - w_b} = \sqrt{|w - w_b|} e^{i\alpha/2}$, $\pi/2 > \alpha > -3\pi/2$, whence $\arg \chi = (\alpha/2) + (\pi/4)$. Thus, $\text{Im } \chi > 0$ for $-\pi/2 < \alpha < \pi/2$, and $\text{Im } \chi < 0$

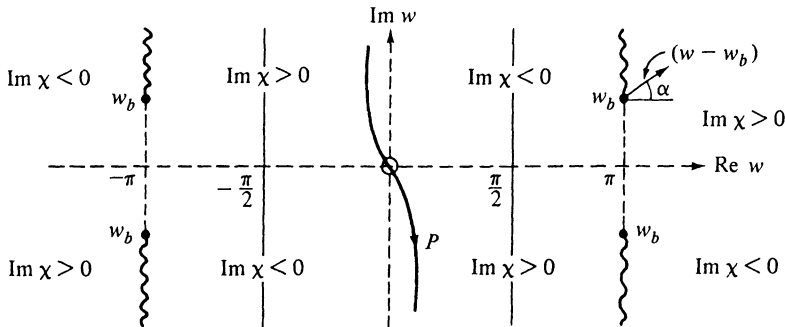


FIG. 6.3.2 Behavior of $\chi = \sqrt{a^2 + 2\rho\rho' \cos w}$, $a^2 > 2\rho\rho' > 0$, in the complex w plane.

for $-3\pi/2 < \alpha < -\pi/2$. Similar considerations apply to the other branch points and lead to a behavior of $\text{Im } \chi$ shown in Fig. 6.3.2. From these considerations and the asymptotic behavior $H_0^{(1)}(x) \propto \exp(ix)$ as $x \rightarrow \infty$, it is verified that the contour of integration in Eq. (8) can be deformed away from the imaginary axis onto a path P as in Fig. 6.3.2, on which $\text{Im } \chi > 0$.

If $k\rho$ or $k\rho'$ in Eq. (8) becomes very large, χ likewise becomes large and the Hankel function may be replaced by its asymptotic approximation in Eq. (5.3.13b),

$$H_\mu^{(1)}(k\chi) \sim \sqrt{\frac{2}{\pi k\chi}} e^{i(k\chi - \pi/4 - \mu\pi/2)}, \quad |k\chi| \gg |\mu|. \quad (12)$$

The integrand then contains an exponential factor $e^{ik\chi(w)}$, with k playing the role of the large parameter, whence a pertinent saddle point of $\chi(w)$ is located at $w = 0$; the functions A to be encountered do not behave exponentially in w . Along the steepest-descent path SDP at $w = 0$, one has, from Eq. (4.2.5),

$$\arg dw = \arg \sqrt{\frac{-2}{i\chi''(0)}} = -\frac{\pi}{4}, \quad (13)$$

so the SDP crosses the saddle point at an angle of -45° . In general, $\chi(w) = \chi(0) + is^2$, $s^2 > 0$, along the SDP, i.e.,

$$\text{Re } \chi(w) = \text{Re } \chi(0) = \rho + \rho'. \quad (14)$$

As $w_i \rightarrow i\infty$, $\cos w \rightarrow (\cosh w_i)e^{-iw_i}$, and $\chi(w) \rightarrow [2\rho\rho' \cos w]^{1/2}$. $\text{Re } \chi(w)$ must be finite [see Eq. (14)], so $w_i \rightarrow \mp\pi$ as $w_i \rightarrow \pm\infty$. Since there are no singularities between the imaginary axis and the SDP, the original contour can be deformed into the steepest-descent path and the integral evaluated according to Eq. (4.2.1b). Thus, to $O(1/\sqrt{k\rho})$ or $O(1/\sqrt{k\rho'})$, for $|\phi - \phi'| \gtrsim \pi$ (i.e., w_p not near the saddle point at $w = 0$),

$$\bar{G}(\rho, \rho') \sim \frac{i}{4} H_0^{(1)}(k|\rho - \rho'|) U(\pi - |\phi - \phi'|) - 2A(\phi, \phi'; 0) C(k\rho) C(k\rho'), \quad (15)$$

where $A(\phi, \phi'; 0)$ is the closed-form expression for the integral on the right-

hand side of Eq. (6), with $w = 0$, and

$$C(\alpha) = \frac{e^{i(\alpha+\pi/4)}}{2\sqrt{2\pi\alpha}}. \quad (15a)$$

This result has a simple physical interpretation in terms of a geometric-optical and diffraction field, as will be emphasized in connection with the various problems treated in Secs. 6.4–6.6.

Higher-order terms in the asymptotic expansion of the diffraction integral may be derived directly from Eq. (3) by using the method described in Eqs. (6.4.8)–(6.4.12).

Transition effects (uniform asymptotic formulation)

In view of Eq. (7) the simple formula in Eq. (15) fails in the vicinity of the shadow boundary $|\phi - \phi'| = \pi$ and must be augmented by a transition term derived by accounting explicitly for the presence of the pole at $w_p = \pi - |\phi - \phi'| \approx 0$ near the saddle point of the integrand in Eq. (8). Upon employing Eq. (12) for $H_0^{(1)}(k\chi)$, utilizing Eq. (7), and recalling the fact that the major contribution to the integral arises from the vicinity of $w = 0$, one may remove from the integrand all slowly varying factors and write

$$\frac{1}{8\pi} \int_{-\infty}^{-i\infty} H_0^{(1)}(k\chi) A(\phi, \phi'; w) dw \sim -\frac{e^{-i\pi/4}}{4\pi\sqrt{2\pi k\chi(0)}} (I + I'), \quad (16)$$

where

$$I = \int_{SDP} \frac{e^{ik\chi(w)}}{w - w_p} dw, \quad \chi(w) = \sqrt{\rho + \rho'^2 + 2\rho\rho' \cos w}, \quad w_p \approx 0, \quad (16a)$$

and I' is given by the same integral with $(w_p - w)^{-1}$ replaced by $D(w)$ in Eq. (7). Since $D(w)$ is regular near $w = 0$, the asymptotic evaluation of I' is straightforward and leads to a result as in Eq. (17a), with $1/w_p$ replaced by $D(0)$.

While the asymptotic evaluation of I , with $\chi(w)$ as indicated, can be carried out via the procedure in Sec. 4.4a, it is simpler and sufficiently accurate for the present purpose to approximate $\chi(w)$ by

$$\chi(w) = \sqrt{(\rho + \rho')^2 + 2\rho\rho'(\cos w - 1)} \approx (\rho + \rho') + \frac{\rho\rho'}{\rho + \rho'} (\cos w - 1), \quad (16b)$$

since the major contribution to I arises from the vicinity of the saddle point $w = 0$. The resulting integral in Eq. (16a) is then identical in form with $I_1(\Omega, \alpha, \beta)$ in Eq. (4.2.23), so the asymptotic expression (4.4.34) can be employed directly. It is useful to group the terms as follows:

$$I \equiv \int_{SDP} \frac{e^{ik\tau \cos w}}{w - w_p} dw \sim I^d + I', \quad (17)$$

where τ stands for $\rho\rho' / (\rho + \rho')$,

$$\bar{I}^d = \sqrt{\frac{2\pi}{k\tau}} \frac{e^{i(k\tau - \pi/4)}}{-w_p}, \quad w_p = \pi - |\phi - \phi'|, \quad (17a)$$

$$\bar{I}' = i\pi(\operatorname{sgn} w_p)e^{ik\tau}\left[F(\xi) - \frac{e^{i\pi/4}}{\sqrt{2\pi}\xi}\right], \quad \xi = \sqrt{k\tau}\left|\sin \frac{w_p}{2}\right|, \quad (17b)$$

and $\operatorname{sgn}(x) = \pm 1$, $x \geq 0$. The function F is defined as

$$F(\xi) = \frac{2}{\sqrt{\pi}} e^{-i2\xi^2} \int_{(1-i)\xi}^{\infty} e^{-y^2} dy, \quad (18)$$

and has the asymptotic approximation

$$F(\xi) \sim \frac{e^{i\pi/4}}{\sqrt{2\pi}\xi} + O\left(\frac{1}{\xi^3}\right), \quad \xi \gg 1, \quad (18a)$$

so that \bar{I}' contributes only when ξ is small. Since $F(\xi)$ remains bounded and the singularity in the second term of Eq. (17b) cancels that due to \bar{I}^d , the asymptotic solution for \bar{I} remains valid as $w_p \rightarrow 0$. For sufficiently large ξ where \bar{I}' is negligible, the result $\bar{I} \sim \bar{I}^d$ represents the usual asymptotic approximation obtained by the ordinary saddle-point technique. \bar{I}' may therefore be regarded as a correction term that must be added to the simple asymptotic solution in the transition region surrounding the shadow boundary, wherein ξ is small. Suppose that \bar{I}' is negligible when $\xi \geq \xi_m$; then the transition region is bounded approximately by the curve

$$\xi_m \sqrt{k\tau} = k\tau \left|\sin \frac{w_p}{2}\right| \approx \frac{k|x|}{2}, \quad (19)$$

where $x = \tau w_p$ is the distance from the curve, a parabola, to the shadow boundary and, for ρ' very large, τ is essentially the distance coordinate along the shadow boundary (see Fig. 6.4.4). From Fig. 4.4.3(a) it is noted that the asymptotic approximation in Eq. (18a) holds with good accuracy when $\xi \geq 3$, so we may put $\xi_m = 3$ in Eq. (19); for greater accuracy, a larger value of ξ_m may be taken.

Upon combining Eqs. (16) and (17), one may write the following correction \bar{G}' to \bar{G} which must be employed in the transition region $|\phi - \phi'| \approx \pi$:

$$\bar{G}'(\mathbf{p}, \mathbf{p}') = -\frac{1}{2}C(k\rho + k\rho') \operatorname{sgn}(\pi - |\phi - \phi'|) \left[F(\xi) - \frac{e^{i\pi/4}}{\xi \sqrt{2\pi}} \right], \quad (20)$$

where ξ and $C(\alpha)$ are defined in Eqs. (17b) and (15a), respectively, and $\tau = \rho\rho' / (\rho + \rho')$. When this expression is added to the result in Eq. (15), the composite formula remains uniformly valid for arbitrary observation points. It is of interest to note that as $|\phi - \phi'| \rightarrow \pi$, $F(\xi) \rightarrow 1$, and the sum of Eqs. (15) and (20) may be written as

$$\bar{G}(\mathbf{p}, \mathbf{p}') \sim \frac{1}{2} \bar{G}_{\text{inc}} + O\left(\frac{1}{k\sqrt{\rho\rho'}}\right), \quad |\phi - \phi'| = \pi, \quad (21)$$

where \bar{G}_{inc} is the incident wavefunction

$$\bar{G}_{\text{inc}} = \frac{i}{4} H_0^{(1)}(k|\mathbf{p} - \mathbf{p}'|) \sim C(k\rho + k\rho'), \quad (21a)$$

and it has been recognized that $|\mathbf{p} - \mathbf{p}'| \rightarrow (\rho + \rho')$ when $|\phi - \phi'| = \pi$. Thus,

for large $k\rho$ and $k\rho'$, the field on the shadow boundary has a value equal to $\frac{1}{2}$ that of the incident field.

The present discussion deals only with the pole singularity at $w_p = \pi - |\phi - \phi'|$; when A in Eq. (7) has other relevant poles descriptive of reflected waves, each pole gives rise to similar transition phenomena near the appropriate angular coordinates.

6.3b Time-harmonic Plane-wave and Point-source Excitations

Solutions in integral form

If the source point ρ' moves to infinity along the angle ϕ' , one obtains in the limit the result for an incident plane wave. In this instance, one of the Hankel functions in Eq. (3) is replaced by the asymptotic form in Eq. (12). Although μ in Eq. (3) also covers an infinite range, the integrand decreases exponentially with increasing μ , and the error made by employing Eq. (12) for all μ can be shown to be proportional to $\exp(-\alpha N)$, where $\alpha = |\phi - \phi'| - \pi$ and $1 \ll N \ll k\rho'$. N is a positive number such that Eq. (12) can be employed in the range $|\mu| \leq N$. As $\rho' \rightarrow \infty$, N can likewise be made arbitrarily large and the error term goes to zero. Substitution of the contour integral representation for $H_\mu^{(1)}(k\rho)$ for imaginary μ ,

$$H_\mu^{(1)}(k\rho) = \frac{1}{\pi} \int_{i\infty}^{-i\infty} e^{ik\rho \cos w + i\mu(w - \pi/2)} dw, \quad (22)$$

then leads to an expression as in Eq. (8), provided that one replaces the Hankel function

$$\frac{i}{4} H_0^{(1)}(k\sqrt{\rho^2 + \rho'^2 + 2\rho\rho' \cos \beta}) \quad \text{by } C(k\rho') e^{ik\rho \cos \beta}, \quad (23)$$

where $C(k\rho')$ is defined in Eq. (15a). For an incident plane wave of unit amplitude, $C \equiv 1$ [see Eq. (5.4.30b)] and one obtains the wavefunction

$$\tilde{u}(\rho; \phi') = e^{-ik\rho \cos(\phi - \phi')} U(\pi - |\phi - \phi'|) - \frac{i}{2\pi} \int_{i\infty}^{-i\infty} e^{ik\rho \cos w} A(\phi, \phi'; w) dw, \quad (24)$$

where A is the closed form for the integral on the right-hand side of Eq. (6). The first term on the right-hand side of Eq. (24) represents the incident plane-wave field in the illuminated region, whereas the second term expresses the diffraction field [see remarks following Eq. (8) for possible reflected wave contributions]. The result for an obliquely incident plane wave is deduced from Eq. (6.2.18).

The three-dimensional scalar Green's function $G(\mathbf{r}, \mathbf{r}')$ appropriate to excitation by a point source located at $\mathbf{r}' = (\rho', \phi', z')$ can be obtained from Eq. (8) by application of the rule stated after Eq. (6.2.5). Since k appears only in the argument of the Hankel functions, application of Eq. (5.4.12d),

$$\int_{-\infty}^{\infty} H_0^{(1)}(\sqrt{k^2 - \zeta^2} q) e^{i\zeta p} d\zeta = -2i \frac{e^{ik\sqrt{q^2 + p^2}}}{\sqrt{q^2 + p^2}}, \quad (25)$$

leads at once to the result

$$G(\mathbf{r}, \mathbf{r}') = \frac{e^{ik|\mathbf{r}-\mathbf{r}'|}}{4\pi|\mathbf{r}-\mathbf{r}'|} U(\pi - |\phi - \phi'|) - \frac{i}{8\pi^2} \int_{i\infty}^{-i\infty} \frac{e^{iky}}{\gamma} A(\phi, \phi'; w) dw, \quad (26)$$

where [see Eq. (5)]

$$\begin{aligned} \gamma &= [\rho^2 + \rho'^2 + (z - z')^2 + 2\rho\rho' \cos w]^{1/2}, \\ |\mathbf{r} - \mathbf{r}'| &= \sqrt{|\mathbf{p} - \mathbf{p}'|^2 + (z - z')^2}. \end{aligned} \quad (26a)$$

Thus, the three-dimensional Green's function $G(\mathbf{r}, \mathbf{r}')$ results from the two-dimensional $\bar{G}(\mathbf{p}, \mathbf{p}')$ in Eq. (8) upon replacement of

$\frac{i}{4} H_0^{(1)}(k\sqrt{\rho^2 + \rho'^2 + 2\rho\rho' \cos \beta})$ by

$$\frac{\exp[ik\sqrt{\rho^2 + \rho'^2 + 2\rho\rho' \cos \beta + (z - z')^2}]}{4\pi\sqrt{\rho^2 + \rho'^2 + 2\rho\rho' \cos \beta + (z - z')^2}}. \quad (27)$$

As before, the first term on the right-hand side of Eq. (26) furnishes the incident point-source field in the illuminated region while the second term yields the diffraction effect [see remarks following Eq. (8) for possible reflected-wave contributions].

Asymptotic evaluation

The diffraction integral for the plane-wave scattering problem in Eq. (24) is already in the standard form, so an asymptotic evaluation for large values of $k\rho$ may be carried out directly by the methods leading to Eqs. (15) and (20). The result to $O(1/\sqrt{k\rho})$, uniformly in $|\phi - \phi'|$, is found to be

$$\bar{u}(\mathbf{p}; \phi') \sim \bar{u}^0 + \bar{u}^d + \bar{u}', \quad (28)$$

where

$$\bar{u}^0 = e^{-ik\rho \cos(\phi - \phi')} U(\pi - |\phi - \phi'|), \quad (28a)$$

$$\bar{u}^d = -\frac{e^{ik\rho + i\pi/4}}{\sqrt{2\pi k\rho}} A(\phi, \phi'; 0), \quad (28b)$$

$$\bar{u}' = -e^{ik\rho} \operatorname{sgn}(\pi - |\phi - \phi'|) \left[\frac{F(\xi)}{2} - \frac{e^{i\pi/4}}{2\sqrt{2\pi}\xi} \right], \quad (28c)$$

with

$$\xi = \sqrt{k\rho} \left| \sin \frac{\pi - |\phi - \phi'|}{2} \right|. \quad (28d)$$

$F(\xi)$ is defined in Eq. (18). As in the result for the line source, the transition term \bar{u}' must be included only when $|\phi - \phi'| \approx \pi$; near other angular directions where $A(\phi, \phi'; 0)$ may diverge [see remarks following Eq. (8)], analogous transition functions must be employed. When $|\phi - \phi'| = \pi$, one has

$$\bar{u}(\mathbf{p}; \phi') \sim \frac{e^{ik\rho}}{2} + O\left(\frac{1}{\sqrt{k\rho}}\right), \quad (29)$$

thereby confirming again that the field on the shadow boundary is asymptotically equal to one half the incident field.

Higher-order terms in the asymptotic expansion of \tilde{u}^d may be derived as in Eqs. (6.4.9)–(6.4.12), subject to the modifications in Sec. 6.4e.

The γ -dependent diffraction integral for the point source in Eq. (26) may be evaluated asymptotically by the same procedure as in Sec. 6.3a, owing to its similarity with the integral in Eq. (8) with $H_0^{(1)}(k\chi) \sim e^{ik\chi}/\sqrt{k\chi}$. Since $\gamma = [\chi^2 + (z - z')^2]^{1/2}$ from Eq. (26a), many of the expressions encountered in the line-source problem can be taken over for the point-source case provided that $\rho^2 + \rho'^2$ is replaced by $\rho^2 + \rho'^2 + (z - z')^2$. Thus, one finds for large $k\rho, k\rho'$, and uniformly in $|\phi - \phi'|$:

$$G(\mathbf{r}, \mathbf{r}') \sim G^o + G^d + G', \quad (30)$$

where

$$G^o = \frac{e^{ik|\mathbf{r}-\mathbf{r}'|}}{4\pi|\mathbf{r}-\mathbf{r}'|} U(\pi - |\phi - \phi'|), \quad (30a)$$

$$G^d = -\frac{e^{ikl+in/4}}{4\pi\sqrt{2\pi k\rho\rho'l}} A(\phi, \phi'; 0), \quad l = \sqrt{(\rho + \rho')^2 + (z - z')^2}, \quad (30b)$$

$$G' = -\frac{e^{ikl}}{8\pi l} \operatorname{sgn}(\pi - |\phi - \phi'|) \left[F(\xi) - \frac{e^{in/4}}{\xi\sqrt{2\pi}} \right], \quad (30c)$$

with

$$\xi = \sqrt{\frac{k\rho\rho'}{l}} \left| \sin \frac{\pi - |\phi - \phi'|}{2} \right|. \quad (30d)$$

$F(\xi)$ is defined in Eq. (18). Transition functions analogous to G' in Eq. (30c) must be included near other angles, where $A(\phi, \phi'; 0)$ may have singularities [see remarks following Eq. (8)]. On the shadow boundary $|\phi - \phi'| = \pi$,

$$G(\mathbf{r}, \mathbf{r}') \sim \frac{e^{ikl}}{8\pi l} + O\left(\frac{1}{\sqrt{k\rho\rho'l}}\right), \quad (31)$$

in accord with a similar result in Eq. (21) (see Fig. 6.4.3 for a geometrical interpretation).

6.3c. Pulsed-source Configurations

When the source configurations in the preceding sections have an impulsive behavior characterized by the delta function $\delta(t - t')$ as in Eq. (5.2.15), the transient solutions may be obtained from the time-harmonic Green's functions by performing an integration as in Eq. (6.2.12) et seq. As noted in Sec. 5.2c, the explicit recovery of the time-dependent result is simplified substantially when the time-harmonic solution has the form given in Eqs. (1.6.37) or (1.6.38). This is indeed the case for the expressions in Eqs. (24) and (26), so the transient response to plane-wave or point-source excitation may be recovered by direct application of Eq. (1.6.39) (see also Sec. 5.2c; A in Sec 5.2c and here denotes different quantities).

Since the time-harmonic plane wave $\exp[-ik\rho \cos(\phi - \phi')]$ corresponds to the plane-wave pulse $\delta[t - t' + (\rho/\bar{c}) \cos(\phi - \phi')]$, the temporal response in the presence of the wedge configuration is given via Eqs. (24) and (1.6.39) for arbitrary ρ, ρ', t, t' by

$$\begin{aligned}\hat{u}(\rho, \phi'; t) = & \delta\left(t - t' + \frac{\rho}{\bar{c}} \cos(\phi - \phi')\right) U(\pi - |\phi - \phi'|) \\ & - \frac{1}{\pi} \frac{\operatorname{Re} A[\phi, \phi'; i \cosh^{-1}(\bar{c}(t - t')/\rho)]}{\sqrt{(t - t')^2 - (\rho/\bar{c})^2}} U\left(t - t' - \frac{\rho}{\bar{c}}\right),\end{aligned}\quad (32)$$

where \bar{c} is the propagation speed in the medium and $A(\phi, \phi'; w)$ is the closed form of the function defined in Eq. (6). The first term on the right-hand side of Eq. (32) represents the incident plane-wave pulse in the illuminated region of Fig. 6.3.1, and the second term yields the diffraction field. Since the incident pulse does not reach the edge $\rho = 0$ until time $t = t'$, no diffraction takes place until $t > t'$. The diffracted pulse spreads cylindrically outward from the edge and has a behavior characteristic of an equivalent line source at the edge [see Eq. (5.4.42)] modified by the amplitude factor $\operatorname{Re} A$. Additional physical implications are discussed in connection with examples in Secs. 6.4 and 6.5 (see Fig. 6.4.5). When $A(\phi, \phi'; w)$ has pole singularities in addition to the one at $w = \pi - |\phi - \phi'|$, other plane-wave pulse contributions, descriptive of the reflected field of geometrical optics, arise [see remarks following Eq. (8) and Sec. 6.5].

For excitation by an impulsive point source, the Green's function $\hat{G}(\mathbf{r}, \mathbf{r}'; t, t')$, which satisfies Eq. (6.2.13) for arbitrary $\mathbf{r}, \mathbf{r}', t, t'$, is obtained via Eq. (26) and the procedure following Eq. (1.6.37):

$$\begin{aligned}\hat{G}(\mathbf{r}, \mathbf{r}'; t, t') = & \frac{\delta(t - t' - |\mathbf{r} - \mathbf{r}'|/\bar{c})}{4\pi|\mathbf{r} - \mathbf{r}'|} U(\pi - |\phi - \phi'|) \\ & + \frac{\bar{c}}{4\pi} \frac{\operatorname{Re} A(\phi, \phi'; i\beta)}{\rho\rho' \sinh\beta} U\left(t - t' - \frac{l}{\bar{c}}\right),\end{aligned}\quad (33)$$

where $\beta = \cosh^{-1}\{[\bar{c}^2(t - t')^2 - \rho^2 - \rho'^2 - (z - z')^2]/2\rho\rho'\}$, and l is defined in Eq. (30b). The interpretation of this result is analogous to the above [see Fig. 6.4.3 and Eq. (5.4.14b)], and also the remarks concerning additional contributions arising from A .

The two-dimensional Green's function in Eq. (8) does not exhibit the structure specified in Eq. (1.6.37), so the formulas in Sec 5.2c cannot be applied directly (note the different meaning of A in Sec. 5.2c). It is possible, however, to achieve the desired format after certain preliminary manipulations. Upon letting $k \rightarrow is/\bar{c}$, where s is positive and \bar{c} is the speed of light in the exterior medium, and recalling that

$$H_\nu^{(1)}(iz) = \frac{2}{\pi i} e^{-i\nu\pi/2} K_\nu(z), \quad (34)$$

where $K_\nu(z)$ is the modified Bessel function, one obtains

$$\tilde{G}(\rho, \rho') = \frac{1}{2\pi} K_0\left(s \frac{|\rho - \rho'|}{\bar{c}}\right) U(\pi - |\phi - \phi'|) + I(\rho, \rho'; s), \quad (35)$$

with

$$I(\rho, \rho'; s) = \frac{i}{4\pi^2} \int_{-i\infty}^{i\infty} K_0\left(\frac{s}{\bar{c}} \sqrt{\rho^2 + \rho'^2 + 2\rho\rho' \cos w}\right) A(\phi, \phi'; w) dw. \quad (36)$$

The Laplace inversion of the first term on the right-hand side of Eq. (35) is given in Eq. (5.4.42). To transform the second term into a representation as in Eq. (1.6.34), introduce

$$K_0(x) = \int_1^\infty \frac{e^{-xt}}{\sqrt{t^2 - 1}} dt, \quad x > 0, \quad (37)$$

to obtain

$$I(\rho, \rho'; s) = \frac{i}{4\pi^2} \int_{-i\infty}^{i\infty} dw A(\phi, \phi'; w) \int_{f/\bar{c}}^\infty \frac{e^{-st}}{\sqrt{\tau^2 - f^2/\bar{c}^2}} d\tau, \quad (38)$$

where

$$f \equiv f(\beta) = \sqrt{\rho^2 + \rho'^2 + 2\rho\rho' \cosh \beta} > 0, \quad \beta = -iw. \quad (38a)$$

The desired formulation results upon interchange of the order of integrations which, in Eq. (38), cover the range $f(\beta) < \bar{c}\tau < \infty$ and $-\infty < \beta < \infty$. If the β integration is performed first, one has $-\psi(\tau) < \beta < \psi(\tau)$, $\psi(\tau) = \cosh^{-1} [\bar{c}^2\tau^2 - \rho^2 - \rho'^2]/2\rho\rho'$, while $f(0) < \bar{c}\tau < \infty$. Thus

$$I(\rho, \rho'; s) = \int_0^\infty e^{-st} Q(\tau) d\tau, \quad (39)$$

where

$$Q(\tau) = \begin{cases} 0, & \bar{c}\tau < (\rho + \rho'), \\ -\frac{1}{4\pi^2} \int_{-\psi(\tau)}^{\psi(\tau)} \frac{A(\phi, \phi'; i\beta)}{\sqrt{\tau^2 - f^2(\beta)/\bar{c}^2}} d\beta, & \bar{c}\tau > (\rho + \rho'). \end{cases} \quad (40a)$$

$$Q(\tau) = \begin{cases} 0, & \bar{c}\tau < (\rho + \rho'), \\ -\frac{1}{4\pi^2} \int_{-\psi(\tau)}^{\psi(\tau)} \frac{A(\phi, \phi'; i\beta)}{\sqrt{\tau^2 - f^2(\beta)/\bar{c}^2}} d\beta, & \bar{c}\tau > (\rho + \rho'). \end{cases} \quad (40b)$$

The line-source Green's function satisfying Eq. (6.2.11) is therefore given for arbitrary ρ, ρ', t, t' by

$$\begin{aligned} \hat{G}(\rho, \rho'; t, t') &= \frac{1}{2\pi\sqrt{(t-t')^2 - |\rho - \rho'|^2/\bar{c}^2}} U(\pi - |\phi - \phi'|) \\ &\times U\left(t - t' - \frac{|\rho - \rho'|}{\bar{c}}\right) \\ &- \left[\frac{1}{4\pi^2} \int_{-\psi(t-t')}^{\psi(t-t')} \frac{\operatorname{Re} A(\phi, \phi'; i\beta)}{\sqrt{(t-t')^2 - f^2(\beta)/\bar{c}^2}} d\beta \right] U\left(t - t' - \frac{\rho + \rho'}{\bar{c}}\right). \end{aligned} \quad (41)$$

A physical interpretation of this result, whose form is more complicated than that for the plane-wave or point-source excitation, is provided in connection with Fig. 6.4.2. It should again be recalled that additional contributions representative of reflected field constituents may be present in Eqs. (32), (33) and (41), as noted already in connection with Eq. (32).

The preceding results simplify substantially for observation times near the time of arrival of the first response [i.e., for values of $(t - t')$ which annul the arguments of the various Heaviside unit functions in Eqs. (32), (33), or (41)]. One observes by inspection that the values of \hat{G} in Eqs. (32) and (33) near the time of arrival of the diffracted wavefront are ascertained directly upon replacement of $A[\phi, \phi'; \Omega]$ by $A[\phi, \phi'; 0]$, whereas the corresponding result in Eq. (41) requires a reduction of the integral as $\psi(t - t') \rightarrow 0$. The reader may verify that the expressions obtained in this manner agree with those predicted from the time-harmonic high-frequency asymptotic formulas in Eqs. (15), (24) and (26), after relations (1.6.45) and (1.6.47) have been invoked.

6.4 PERFECTLY ABSORBING WEDGE

A wedge configuration analyzed most simply by the angular transmission analysis is the “perfectly absorbing” wedge defined by the condition that all angularly propagating waves are absorbed completely at the wedge faces; the “black screen” investigated by Sommerfeld¹ belongs to this category, although his analysis differs from the one carried out here. While this boundary condition is not easily phrased as a relation between the *total* electric and magnetic fields at the reflectionless wedge surfaces $\phi = 0$ and $\phi = \varphi$, its specification in terms of a *mode* propagating along the ϕ direction is elementary: $g(\phi, \phi'; \mu)$ must comprise only outgoing waves from the source location $\phi = \phi'$. Thus, the angular Green’s function defined in Eq. (6.2.7) is given by Eq. (3.4.55); the reflectionless condition on the wedge faces is the same for E modes and H modes, so no distinction need be made. With $g_\infty^\infty \equiv g_\infty$, one has

$$g_\infty(\phi, \phi'; \mu) = \frac{e^{i\mu|\phi-\phi'|}}{-2i\mu}, \quad \text{Im } \mu > 0. \quad (1)$$

It is observed from the structure of the Green’s function that the condition of perfect absorption (matched condition) at $\phi = 0, \varphi$, is equivalent to regarding the ϕ space as being infinitely extended (hence the subscript ∞), and to imposing a radiation condition at $|\phi| = \infty$. For the analogous result pertaining to bilaterally unbounded transmission along a rectilinear coordinate, see Eq. (5.4.7), with $j \rightarrow -i$. The behavior of g_∞ in Eq. (1) evidently conforms with that in Eq. (6.3.2), and substitution into Eq. (6.3.6) permits the closed-form evaluation of $A(\phi, \phi'; w)$:

$$A(\phi, \phi'; w) = i \int_0^{i\infty} (1 - e^{i2\mu\pi}) e^{i\mu(w - \pi + |\phi - \phi'|)} d\mu \quad (2a)$$

$$= \frac{1}{\pi - |\phi - \phi'| - w} + \frac{1}{\pi + |\phi - \phi'| + w}. \quad (2b)$$

Unlike the integral representation in Eq. (2a), the result in Eq. (2b) is defined for all values of $|\phi - \phi'|$, and its analytic structure in w reveals the presence of a simple pole at $w_p = \pi - |\phi - \phi'|$ as specified in Eq. (6.3.7). The second pole

at $w = -(\pi + |\phi - \phi'|)$ never crosses the imaginary axis in the complex w plane, so the solutions given in Sec. 6.3 apply without modification.

6.4a Time-harmonic Line-source Excitation

When the perfectly absorbing wedge is excited by a line source of electric current (Fig. 6.4.1) having a density prescribed by

$$\hat{\mathbf{J}}(\mathbf{r}, t) = I\delta(\rho - \rho')e^{-i\omega t}\mathbf{z}_0, \quad (3a)$$

or by a line source of magnetic current with

$$\hat{\mathbf{M}}(\mathbf{r}, t) = V\delta(\rho - \rho')e^{-i\omega t}\mathbf{z}_0, \quad (3b)$$

the electromagnetic fields E_z , H_ρ , H_ϕ , and H_z , E_ρ , E_ϕ excited by the electric and magnetic currents, respectively, can be derived from a two-dimensional scalar Green's function [see Eqs. (6.2.1) and (6.2.2)]. Since the boundary conditions on the perfectly absorbing wedge faces are the same in the two cases,

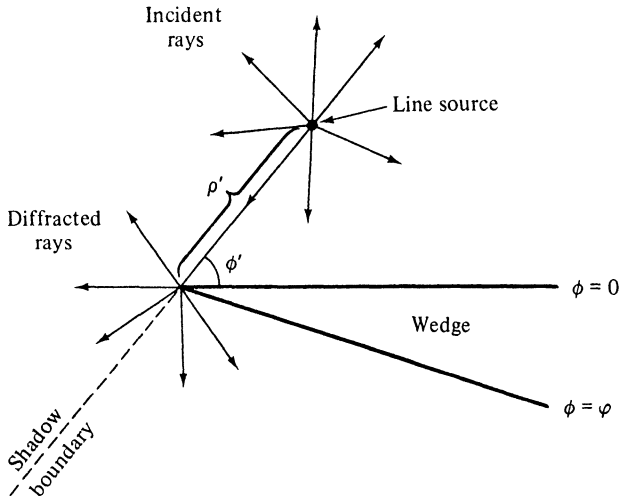


FIG. 6.4.1. Line-source excitation of a perfectly absorbing wedge.

the E -mode and H -mode Green's functions are identical and shall be denoted by $\bar{G}_\infty(\rho, \rho')$, which satisfies the inhomogeneous wave equation

$$\left(\frac{1}{\rho} \frac{\partial}{\partial \rho} \rho \frac{\partial}{\partial \rho} + \frac{1}{\rho^2} \frac{\partial^2}{\partial \phi^2} + k^2 \right) \bar{G}_\infty(\rho, \rho') = -\frac{\delta(\rho - \rho')}{\rho'} \delta(\phi - \phi') \quad (4)$$

in the domain $0 < (\rho, \rho') < \infty$, $-\infty < (\phi, \phi') < \infty$, subject to boundedness at $\rho = 0$ and a radiation condition at $\rho \rightarrow \infty$, $|\phi| \rightarrow \infty$. The subscript ∞ denotes the solution for the angularly unbounded domain $-\infty < \phi < \infty$. The solution in the geometric-optical shadow region $|\phi - \phi'| > \pi$ is given via Eqs. (6.3.3) and (1) by

$$\bar{G}_\infty(\rho, \rho') = \frac{i}{8} \int_0^{i\infty} (1 - e^{i2\mu\pi}) e^{i\mu|\phi - \phi'|} H_\mu^{(1)}(k\rho) H_\mu^{(1)}(k\rho') d\mu, \quad (5)$$

whereas the result obtained from Eqs. (6.3.8) and (2) is valid for all $|\phi - \phi'|$. For $k\rho \gg 1$, $k\rho' \gg 1$, but with $|\phi - \phi'| \approx \pi$, one has the asymptotic approximation given in Eq. (6.3.15),

$$\bar{G}_\infty \sim \bar{G}_\infty^0 + \bar{G}_\infty^d, \quad (6)$$

$$\bar{G}_\infty^0 = \frac{i}{4} H_0^{(1)}(k|\rho - \rho'|) U(\pi - |\phi - \phi'|), \quad (6a)$$

$$\bar{G}_\infty^d = -2A(\phi, \phi'; 0)C(k\rho)C(k\rho') = -iA(\phi, \phi'; 0) \frac{e^{ik(\rho + \rho')}}{4\pi k \sqrt{\rho\rho'}}, \quad (6b)$$

$$A(\phi, \phi'; 0) = \frac{1}{\pi - |\phi - \phi'|} + \frac{1}{\pi + |\phi - \phi'|}, \quad (6c)$$

whereas for arbitrary $|\phi - \phi'|$, one must add to Eq. (6) the transition function from Eq. (6.3.20):

$$\bar{G}_\infty^t(\rho, \rho') = -\frac{e^{i[k(\rho + \rho') + \pi/4]}}{4\sqrt{2\pi k(\rho + \rho')}} \left[F(\xi) - \frac{e^{i\pi/4}}{\xi\sqrt{2\pi}} \right] \text{sgn}(\pi - |\phi - \phi'|), \quad (7)$$

where

$$\xi = \sqrt{\frac{k\rho\rho'}{\rho + \rho'}} \left| \cos \frac{\phi - \phi'}{2} \right|. \quad (7a)$$

and $F(\xi)$ is defined in Eq. (6.3.18). $U(\alpha)$ denotes the Heaviside unit function and $C(\alpha)$ is defined in Eq. (6.3.15a).

Discussion

The \bar{G}_∞^0 term represents the incident field in the illuminated region $|\phi - \phi'| < \pi$, whereas the term \bar{G}_∞^d furnishes to $O(1/\sqrt{k\rho})$, $O(1/\sqrt{k\rho'})$ the diffraction field exterior to the transition region surrounding the light-shadow boundary [see Eq. (9) for a calculation of higher-order terms]. The diffracted contribution associated with the factor $C(k\rho)$ can be interpreted as an outgoing cylindrical wave that emanates from the edge and has an angular distribution given by $-2A(\phi, \phi'; 0)$. This wave is excited by the cylindrical wave incident from the source and the factor $C(k\rho')$ yields precisely the strength of the incident wave at the wedge apex. The process can be schematized clearly through the use of diffracted rays (see Sec. 1.7d). In Fig. 6.4.1, the incident field is represented by rays emanating radially from the source, with the strength of the field along an incident ray given by

$$\frac{i}{4} H_0^{(1)}(k|\rho - \rho'|) \sim C(k|\rho - \rho'|) = \frac{e^{i(k|\rho - \rho'| + \pi/4)}}{2\sqrt{2\pi k|\rho - \rho'|}}.$$

The incident rays exist everywhere in the illuminated region $|\phi - \phi'| < \pi$. Upon striking the wedge surface, an incident ray is completely absorbed, so no reflected rays exist. The ray striking the edge, however, is scattered in all directions and gives rise to the spectrum of diffracted rays. The field amplitude

along a diffracted ray excited by an incident ray (local plane wave) of unit amplitude is given by $-2A(\phi, \phi'; 0)C(k\rho)$ as noted from Eq. (6.3.28b). In the present case, the field along the incident ray striking the edge has an amplitude $C(k\rho')$ whence this factor appears in Eq. (6b). This simple ray-optical interpretation breaks down in the transition region $|\phi - \phi'| \approx \pi$, where the amplitude factor of the local plane wave varies rapidly, and the more complicated description involving \tilde{G}_∞^d must be employed [see Fig. 6.4.4 and Eq. (6.3.19) concerning the extent of the transition region].

Attention may again be called to the above-noted absence of a geometrically reflected wave contribution and also to the lack of dependence of \tilde{G}_∞ on the wedge angle $\phi = \varphi$ in Fig. 6.4.1. This is a direct consequence of the wedge boundary condition that all “angularly propagating waves” are completely absorbed. Because of this condition of angular matching, the location of the wedge faces is of no importance; the matched condition is disturbed only near the apex $\rho = 0$, whence diffraction phenomena arise from this region. While the physical realizability of this type of absorber is questionable, it provides a useful and simple mathematical model for the study of diffraction by absorbing structures and can give physical insight into diffraction effects encountered in physically more meaningful, but mathematically more complicated configurations.

Higher-order terms in the asymptotic expansion

The result given in Eq. (6b) represents to $O(1/\sqrt{k\rho})$, $O(1/\sqrt{k\rho'})$ the asymptotic solution for $\tilde{G}_\infty \sim \tilde{G}_\infty^d$ in the shadow region. To obtain higher-order terms in the asymptotic representation of the diffraction field, it is convenient to proceed directly from Eq. (5) and to substitute for the Hankel functions the complete expansions

$$H_\mu^{(1)}(k\rho) \sim \sqrt{\frac{2}{\pi k\rho}} e^{i\{k\rho - \mu\pi/2 - \pi/4\}} \sum_{m=0}^{\infty} \frac{(\mu, m)}{(-2ik\rho)^m}, \quad k\rho \gg |\mu|, \quad (8a)$$

$$(\mu, m) = \frac{(4\mu^2 - 1^2)(4\mu^2 - 3^2) \dots [4\mu^2 - (2m-1)^2]}{2^{2m} m!}, \quad (\mu, 0) \equiv 1, \quad (8b)$$

and similarly for $H_\mu^{(1)}(k\rho')$. Inversion of the orders of summation and integration yields the following asymptotic series for \tilde{G}_∞^d :

$$\tilde{G}_\infty^d(\rho, \rho') \sim C(k\rho)C(k\rho') \sum_{m=0}^{\infty} \sum_{n=0}^{\infty} \frac{I_{mn}(\phi, \phi')}{(-2ik\rho)^m (-2ik\rho')^n}, \quad (9)$$

where

$$I_{mn}(\phi, \phi') = -2i \int_0^\infty (e^{-i\mu n} - e^{i\mu n}) e^{i|\mu| |\phi - \phi'|} (\mu, m)(\mu, n) d\mu, \quad |\phi - \phi'| > \pi \quad (9a)$$

and $C(\alpha) = (8\pi\alpha)^{-1/2} \exp(i\alpha + i\pi/4)$. Use of the asymptotic approximation (8) for all values of μ in the integral of Eq. (5) involves an exponentially small error that can be neglected [see discussion preceding Eq. (6.3.22)], and termwise integration of the resulting asymptotic series is permitted.

Since

$$(\mu, m) = \frac{1}{m} [\mu^2 - \frac{1}{4} - m(m-1)](\mu, m-1), \quad (10)$$

and a multiplicative factor μ^2 in the integrand of Eq. (9a) can be replaced by the differentiation $-\partial^2/\partial\phi^2$ when $\phi \neq \phi'$, there exists among the diffraction coefficients I_{mn} the recursion relation

$$I_{mn} = L_m(\phi)I_{m-1,n}, \quad m = 1, 2, \dots, \quad (11a)$$

where

$$L_m(\phi) = -\frac{1}{m} \left[\frac{\partial^2}{\partial\phi^2} + m(m-1) + \frac{1}{4} \right]. \quad (11b)$$

Application of the operator $L_n(\phi)$ on I_{mn} increases by unity the index n . Thus, the higher-order diffraction coefficients can be derived from I_{00} by successive application of $L_m(\phi)$ and $L_n(\phi)$, and, by comparing Eqs. (2a) and (9a) with $m = n = 0$, one observes that

$$I_{00}(\phi, \phi') = -2A(\phi, \phi'; 0) = \frac{-2}{\pi - |\phi - \phi'|} - \frac{2}{\pi + |\phi - \phi'|}. \quad (12)$$

While the above derivation is subject to the restriction $|\phi - \phi'| > \pi$, it is noted from Eq. (6.3.8) that the diffraction integral exhibits the same functional dependence $A(\phi, \phi'; w)$ for all values of $|\phi - \phi'|$. Hence, the asymptotic expansion (9) for \hat{G}_∞^d is actually valid for all ϕ, ϕ' outside the transition region $|\phi - \phi'| \approx \pi$, provided that the I_{mn} are represented in closed form via Eqs. (11) and (12), and not in terms of the integral formula (9a), which converges only when $|\phi - \phi'| > \pi$. Evidently, the lowest-order result $C(k\rho)C(k\rho')I_{00}(\phi, \phi')$ agrees with the one in Eq. (6b) derived by an alternative method.

6.4b Impulsive Line-source Excitation

When the line source in Fig. 6.4.1 has an impulsive time behavior characterized by $\delta(t - t')$, the fields are derivable from the Green's function $\hat{G}_\infty(\rho, \rho'; t, t')$, which is defined by

$$\begin{aligned} & \left(\frac{1}{\rho} \frac{\partial}{\partial\rho} \rho \frac{\partial}{\partial\rho} + \frac{1}{\rho^2} \frac{\partial^2}{\partial\phi^2} - \frac{1}{\bar{c}^2} \frac{\partial^2}{\partial t'^2} \right) \hat{G}_\infty(\rho, \rho'; t, t') \\ &= -\frac{\delta(\rho - \rho')}{\rho'} \delta(\phi - \phi') \delta(t - t'), \end{aligned} \quad (13)$$

subject to boundedness at $\rho = 0$, and quiescence for $t < t'$. The solution is given in Eq. (6.3.41) upon substitution of $A(\phi, \phi'; i\beta)$ from Eq. (2b). For observation times $t \approx t' + (\rho + \rho')/\bar{c}$, the second term in Eq. (6.3.41), to be denoted by \hat{G}_∞^d , may be simplified as follows [see also remarks following Eq. (6.3.41)]:

$$\hat{G}_\infty^d \approx -\frac{A(\phi, \phi'; 0)\bar{c}}{4\pi\sqrt{\rho\rho'}} U\left(t - t' - \frac{\rho + \rho'}{\bar{c}}\right), \quad (14a)$$

and furnishes the behavior of the diffraction field in the vicinity of the diffracted wavefront. In contrast, near the incident wavefront where $t \approx t' + |\rho - \rho'|/\bar{c}$, the first term in Eq. (6.3.41) yields

$$\hat{G}_\infty^0 \approx \frac{\bar{c}}{2\pi\sqrt{2|\rho - \rho'|}} \frac{1}{\sqrt{\bar{c}(t - t') - |\rho - \rho'|}} \times U(\pi - |\phi - \phi'|)U\left(t - t' - \frac{|\rho - \rho'|}{\bar{c}}\right), \quad (14b)$$

whence it is observed that the field discontinuity across a wavefront is weakened by diffraction.

As noted already, the first term on the right-hand side of Eq. (6.3.41) represents the response in the absence of the wedge and exists only outside the shadow region of Fig. 6.4.1; it constitutes the geometric-optical contribution. The second term represents a cylindrically spreading diffracted pulse which exists in the entire region exterior to the wedge and reaches the observation point $P(\rho, \phi)$ at time $t - t' = (\rho + \rho')/\bar{c}$, i.e., after a time interval required to travel both the distance ρ' from the source point to the edge and the distance ρ from the edge to the observation point. In view of the "absorbing" wedge faces, there is no reflected-pulse contribution. The incident and diffracted wave fronts are sketched in Fig. 6.4.2. The normals to the wavefronts, the rays, are equivalent to those sketched in Fig. 6.4.1.

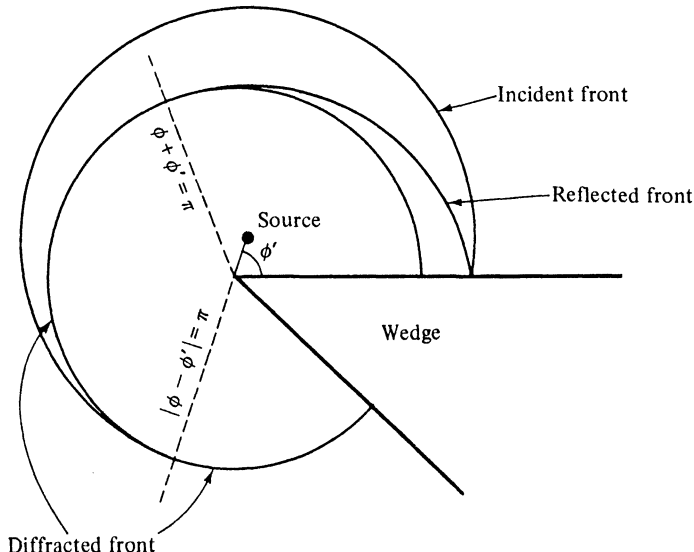


FIG. 6.4.2 Diffraction of cylindrical pulse by a wedge (omit reflected front for perfectly absorbing case). The incident front is centered at the source, the reflected front at the source image with respect to the horizontal wedge face, and the diffracted front is centered at the edge.

6.4c Time-harmonic Point-source Excitation

The electromagnetic fields radiated by a z -directed element of electric current

$$\hat{\mathbf{J}}(\mathbf{r}, t) = J^o \delta(\mathbf{r} - \mathbf{r}') e^{-i\omega t} \mathbf{z}_0 \quad (15a)$$

or magnetic current

$$\hat{\mathbf{M}}(\mathbf{r}, t) = M^o \delta(\mathbf{r} - \mathbf{r}') e^{-i\omega t} \mathbf{z}_0 \quad (15b)$$

in the presence of a perfectly absorbing wedge can be ascertained via the discussion in Sec. 6.2a from a scalar Green's function that satisfies the equation

$$\left(\frac{1}{\rho} \frac{\partial}{\partial \rho} \rho \frac{\partial}{\partial \rho} + \frac{1}{\rho^2} \frac{\partial^2}{\partial \phi^2} + \frac{\partial^2}{\partial z^2} + k^2 \right) G_\infty(\mathbf{r}, \mathbf{r}') = -\frac{\delta(\rho - \rho')}{\rho'} \delta(\phi - \phi') \delta(z - z') \quad (16)$$

in the domain $0 < (\rho, \rho') < \infty$, $-\infty < (\phi, \phi') < \infty$, $-\infty < (z, z') < \infty$, subject to the boundary conditions

$$G_\infty \text{ finite at } \rho = 0; \text{ radiation condition at } \rho \rightarrow \infty, \phi \rightarrow \pm\infty, z \rightarrow \pm\infty. \quad (16a)$$

From Eqs. (6.2.10), (6.3.1), and (6.4.1), the following representation applies in the geometric-optical shadow region $|\phi - \phi'| > \pi$ (see Fig. 6.3.1):

$$G_\infty(\mathbf{r}, \mathbf{r}') = \frac{1}{8\pi} \int_{-\infty}^{\infty} d\zeta \int_0^{i\infty} \mu (1 - e^{i2\mu\pi}) H_\mu^{(1)}(\sqrt{k^2 - \zeta^2}\rho) H_\mu^{(1)}(\sqrt{k^2 - \zeta^2}\rho') \times \frac{e^{i\mu|\phi - \phi'|}}{-2i\mu} e^{i\zeta(z - z')} d\mu, \quad (17)$$

whereas for *arbitrary* observation points, the alternative formulation in Eq. (6.3.26) is appropriate, with $A(\phi, \phi'; w)$ taken from Eq. (2b).

For large values of $k\rho$ and $k\rho'$ the asymptotic approximation for $G_\infty(\mathbf{r}, \mathbf{r}')$ is given in Eqs. (6.3.30), with $A(\phi, \phi'; 0)$ substituted from Eq. (2b). The three constituents in Eq. (6.3.30) have direct physical interpretations. G_∞^0 in Eq. (6.3.30a) represents the incident spherical wave in the illuminated region (i.e., the region wherein the source point \mathbf{r}' is visible from the observation point \mathbf{r}); since the perfectly absorbing wedge faces do not give rise to a reflected field, G_∞^0 furnishes the entire geometric-optical contribution. G_∞^d in Eq. (6.3.30b) provides the diffraction field exterior to the transition region $|\phi - \phi'| \approx \pi$ surrounding the light-shadow boundary. Viewed in terms of geometrical rays, an incident ray striking the edge gives rise to a cone of diffracted rays, with the cone angle α equal to the angle between the incident ray and the edge as shown in Fig. 6.4.3. The length parameter l appearing in the exponential $\exp(ikl)$ expresses precisely the phase increment for a local plane-wave field following the trajectory $(l_1 + l_2)$ between the source and observation points, in accord with the ray-optical interpretation. For observation points lying near the shadow boundary $|\phi - \phi'| = \pi$, the transition function G_∞^t in Eq. (6.3.30c) is effective and assures the continuity of the total field G_∞ .

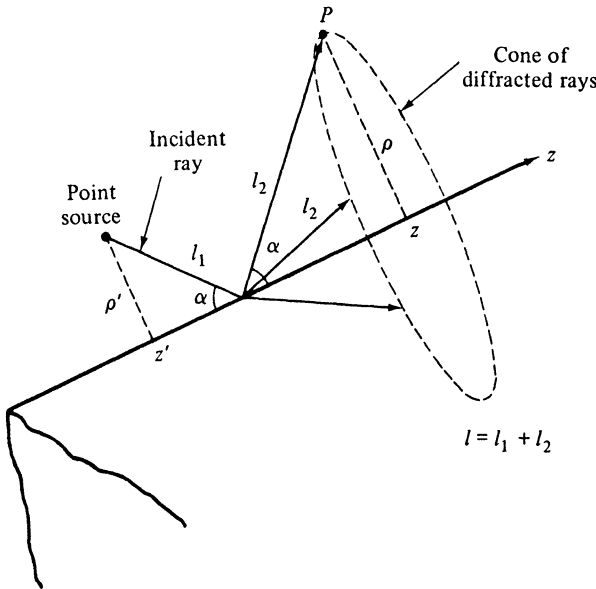


FIG. 6.4.3 Diffracted rays caused by an incident spherical wave.

6.4d Impulsive Point-Source Excitation

When the point source has the impulsive temporal behavior $\delta(t - t')$, the relevant scalar Green's function is defined by the equation

$$\begin{aligned} \left(\frac{1}{\rho} \frac{\partial}{\partial \rho} \rho \frac{\partial}{\partial \rho} + \frac{1}{\rho^2} \frac{\partial^2}{\partial \phi^2} + \frac{\partial^2}{\partial z^2} - \frac{1}{c^2} \frac{\partial^2}{\partial t^2} \right) \hat{G}_\infty(\mathbf{r}, \mathbf{r}'; t, t') \\ = -\frac{\delta(\rho - \rho')}{\rho'} \delta(\phi - \phi') \delta(z - z') \delta(t - t'), \end{aligned} \quad (18)$$

in the domain $0 < (\rho, \rho') < \infty$, $-\infty < (\phi, \phi') < \infty$, $-\infty < (z, z') < \infty$, $-\infty < (t, t') < \infty$, subject to finiteness at $\rho = 0$, and to quiescence when $t < t'$. In an angular transmission representation, the solution for \hat{G}_∞ in the shadow region $|\phi - \phi'| > \pi$ is given by $(2\pi)^{-1} \int_{-\infty}^{\infty} G_\infty(\mathbf{r}, \mathbf{r}') \exp[-i\omega(t - t')] d\omega$, with the time-harmonic Green's function G_∞ taken from Eq. (17) [see Eq. (6.2.14)]. Alternatively, and more directly, one has the closed form solution for arbitrary $\mathbf{r}, \mathbf{r}', t, t'$ in Eq. (6.3.33), the first term of which represents the incident spherical pulse in the illuminated region while the second term [with use of Eq. (2b)] represents the diffraction field \hat{G}_∞^d . In this instance, the diffracted wavefront reaches the observation point along a ray path l_1 that strikes the edge and is reflected therefrom along l_2 at the incidence angle. The diffracted rays, perpendicular to the wavefront, lie on a cone as shown in Fig. 6.4.3.

6.4e Time-harmonic Plane-wave Excitation

By moving the line source in Fig. 6.4.1 to infinity along the direction ϕ' , one may derive the result for plane-wave incidence, with the incident wave,

when properly normalized, given by $\exp[-ik\rho \cos(\phi - \phi') - i\omega t]$. The corresponding wave function $\bar{u}_\infty(\rho, \phi')$ for the perfectly absorbing wedge satisfies the homogeneous wave equation

$$\left(\frac{1}{\rho} \frac{\partial}{\partial \rho} \rho \frac{\partial}{\partial \rho} + \frac{1}{\rho^2} \frac{\partial^2}{\partial \phi'^2} + k^2 \right) \bar{u}_\infty(\rho, \phi') = 0 \quad (19)$$

in the domain $0 < \rho < \infty$, $-\infty < (\phi, \phi') < \infty$, subject to boundedness at $\rho = 0$, and a radiation condition on the scattered portion $\bar{u}_\infty^d(\rho, \phi')$ at $(\rho, |\phi|) \rightarrow \infty$. In the shadow region $|\phi - \phi'| > \pi$, the solution may be derived from Eq. (5) via the replacement of $H_\mu^{(1)}(k\rho')$ by the first term of its asymptotic expansion in Eq. (8a) and use of the normalization condition in Eq. (5.4.30b),

$$C(k\rho') = \frac{1}{2\sqrt{2\pi k\rho'}} e^{i(k\rho' + \pi/4)} \rightarrow 1, \quad (20)$$

to furnish an incident plane wave of unit amplitude. Thus,

$$\bar{u}_\infty(\rho, \phi') = \frac{i}{2} \int_0^{i\infty} (1 - e^{i2\mu\pi}) e^{i\mu[|\phi - \phi'| - \pi/2]} H_\mu^{(1)}(k\rho) d\mu, \quad |\phi - \phi'| > \pi. \quad (21)$$

Alternatively, the representation in Eq. (6.3.24) may be employed for arbitrary ρ, ϕ, ϕ' , with $A(\phi, \phi'; w)$ substituted from Eq. (2b).

For $k\rho \gg 1$, an asymptotic form of the solution, $\bar{u}_\infty \sim \bar{u}_\infty^0 + \bar{u}_\infty^d + \bar{u}_\infty^t$, is given in Eq. (6.3.28), with $A(\phi, \phi'; 0)$ taken from Eq. (2b). \bar{u}_∞^0 in Eq. (6.3.28a) represents the plane wave incident along the direction ϕ' ; because of the presence of the wedge (Fig. 6.4.4), its domain of existence is the region $|\phi - \phi'| < \pi$, the illuminated region deduced from simple geometric-optical considerations. \bar{u}_∞^d in Eq. (6.3.28b) can be interpreted as an outgoing cylindrical wave that appears to emanate from the edge $\rho = 0$; because of the cylindrical "spreading coefficient," the cylindrical wave is smaller than the incident-wave contribution by a factor $O(1/\sqrt{k\rho})$. The cylindrical wave contributes both in the illuminated and shadow regions and represents the diffraction effects almost everywhere; this simple description of the diffraction field fails in the vicinity of the shadow boundary $|\phi - \phi'| = \pi$, where the cylindrical-wave amplitude diverges like $1/(\pi - |\phi - \phi'|)$. In this geometric-optical transition region, whose width may be characterized as in Eq. (6.3.19), the transition function \bar{u}_∞^t in Eq. (6.3.28c) assumes importance. These considerations are schematized in Fig. 6.4.4.

Higher-order terms in the asymptotic expansion for the diffracted wave \bar{u}_∞^d may be derived as for the line-source problem. In fact, it is found that \bar{u}_∞^d is given by the right-hand side of Eq. (9) provided that $C(k\rho') = 1$ and only the terms I_{mo} , $m = 0, 1, 2, \dots$, are retained. Closed-form expressions for I_{mo} are derived via Eqs. (11) and (12), and the resulting form of \bar{u}_∞^d is valid for all $|\phi - \phi'| \neq \pi$.

Results for oblique incidence with respect to the z axis follow directly from Eq. (6.2.18).

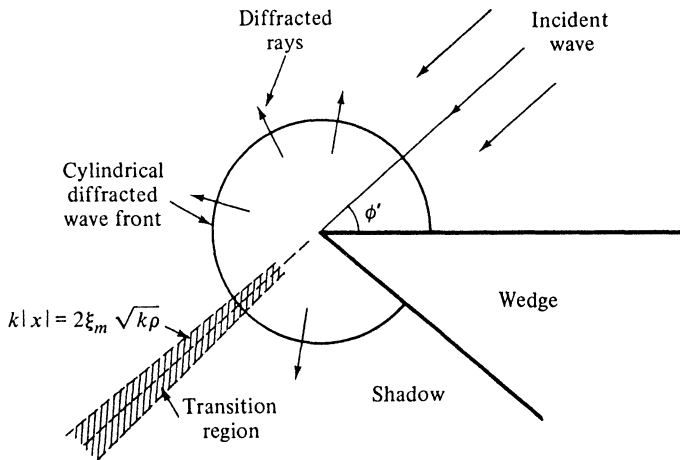


FIG. 6.4.4 Geometrical interpretation of asymptotic field solution for an incident plane wave.

6.4f Impulsive Plane-wave Excitation

When the incident field has the form of a plane-wave pulse $\delta[t - t' + (\rho/\bar{c}) \cos(\phi - \phi')]$, the wave function $\hat{u}_\infty(\rho, \phi'; t, t')$ for the perfectly absorbing wedge satisfies the time-dependent wave equation,

$$\left(\frac{1}{\rho} \frac{\partial}{\partial \rho} \rho \frac{\partial}{\partial \rho} + \frac{1}{\rho^2} \frac{\partial^2}{\partial \phi^2} - \frac{1}{\bar{c}^2} \frac{\partial^2}{\partial t'^2} \right) \hat{u}_\infty(\rho, \phi'; t, t') = 0, \quad (22)$$

in the domain $0 < \rho < \infty$, $-\infty < (\phi, \phi') < \infty$, $-\infty < (t, t') < \infty$, subject to boundedness at $\rho = 0$, and quiescence for $t < t'$. \bar{c} is the propagation speed in the medium.

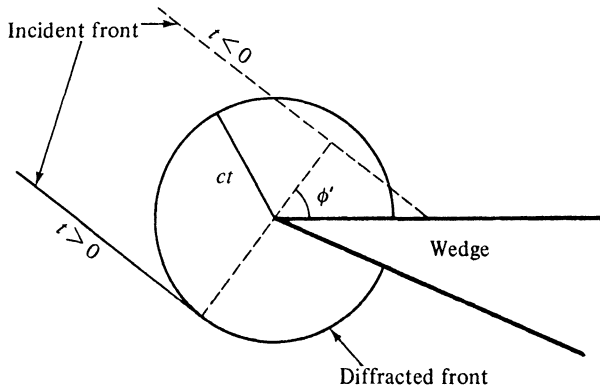


FIG. 6.4.5 Diffraction of plane-wave-pulse by a perfectly absorbing wedge.

The solution for arbitrary (ρ, t) is given in Eq. (6.3.32), with $A(\phi, \phi'; w)$ taken from Eq. (2b), and its physical interpretation for $t' = 0$ is seen from Fig. 6.4.5. Diffraction does not take place until observation times $t > 0$ since the incident pulse does not reach the edge until $t = 0$. Absence of a reflected pulse is attributed to the perfectly absorbing wedge faces.

6.5 PERFECTLY CONDUCTING WEDGE AND HALF-PLANE

6.5a Angular Transmission Representation

When the wedge faces at $\phi = 0, \varphi$ in Fig. 6.4.1 are perfectly conducting, it is necessary to distinguish between the boundary conditions satisfied by the E and H mode potential functions in Secs. 5.2 and 6.2 (see Reference 2 for a listing of various results and literature citations). For the E modes with respect to z (i.e., $H_z \equiv 0$), the potential functions vanish on the wedge faces, whereas for the H modes (with $E_z \equiv 0$), the normal derivatives vanish [see Eqs. (2.3.36a) and (2.3.37a)]. In terms of the one-dimensional angular Green's functions satisfying Eq. (6.2.7), these requirements imply that

$$g'(\phi, \phi'; \mu) = 0 \text{ at } \phi = 0, \varphi, \quad \text{for } E\text{-mode case,} \quad (1a)$$

$$\frac{d}{d\phi} g''(\phi, \phi'; \mu) = 0 \text{ at } \phi = 0, \varphi, \quad \text{for } H\text{-mode case,} \quad (1b)$$

where the ' and '' superscripts have been introduced to distinguish the two situations. In Eq. (6.2.7), p has been replaced by μ as in Sec. 6.3, and the subscript ϕ has been deleted. Solutions may be given in the closed forms of Eqs. (3.4.51),

$$g'(\phi, \phi'; \mu) = \frac{\sin \mu \phi_- \sin \mu(\varphi - \phi_+)}{\mu \sin \mu \varphi}, \quad (2a)$$

$$g''(\phi, \phi'; \mu) = \frac{\cos \mu \phi_- \cos \mu(\varphi - \phi_+)}{-\mu \sin \mu \varphi}, \quad (2b)$$

where ϕ_- and ϕ_+ denote the lesser and greater, respectively, of the angle coordinates ϕ and ϕ' . Alternatively, in terms of a series representation involving images in an infinitely extended ϕ space [Eq. (3.4.59)],

$$g'(\phi, \phi'; \mu) = \sum_{n=-\infty}^{\infty} g_{\infty}(\phi, 2n\varphi + \phi'; \mu) \mp \sum_{n=-\infty}^{\infty} g_{\infty}(\phi, 2n\varphi - \phi'; \mu) \quad (3)$$

where g_{∞} denotes the Green's function in Eq. (6.4.1). Substitution of these expressions into Eq. (6.3.3), or its counterparts derived from Eqs. (6.2.10), (6.2.12), and (6.2.14), provides the solution for the multidimensional scalar Green's functions in the geometrical-optical shadow region.

To obtain an angular transmission representation for the Green's functions valid everywhere, it is necessary to evaluate the function $A(\phi, \phi'; w)$ defined in Eq. (6.3.6). Substitution of Eq. (3) into Eq. (6.3.6), interchange of the order of summation and integration, and use of Eq. (6.4.2b) yields

$$A(\phi, \phi' ; w) = B(\phi, \phi' ; w) \mp B(\phi, -\phi' ; w), \quad \text{for } \begin{cases} E \text{ modes,} \\ H \text{ modes,} \end{cases} \quad (4)$$

where $B = B_1 + B_2$ with

$$B_{1,2}(\phi, \phi' ; w) = \sum_{n=-\infty}^{\infty} \frac{1}{\pi \mp [w - (\phi - \phi') + 2n\varphi]}, \quad \phi < \phi'. \quad (5)$$

This series can be summed into a closed form via the representation for the cotangent function,

$$\cot x = \frac{1}{x} + 2x \sum_{n=1}^{\infty} \frac{1}{x^2 - (n\pi)^2} = \sum_{n=-\infty}^{\infty} \frac{1}{x - n\pi}. \quad (6)$$

The last expression in Eq. (6) has the same form as the series in Eq. (5); while it diverges as written there, the series obtained by grouping together terms with $\pm n$, i.e., $[(x - n\pi)^{-1} + (x + n\pi)^{-1}]$, does converge and yields the first equality in Eq. (6). The series in Eq. (5) is to be understood in this sense, and it is assumed that the images have been grouped so as to yield a convergent result. Thus,

$$B_{1,2} = \frac{\pi}{2\varphi} \cot \left[\frac{\pi}{2\varphi} [\pi \mp w \pm (\phi - \phi')] \right], \quad (7)$$

and B can be expressed compactly by use of the formula

$$\cot(\alpha + \beta) + \cot(\alpha - \beta) = \frac{2 \sin 2\alpha}{\cos 2\beta - \cos 2\alpha}. \quad (8)$$

An analogous expression may be derived for $\phi > \phi'$.

When these results are substituted into Eqs. (6.3.8), (6.3.24), or (6.3.26), one obtains expressions for the various Green's functions at arbitrary observation points. In addition to the pole singularity of $A(\phi, \phi' ; w)$ at $\pi - |\phi - \phi'|$, which has been accounted for explicitly in Sec. 6.3, attention must be given to possible residue contributions from other poles, to be considered subsequently [see remarks following Eq. (6.3.8)]. Since the functions multiplying $A(\phi, \phi' ; w)$ in the diffraction integrals are even functions of w and the integration interval is symmetrical about $w = 0$, these integrals are affected only by the even part (in w) of A or B . The result is therefore unchanged if w in B_1 and (or) B_2 is replaced by $-w$, and one may construct a variety of functions $B(\phi, \phi' ; w)$, giving rise to the same diffraction integral (i.e., having the same even part).† Several representations derived in the literature by alternative methods of analysis are given below. From Eqs. (7) and (8), one obtains directly

$$B(\phi, \phi' ; w) = \frac{\pi}{\varphi} \sin \frac{\pi^2}{\varphi} \frac{1}{\cos [(\pi/\varphi)(w - \phi + \phi')] - \cos(\pi^2/\varphi)}, \quad (9a)$$

while replacement of w by $-w$ in B_2 yields¹

$$B(\phi, \phi' ; w) = \frac{\pi}{\varphi} \frac{\sin [(\pi/\varphi)(\pi - w)]}{\cos [(\pi/\varphi)(\phi - \phi')] - \cos [(\pi/\varphi)(\pi - w)]}. \quad (9b)$$

Or, upon writing $2B_1(w) = B_1(w) + B_1(-w)$,

† These remarks apply also to Sec. 6.4.

$$B_1 = \frac{\pi}{2\varphi} \frac{\sin [(\pi/\varphi)(\pi + \phi - \phi')]}{\cos(\pi w/\varphi) - \cos[(\pi/\varphi)(\pi + \phi - \phi')]} \quad (9c)$$

whence³

$$\begin{aligned} B(\phi, \phi' ; w) = & \frac{\pi}{2\varphi} \left[\frac{\sin [(\pi/\varphi)(\pi + \phi - \phi')]}{\cos(\pi w/\varphi) - \cos[(\pi/\varphi)(\pi + \phi - \phi')]} \right. \\ & \left. + \frac{\sin [(\pi/\varphi)(\pi - \phi + \phi')]}{\cos(\pi w/\varphi) - \cos[(\pi/\varphi)(\pi - \phi + \phi')]} \right]. \end{aligned} \quad (9d)$$

These representations for B are, of course, equal only in connection with the diffraction integrals. It is noted that the contributing part of B is an even function of $\phi - \phi'$, so this quantity can be replaced by $|\phi - \phi'|$.

The pole singularities of $A(\phi, \phi' ; w)$ in the complex w plane are made evident by the series representation in Eq. (5). When $|\phi - \phi'| > \pi$ and $0 \leq (\phi, \phi') \leq \varphi$, none of the poles crosses the integration path along the imaginary axis in the complex w plane, so no residue contributions appear; as in Eq. (6.3.5), this condition corresponds to observation points located in the geometrical shadow region of Fig. 6.4.1 and can be satisfied only for wedge angles $\varphi > \pi$. However, when the angular interval between the observation point coordinate ϕ and the coordinate ϕ' of the source point or $\phi'_n, \hat{\phi}'_n$ of an image point is less than $\pm\pi$, a relevant pole singularity traverses the integration path and gives rise to a residue term. Thus, the first term on the right-hand side of Eq. (6.3.8) is now replaced by the finite sums

$$\begin{aligned} \bar{G}^0(\rho, \rho') = & \sum_n \frac{i}{4} H_0^{(1)}[kR(\phi'_n)] U(\pi - |\phi - \phi'_n|) \\ & \mp \sum_n \frac{i}{4} H_0^{(1)}[kR(\hat{\phi}'_n)] U(\pi - |\phi - \hat{\phi}'_n|), \end{aligned} \quad (10)$$

where $n = 0, \pm 1, \dots, 0 \leq (\phi, \phi') \leq \varphi$. The upper and lower sign in Eq. (10) applies to the E modes and H modes, respectively, and

$$\phi'_n = 2n\varphi + \phi', \hat{\phi}'_n = 2n\varphi - \phi', R(\alpha) = \sqrt{\rho^2 + \rho'^2 - 2\rho\rho' \cos(\phi - \alpha)}. \quad (10a)$$

$R(\alpha)$ represents the distance from the observation point (ρ, ϕ) to a (real or image) source point at (ρ', α) . A similar modification occurs in Eqs. (6.3.24) and (6.3.26) pertaining to plane-wave and point-source excitation, respectively. The term corresponding to $\phi'_0 = \phi'$ in Eq. (10) represents the incident wave in the illuminated region, whereas the other terms represent exactly the singly and multiply reflected waves predicted on the basis of geometrical optics. It is evident that many reflections are possible for small wedge angles φ , whereas, when $\varphi > \pi$, a maximum of three terms remains in the series: $\phi'_0, \hat{\phi}'_0, \phi'_1$. These conclusions are schematized in Fig. 6.5.1, from which it is observed that an observation point P in a trough region $\varphi < \pi$ may be reached by the direct ray a , two singly reflected rays $b_{1,2}$, doubly reflected rays c , etc., each of which is represented by a term in Eq. (10), with the \mp signs accounting for the reflec-

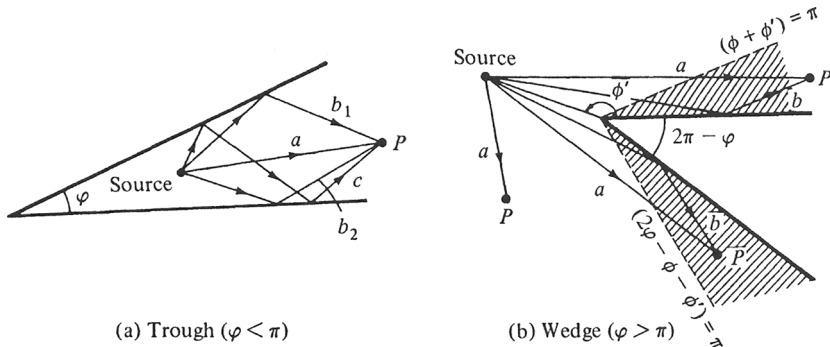


FIG. 6.5.1 Geometric-optical contributions.

tion coefficients -1 and $+1$ for E modes and H modes, respectively, at a perfect conductor. In the wedge-shaped region $\varphi > \pi$, on the other hand, there is at most one singly reflected ray that contributes only when the observation point lies in the shaded region, whereas no reflected contribution arises for other observation-point locations. The Heaviside unit functions in Eq. (10) provide for these limited domains of existence of a particular geometric-optical ray species.

One observes from Eq. (9a) that $B \equiv 0$ when $\varphi = \pi/n$, where n is any positive integer. Hence, the diffraction integrals vanish identically, and the line-source excited field is representable *exactly* in closed form by its image contributions in Eq. (10), with analogous conclusions applicable to plane-wave or point-source excitation.

6.5b Radial Transmission Representation

While the angular transmission representation discussed in Sec. 6.5a is useful for the calculation of the quasi-optic field in the range of large $k\rho$ and $k\rho'$, it is inappropriate when either the source point or the observation point lies near the edge ($k\rho'$ or $k\rho$ small). In this parameter range, it is useful to employ a radial transmission formulation, which involves a one-dimensional Green's function $g_\rho(\rho, \rho'; \mu)$ in the radial domain, and eigenfunctions $\Phi_\mu(\phi)$ in the angular domain. The two-dimensional Green's function $\bar{G}(\rho, \rho')$ corresponding to excitation by a time-harmonic line source is now represented by (see Sec. 3.3c)

$$\bar{G}(\rho, \rho') = \sum_{\mu} \Phi_{\mu}(\phi) \Phi_{\mu}(\phi') g_{\rho}(\rho, \rho'; \mu), \quad (11)$$

which formulation is alternative to the one given in Eq. (6.2.8), and may be derived therefrom by passing to the complex μ plane and deforming contours as in Sec. 3.3c. The orthonormal angular eigenfunctions are listed in Eqs. (3.2.47) and (3.2.48), and the radial Green's function g_{ρ} is given in Eq. (3.4.93). Thus,¹

$$\bar{G}'(\rho, \rho') = \frac{\pi i}{\varphi} \sum_{m=1}^{\infty} J_m(k\rho_{<}) H_m^{(1)}(k\rho_{>}) \sin \mu\phi \sin \mu\phi', \quad \mu = \frac{m\pi}{\varphi}, \quad (12)$$

and

$$\bar{G}''(\rho, \rho') = \frac{\pi i}{2\varphi} J_0(k\rho_{<}) H_0^{(1)}(k\rho_{>}) + \frac{\pi i}{\varphi} \sum_{m=1}^{\infty} J_m(k\rho_{<}) H_m^{(1)}(k\rho_{>}) \cos \mu\phi \cos \mu\phi'. \quad (13)$$

Since $J_\mu(k\rho_{<}) \sim (k\rho_{<}/\mu)^\mu$, $\mu \gg k\rho_{<}$, the series converges rapidly and can be used for numerical evaluation when either the source point or the observation point is located near the edge. In particular, the behavior of \bar{G}' and \bar{G}'' near the edge is given by

$$\bar{G}' \propto (k\rho)^{\pi/\alpha}, \quad \bar{G}'' \propto \text{constant} + O[(k\rho)^{\pi/\alpha}], \quad \text{as } \rho \rightarrow 0. \quad (14)$$

One may verify that the electromagnetic fields derived from Eqs. (12) and (13) satisfy the edge conditions in Eq. (1.5.37).

In view of the remarks made in connection with Eq. (6.2.5), one may derive the corresponding representations for the three-dimensional Green's functions $G'(\mathbf{r}, \mathbf{r}')$ and $G''(\mathbf{r}, \mathbf{r}')$ from Eqs. (12) and (13) upon

$$\text{replacing } k \text{ by } \sqrt{k^2 - \zeta^2} \text{ and performing the operation } (1/2\pi) \int_{-\infty}^{\infty} d\zeta e^{i\zeta(z-z')}, \quad (15)$$

with $\text{Im } \sqrt{k^2 - \zeta^2} \geq 0$.

By letting $\rho' \rightarrow \infty$, one may derive from Eqs. (12) and (13) the result for excitation by an incident plane wave $\exp[-ik\rho \cos(\phi - \phi')]$. Since $J_\mu(k\rho_{<})$ decays when $\mu > k\rho_{<}$, the contributing range of the series is bounded in μ , and negligible error is introduced through use of the asymptotic approximation in Eq. (6.3.12) for all relevant μ as $k\rho_{>} \rightarrow \infty$. Imposition of the normalization condition Eq. (5.4.30b) yields the following expressions for the wavefunctions:

$$\bar{u}'(\rho, \phi') = \frac{4\pi}{\varphi} \sum_{m=1}^{\infty} J_m(k\rho) \sin \mu\phi \sin \mu\phi' e^{-i\mu\pi/2}, \quad \mu = \frac{m\pi}{\varphi}, \quad (16a)$$

$$\bar{u}''(\rho, \phi') = \frac{2\pi}{\varphi} \left\{ J_0(k\rho) + 2 \sum_{m=1}^{\infty} J_m(k\rho) \cos \mu\phi \cos \mu\phi' e^{-i\mu\pi/2} \right\}. \quad (16b)$$

Results for oblique incidence are obtained at once via Eq. (6.2.18).

6.5c Time-harmonic Line-source Excitation

The electromagnetic fields excited by a line source of electric or magnetic currents may be inferred from the scalar E -and H -mode Green's functions $\bar{G}'(\rho, \rho')$ and $\bar{G}''(\rho, \rho')$, respectively, as in Eqs (6.2.1b) and (6.2.2b).² These Green's functions satisfy in the domain $0 < (\rho, \rho') < \infty$, $0 \leq (\phi, \phi') \leq \varphi$ the wave equation (6.2.3), subject to the boundary conditions

$$\bar{G}' = 0, \quad \frac{\partial \bar{G}''}{\partial \phi} = 0 \quad \text{at } \phi = 0, \varphi, \quad (17)$$

boundedness at $\rho = 0$, and a radiation condition at $\rho \rightarrow \infty$. For arbitrary values of (ρ, ρ') , the solution is given in a radial transmission representation by Eqs. (12) and (13), and in an angular transmission representation by Eq. (6.3.8),

subject to the modifications in Eqs. (4) and (10). When the wedge angle $\phi > \pi$, only three terms contribute to the geometric-optical series in Eq. (10), and one obtains the result

$$\bar{G}(\rho, \rho') = \bar{G}^0(\rho, \rho') + \bar{G}_1(\rho, \rho'), \quad (18)$$

where

$$\begin{aligned} \bar{G}^0(\rho, \rho') = & \frac{i}{4} H_0^{(1)}[kR(\phi')](U(\pi - |\phi - \phi'|)) \\ & \mp \frac{i}{4} H_0^{(1)}[kR(-\phi')]U(\pi - \phi - \phi') \\ & \mp \frac{i}{4} H_0^{(1)}[kR(2\phi - \phi')]U[\pi - (2\phi - \phi - \phi')]. \end{aligned} \quad (18a)$$

$U(x)$ is the Heaviside unit function defined in Eq. (6.3.8) and \bar{G}_1 is the diffraction integral

$$\bar{G}_1(\rho, \rho') = \frac{1}{8\pi} \int_{i\infty}^{-i\infty} H_0^{(1)}(k\chi)[B(\phi, \phi'; w) \mp B(\phi, -\phi'; w)]dw. \quad (18b)$$

The upper sign is appropriate to the E -mode Green's function \bar{G}' , while the lower sign yields the H -mode Green's function \bar{G}'' . R is defined in Eq. (10a), various forms for B are given in Eqs. (9), and

$$\chi = (\rho^2 + \rho'^2 + 2\rho\rho' \cos w)^{1/2}.$$

When $k\rho \gg 1$, $k\rho' \gg 1$, but with $|\phi - \phi'|, (\phi + \phi'), (2\phi - \phi - \phi') \approx \pi$, one has the asymptotic approximation

$$\bar{G} \sim \bar{G}^0 + \bar{G}^d, \quad (19)$$

with \bar{G}^0 taken from Eq. (18a) [which may be simplified for large arguments by use of Eq. (6.3.12)], and \bar{G}^d obtained as in Eq. (6.3.15):

$$\begin{aligned} \bar{G}^d = & -2C(k\rho)C(k\rho')[B(\phi, \phi'; 0) \pm B(\phi, -\phi'; 0)] \\ = & \frac{-ie^{ik(\rho+\rho')}}{4k\sqrt{\rho\rho'\varphi}} \left(\sin \frac{\pi^2}{\varphi} \right) \left[\frac{1}{\cos[(\pi/\varphi)(\phi - \phi')] - \cos(\pi^2/\varphi)} \right. \\ & \left. \mp \frac{1}{\cos[(\pi/\varphi)(\phi + \phi')] - \cos(\pi^2/\varphi)} \right], \quad \text{for } \begin{array}{l} E \text{ modes,} \\ H \text{ modes.} \end{array} \end{aligned} \quad (19a)$$

For arbitrary ϕ and ϕ' , the following transition functions must be added to Eq. (19):

$$\begin{aligned} \bar{G}'(\rho, \rho') = & \bar{G}'_\infty(\rho; \rho', \phi') \mp \bar{G}'_\infty(\rho; \rho', -\phi') \mp \bar{G}'_\infty(\rho; \rho', 2\phi - \phi'), \\ & \text{for } \begin{array}{l} E \text{ modes,} \\ H \text{ modes,} \end{array} \end{aligned} \quad (20)$$

where $\bar{G}'_\infty(\rho; \rho', \phi')$ is given in Eq. (6.4.7), it being recalled that $\bar{G}'_\infty(\rho; \rho', \phi')$ is to be so used that $\xi \rightarrow 0$ implies that $\pi - |\phi - \phi'| \rightarrow 0$.

Discussion

The physical interpretation of the result in Eq. (19) in terms of geometric-optical and diffraction effects proceeds as for the perfectly absorbing wedge in

Sec. 6.4a. As in Fig. 6.4.1, the diffracted contribution \bar{G}^d is in the form of a cylindrical wave emanating from the edge and penetrating all the various geometric-optical domains. Owing to the perfect reflectivity of the wedge faces in the present case, the geometric-optical field \bar{G}^0 includes not only the incident field in the illuminated region but also the fields reflected from the sides of the wedge, which latter contributions have already been analyzed in connection with Fig. 6.5.1. The diffracted field amplitude in Eq. (19a) diverges on the shadow boundary $|\phi - \phi'| = \pi$ and also on the lines $\phi = \pi - \phi'$, $\phi = (2\phi - \phi' - \pi)$ which bound the domain of existence of the waves reflected according to geometrical optics from the wedge faces at $\phi = 0$ and $\phi = \varphi$, respectively [see Fig. 7.4.5(a) for a plot of the diffracted field variation]. Continuity of \bar{G} through these transition regions is assured by use of the transition functions in Eq. (20), only one of which is relevant at a time since these functions are negligibly small outside their particular transition domain. As noted from Eq. (5), the behavior of $B(\phi, \phi'; w)$ near $w_p = \pi - |\phi - \phi'|$ or $w_{\hat{p}} = \pi - |\phi - \hat{\phi}'_n|$, where ϕ'_n and $\hat{\phi}'_n$ are the image locations in Eq. (10a), is of the same form as for the previously investigated case $w_p = \pi - |\phi - \phi'|$. The relevant transition functions may therefore be inferred directly from the infinite angular space problem in Sec. 6.4, with one transition function corresponding to each image solution. For a restricted range of observation angles $0 \leq \phi \leq \varphi$, only a limited number of these may become contributory [see Eq. (10)]. In connection with the field values *on* the boundaries of the various geometric-optical domains, see Eq. (6.3.21) and its analogue for the reflected waves.

Higher-order terms in the asymptotic expansion for \bar{G}^d may be derived by considerations analogous to those in Eqs. (6.4.9) et seq., starting from Eqs. (2) and (6.3.3).

6.5d Impulsive Line-source Excitation

When the line source has the impulsive time dependence $\delta(t - t')$, the fields are derivable from the Green's function $\hat{G}(\rho, \rho'; t, t')$, which satisfies the differential equation (6.4.13), subject to the stated boundary conditions, with the modification for the ϕ domain given Eq. (17).³ The result for arbitrary ρ, ρ', t, t' , may be taken directly from Eq. (6.3.41), with $A(\phi, \phi'; i\beta)$ inserted from Eqs. (4) and (9b), and additional terms included to account for the reflected fields corresponding to Eq. (10):

$$\begin{aligned} \hat{G}(\rho, \rho'; t, t') = & \sum_n \left\{ \frac{U(\pi - |\phi - \phi'_n|)U(t - t' - [R(\phi'_n)/\bar{c}])}{2\pi\sqrt{(t - t')^2 - [R^2(\phi'_n)/\bar{c}^2]}} \right. \\ & \mp \left. \frac{U(\pi - |\phi - \hat{\phi}'_n|)U(t - t' - [R(\hat{\phi}'_n)/\bar{c}])}{2\pi\sqrt{(t - t')^2 - [R^2(\hat{\phi}'_n)/\bar{c}^2]}} \right\} \\ & - \left\{ \frac{1}{4\pi^2} \int_{-\cosh^{-1}M}^{\cosh^{-1}M} \frac{d\beta}{\sqrt{(t - t')^2 - [f^2(\beta)/\bar{c}^2]}} \right. \\ & \times \left. [\operatorname{Re} B(\phi, \phi'; i\beta) \mp \operatorname{Re} B(\phi, -\phi'; i\beta)] \right\} U\left(t - t' - \frac{\rho + \rho'}{\bar{c}}\right), \quad (21) \end{aligned}$$

where the upper and lower signs refer to the *E*- and *H*-mode cases, respectively;

the various definitions in Eq. (10a) apply, $f(\beta) = (\rho^2 + \rho'^2 + 2\rho\rho' \cosh \beta)^{1/2}$, $M = [\bar{c}^2(t - t')^2 - \rho^2 - \rho'^2]/2\rho\rho'$, and, from Eqs. (9), with $\psi = (\phi - \phi')$,

$$\operatorname{Re} B(\phi, \phi'; i\beta) =$$

$$\frac{(\pi/\varphi) [\cos(\pi\psi/\varphi) \cosh(\pi\beta/\varphi) - \cos(\pi^2/\varphi)] \sin(\pi^2/\varphi)}{\cosh^2(\pi\beta/\varphi) + \cos^2(\pi\psi/\varphi) - \sin^2(\pi^2/\varphi) - 2\cos^2(\pi^2/\varphi) \cos(\pi\psi/\varphi) \cosh(\pi\beta/\varphi)} \quad (21a)$$

When the wedge angle $\varphi > \pi$, only the terms with $\phi'_0, \hat{\phi}'_0, \hat{\phi}'_1$ contribute. The physical interpretation of this result is discussed in connection with Fig. 6.4.2. For angles $\varphi = (\pi/n)$, $n = 1, 2, \dots$, one has $B \equiv 0$, and the geometrical optics portion of the solution is exact.

6.5e Time-harmonic Point-source Excitation

The fields excited by a longitudinal electric or magnetic dipole as in Eqs. (6.4.15) may be inferred from the scalar E -mode Green's function $G'(\mathbf{r}, \mathbf{r}')$ and the scalar H -mode Green's function $G''(\mathbf{r}, \mathbf{r}')$, respectively, which satisfy Eq. (6.4.16) in the domain $0 < (\rho, \rho') < \infty$, $0 \leq (\phi, \phi') \leq \varphi$, $-\infty < (z, z') < \infty$, subject to the boundary conditions

$$G' = 0, \quad \frac{\partial G''}{\partial \phi} = 0 \quad \text{at } \phi = 0, \varphi, \quad (22)$$

boundedness at $\rho = 0$, and a radiation condition at $r \rightarrow \infty$.^{2,3}

For arbitrary values of \mathbf{r} and \mathbf{r}' , solutions are given in a radial transmission representation by [see Eqs (12), (13), and (15)]

$$G(\mathbf{r}, \mathbf{r}') = \frac{i}{4\varphi} \int_{-\infty}^{\infty} d\zeta \sum_{m=0}^{\infty} \epsilon_m J_m(\sqrt{k^2 - \zeta^2} \rho_{<}) \times H_{\mu}^{(1)}(\sqrt{k^2 - \zeta^2} \rho_{>}) e^{i\zeta(z-z')} \begin{cases} \sin \mu\phi \sin \mu\phi' \\ \cos \mu\phi \cos \mu\phi' \end{cases}, \quad \begin{array}{ll} \text{for } E \text{ modes,} \\ \text{for } H \text{ modes,} \end{array} \quad (23)$$

where $\epsilon_m = 1$, $m = 0$, while $\epsilon_m = 2$, $m \geq 1$, and $\mu = m\pi/\varphi$. The integration path proceeds as in Fig. 5.3.6a, with $\operatorname{Im} \sqrt{k^2 - \zeta^2} \geq 0$. In an angular transmission representation, the solution for arbitrary \mathbf{r} and \mathbf{r}' is given by Eq. (6.3.26), provided that $A(\phi, \phi'; w)$ is taken from Eqs. (4) and (9), and that additional geometric-optical constituents analogous to those in Eq. (10) are included. Thus,

$$G(\mathbf{r}, \mathbf{r}') = G^0(\mathbf{r}, \mathbf{r}') + G_1(\mathbf{r}, \mathbf{r}'), \quad (24)$$

where G^0 is the geometric-optical contribution,

$$G^0(\mathbf{r}, \mathbf{r}') = \sum_n \left\{ \frac{e^{ik|\mathbf{r}-\mathbf{r}'_n|}}{4\pi|\mathbf{r}-\mathbf{r}'_n|} U(\pi - |\phi - \phi'_n|) \mp \frac{e^{ik|\mathbf{r}-\hat{\mathbf{r}}'_n|}}{4\pi|\mathbf{r}-\hat{\mathbf{r}}'_n|} U(\pi - |\phi - \hat{\phi}'_n|) \right\}, \quad \begin{array}{ll} \text{for } E \text{ modes,} \\ \text{for } H \text{ modes,} \end{array} \quad (24a)$$

and $|\mathbf{r} - \mathbf{r}'_n| = \sqrt{R^2(\phi'_n) + (z - z')^2}$, $|\mathbf{r} - \hat{\mathbf{r}}'_n| = \sqrt{R^2(\hat{\phi}'_n) + (z - z')^2}$, with R defined in Eq. (10a). The function G_1 is given in the integral form

$$G_1(\mathbf{r}, \mathbf{r}') = -\frac{i}{8\pi^2} \int_{i\infty}^{-i\infty} \frac{e^{iky}}{\gamma} [B(\phi, \phi'; w) \mp B(\phi, -\phi'; w)] dw, \quad \begin{array}{l} \text{for } E \text{ modes,} \\ \text{for } H \text{ modes,} \end{array} \quad (24b)$$

where $\gamma = [\rho^2 + \rho'^2 + (z - z')^2 + 2\rho\rho' \cos w]^{1/2}$.

When $k\rho$ and $k\rho'$ are large, $G(\mathbf{r}, \mathbf{r}')$ has the asymptotic approximation

$$G(\mathbf{r}, \mathbf{r}') \sim G^o(\mathbf{r}, \mathbf{r}') + G^d(\mathbf{r}, \mathbf{r}') + G'(r, r'), \quad (25)$$

where G^o is given in Eq. (24a), G^d is the diffracted contribution in Eq. (6.3.30b),

$$\begin{aligned} G^d = & -\frac{e^{i(kl+\pi/4)}}{4\rho\sqrt{2\pi k\rho\rho'l}} \sin \frac{\pi^2}{\varphi} \\ & \times \left[\frac{1}{\cos[(\pi/\varphi)(\phi - \phi')] - \cos(\pi^2/\varphi)} \mp \frac{1}{\cos[(\pi/\varphi)(\phi + \phi')] - \cos(\pi^2/\varphi)} \right], \\ & \begin{array}{l} \text{for } E \text{ modes,} \\ \text{for } H \text{ modes,} \end{array} \end{aligned} \quad (25a)$$

and G' is the transition function,

$$G'(\mathbf{r}; \rho', \phi', z') = \sum_n [G'_n(\mathbf{r}; \rho', \phi'_n, z') \mp G'_\infty(\mathbf{r}; \rho', \hat{\phi}'_n, z')], \quad \begin{array}{l} \text{for } E \text{ modes,} \\ \text{for } H \text{ modes.} \end{array} \quad (25b)$$

$G'_\infty(\mathbf{r}; \rho', \phi', z')$ is given in Eq. (6.3.30c), and l is defined in Eq. (6.3.30b) (see also Fig. 6.4.3 for a physical interpretation). For wedge angles $\varphi > \pi$, only the contributions from $\phi'_0 = \phi'$, $\hat{\phi}'_0 = -\phi'$ and $\hat{\phi}'_1 = 2\varphi - \phi'$ are relevant in Eqs. (24a) and (25b). G' is negligible except for observation points in transition regions defined by $|\phi - \phi'_n| \approx \pi$ or $|\phi - \hat{\phi}'_n| \approx \pi$.

6.5f Impulsive Point-source Excitation

When the point source has the temporal behavior $\delta(t - t')$, the fields can be derived from the scalar Green's functions $\hat{G}'(\mathbf{r}, \mathbf{r}'; t, t')$ and $\hat{G}''(\mathbf{r}, \mathbf{r}'; t, t')$ corresponding to the E and H -mode cases, respectively. They satisfy Eq. (6.4.18) in the domain $0 < (\rho, \rho') < \infty$, $0 \leq (\phi, \phi') \leq \varphi$, $-\infty < (z, z') < \infty$, $-\infty < (t, t') < \infty$, subject to the stated boundary conditions, with the modification for the ϕ domain as in Eq. (22). The solution for arbitrary $\mathbf{r}, \mathbf{r}', t, t'$ is taken from Eq. (6.3.33), with the inclusion of reflected geometric-optical contributions:

$$\begin{aligned} \hat{G}(\mathbf{r}, \mathbf{r}'; t, t') = & \sum_n \left\{ \frac{\delta(t - t' - |\mathbf{r} - \mathbf{r}'_n|/\bar{c})}{4\pi|\mathbf{r} - \mathbf{r}'_n|} U(\pi - |\phi - \phi'_n|) \right. \\ & \mp \left. \frac{\delta(t - t' - |\mathbf{r} - \hat{\mathbf{r}}'_n|/\bar{c})}{4\pi|\mathbf{r} - \hat{\mathbf{r}}'_n|} U(\pi - |\phi - \hat{\phi}'_n|) \right\} \\ & + \frac{\bar{c}}{4\pi} \frac{[\operatorname{Re} B(\phi, \phi'; i\beta) \mp \operatorname{Re} B(\phi, -\phi'; i\beta)]}{\rho\rho' \sinh \beta} U\left(t - t' - \frac{l}{\bar{c}}\right), \\ & \begin{array}{l} \text{for } E \text{ modes,} \\ \text{for } H \text{ modes,} \end{array} \end{aligned} \quad (26)$$

where \mathbf{r}'_n , $\hat{\mathbf{r}}'_n$, l , β are defined in Eqs. (24a), (6.3.30b), and (6.3.33), respectively, and $\operatorname{Re} \mathbf{B}$ is taken from Eq. (21a).

6.5g Time-harmonic Plane-wave Excitation

When a plane wave $\exp[-ik\rho \cos(\phi - \phi') - i\omega t]$ is incident on the perfectly conducting wedge from the direction ϕ' , the corresponding wave function $\bar{u}(\rho, \phi')$ satisfies Eq. (6.4.19) in the domain $0 < \rho < \infty$, $0 \leq (\phi, \phi') \leq \varphi$, subject to boundedness at $\rho = 0$, a radiation condition on the scattered portion at $\rho \rightarrow \infty$, and to

$$\bar{u}'(\rho, \phi') = 0, \quad \frac{\partial \bar{u}''(\rho, \phi')}{\partial \phi} = 0 \quad \text{at } \phi = 0, \varphi. \quad (27)$$

The *E*-mode function \bar{u}' is relevant when the electric vector in the incident field is parallel to the z axis, whereas the *H*-mode function \bar{u}'' applies to magnetic-field polarization parallel to z .^{2,3}

In a radial transmission representation, the solution is given by Eqs. (16), whereas in an angular transmission representation, the solution follows from Eq. (6.3.24) provided that one includes geometric-optical reflected contributions as in Eq. (10) and inserts $A(\phi, \phi'; w)$ from Eqs. (4) and (9):

$$\bar{u}(\rho, \phi') = \bar{u}^o(\rho, \phi') + \bar{u}_1(\rho, \phi'), \quad (28)$$

where \bar{u}^o is the geometric-optical field

$$\begin{aligned} \bar{u}^o(\rho, \phi') = & e^{-ik\rho \cos(\phi - \phi')} U(\pi - |\phi - \phi'|) \mp e^{-ik\rho \cos(\phi + \phi')} U(\pi - \phi - \phi') \\ & \mp e^{-ik\rho \cos(2\varphi - \phi - \phi')} U[\pi - (2\varphi - \phi - \phi')], \end{aligned} \quad (28a)$$

while \bar{u}_1 is the diffraction integral

$$\bar{u}_1(\rho, \phi') = \frac{-i}{2\pi} \int_{i\infty}^{-i\infty} e^{ik\rho \cos w} [B(\phi, \phi'; w) \mp B(\phi, -\phi'; w)] dw. \quad (28b)$$

The upper and lower signs correspond to the *E*- and *H*-mode wavefunctions, respectively, and the formula in Eq. (28a) is valid when $\varphi > \pi$; for arbitrary values of φ , additional terms as in Eq. (10) are required.

For large values of $k\rho$, the following asymptotic approximation applies:

$$\bar{u}(\rho, \phi') \sim \bar{u}^o(\rho, \phi') + \bar{u}^d(\rho, \phi') + \bar{u}'(\rho, \phi'), \quad (29)$$

where, for $\varphi > \pi$, \bar{u}^o is given in Eq. (28a), while the diffracted field \bar{u}^d is obtained directly from Eq. (19a) subject to the normalization in Eq. (6.4.20) [see also Eqs. (6.3.28)]:

$$\begin{aligned} \bar{u}^d(\rho, \phi') = & -\frac{e^{i(k\rho + \pi/4)} \sqrt{\pi}}{\varphi \sqrt{2k\rho}} \sin \frac{\pi^2}{\varphi} \\ & \times \left[\frac{1}{\cos[(\pi/\varphi)(\phi - \phi')] - \cos(\pi^2/\varphi)} \mp \frac{1}{\cos[(\pi/\varphi)(\phi + \phi')] - \cos(\pi^2/\varphi)} \right]. \end{aligned} \quad (29a)$$

In the transition regions surrounding the shadow boundary $|\phi - \phi'| = \pi$ or the reflected wave boundaries $\phi = \pi - \phi'$, $\phi = 2\varphi - \phi' - \pi$, one must employ the appropriate transition function contained in

$$\bar{u}'(\rho, \phi') = \bar{u}_\infty(\rho, \phi') \mp \bar{u}_\infty(\rho, -\phi') \mp \bar{u}_\infty(\rho, 2\varphi - \phi'), \quad \begin{array}{l} E \text{ modes,} \\ H \text{ modes,} \end{array} \quad (29b)$$

with $\bar{u}_\infty(\rho, \phi')$ given in Eq. (6.3.28c).

The physical interpretation of the asymptotic result is analogous to that in Fig. 6.4.4, provided that the reflected-wave contribution in \bar{u}^o is included.

For oblique incidence, the solution follows from an application of Eq. (6.2.18).

6.5h Impulsive Plane-wave Excitation

When the incident field is in the form of the plane-wave pulse $\delta[t - t' + (\rho/\tilde{c}) \cos(\phi - \phi')]$, the wavefunctions $\hat{u}'(\rho, \phi'; t, t')$ and $\hat{u}''(\rho, \phi'; t, t')$ corresponding to the E - and H -mode cases, respectively, satisfy the wave equation (6.4.22) in the domain $0 < \rho < \infty$, $0 \leq (\phi, \phi') \leq \varphi$, $-\infty < (t, t') < \infty$, subject to the stated boundary conditions, with modifications for the ϕ domain as in Eq. (27). The solution for arbitrary ρ, ϕ', t, t' is given by Eqs. (6.3.32) and (4), provided that geometric-optical reflected wave contributions are included:

$$\begin{aligned} \hat{u}'(\rho, \phi'; t, t') = & \delta\left[t - t' + \frac{\rho}{\tilde{c}} \cos(\phi - \phi')\right] U(\pi - |\phi - \phi'|) \\ & \mp \delta\left[t - t' + \frac{\rho}{\tilde{c}} \cos(\phi + \phi')\right] U(\pi - \phi - \phi') \\ & \mp \delta\left[t - t' + \frac{\rho}{\tilde{c}} \cos(2\varphi - \phi - \phi')\right] U[\pi - (2\varphi - \phi - \phi')] \\ & - \frac{1}{\pi} \frac{U(t - t' - \rho/\tilde{c})}{\sqrt{(t - t')^2 - (\rho/\tilde{c})^2}} [\operatorname{Re} B(\phi, \phi'; i\beta) \mp \operatorname{Re} B(\phi, -\phi'; i\beta)], \\ & \quad \begin{array}{l} E \text{ modes,} \\ H \text{ modes,} \end{array} \quad (30) \end{aligned}$$

where $\beta = \cosh^{-1}[\tilde{c}(t - t')/\rho]$, $\operatorname{Re} B$ is given in Eq. (21a), and it has been assumed that $\varphi > \pi$. The physical interpretation of this result is the same as in Fig. 6.4.5, with inclusion of the reflected-wave fronts.

6.5i Special Case: the Half-plane

Although the formulas in the preceding sections apply for all wedge angles $0 < \varphi \leq 2\pi$, simplifications occur for certain special values of φ . It has already been noted that when $\varphi = \pi/n$, $n = 1, 2, \dots$, the geometrical optics field derived by the theory of images provides the exact solution. Another important special case is provided by $\varphi = 2\pi$, in which instance the wedge degenerates into a half-plane. While this obstacle configuration still gives rise to diffraction, many of the previously derived solutions can be reduced to a simpler form.^{3,4}

Time-harmonic line-source excitation

When $\varphi = 2\pi$, the diffraction integral in Eq. (18b) can be reduced to a more elegant form derived first by MacDonald.⁵ Instead of dealing directly with Eq. (18b), it is preferable to start from the pulse solution in Eq. (39) and to recover therefrom the time-harmonic result upon multiplication by $\exp(-i\omega t')$ and integration over t' from $-\infty$ to $+\infty$. Since

$$\begin{aligned} Q &= \int_{-\infty}^{\infty} U[\hat{t} - \beta] \frac{e^{-i\omega t'}}{\sqrt{(\tilde{c}\hat{t})^2 - R^2(\phi')}} dt' \\ &= \int_{-\infty}^{t-\beta} \frac{e^{-i\omega t'}}{\sqrt{(\tilde{c}\hat{t})^2 - R^2(\phi')}} dt', \quad \beta \text{ real}, \end{aligned} \quad (31)$$

where $\hat{t} = t - t'$, the change of variable $\tilde{c}\hat{t} = R(\phi') \cosh x$, with $R(\phi')$ defined in Eq. (10a), yields

$$Q = \frac{1}{\tilde{c}} e^{-i\omega t} \int_{\xi'}^{\infty} e^{ikR(\phi') \cosh x} dx, \quad \xi' = \cosh^{-1} \left[\frac{\tilde{c}\beta}{R(\phi')} \right], \quad k = \frac{\omega}{\tilde{c}}. \quad (31a)$$

If $\beta = R(\phi')/\tilde{c}$, one has $\xi' = 0$, and the resulting integral is recognized as [see Eq. (6.3.22), with $\mu = 0$]

$$\int_0^{\infty} e^{ikR(\phi') \cosh x} dx = \frac{\pi i}{2} H_0^{(1)}[kR(\phi')]. \quad (32)$$

Upon omitting the common time factor $\exp(-i\omega t)$, one finds the desired expression for the steady-state Green's function ($\phi' < \pi$):

$$\bar{G}(\rho, \rho') = I(\rho; \rho', \phi') \mp I(\rho; \rho', -\phi'), \quad (33)$$

where

$$\begin{aligned} I(\rho; \rho', \phi') &= \frac{i}{4} H_0^{(1)}[kR(\phi')] U(\pi - |\phi - \phi'|) \\ &\quad - \frac{1}{4\pi} \operatorname{sgn}(\pi - |\phi - \phi'|) \int_{\xi}^{\infty} e^{ikR(\phi') \cosh x} dx, \\ \xi &= \cosh^{-1} \left[\frac{\rho + \rho'}{R(\phi')} \right]. \end{aligned} \quad (33a)$$

The upper sign in Eq. (33) refers to the *E*-mode case while the lower sign refers to the *H*-mode case. In view of Eq. (32), Eq. (33a) can also be written as

$$I(\rho; \rho', \phi') = \frac{1}{4\pi} \int_{-\xi}^{\infty} e^{ikR(\phi') \cosh x} dx, \quad |\phi - \phi'| < \pi, \quad (34)$$

so the result for $\bar{G}(\rho, \rho')$ can be expressed solely in terms of the integral of $\exp[ikR(\phi') \cosh x]$.

A series representation of the solution may be obtained from Eqs. (12) and (13) with $\mu = m/2$.

Impulsive line-source excitation

When $\varphi = 2\pi$, the integral appearing in Eq. (21) can be expressed in closed form³ because of the simplification

$$\operatorname{Re} B(\phi, \phi'; i\beta) = \frac{\cos(\psi/2) \cosh(\beta/2)}{\cosh \beta + \cos \psi}, \quad \varphi = 2\pi. \quad (35)$$

Introduction into the integral in Eq. (21) of the successive changes of variable

$$\cosh \beta = 1 + v^2, \quad \cosh \frac{\beta}{2} d\beta = \sqrt{2} dv, \quad (36a)$$

and

$$v = b \sin \gamma, \quad b = \sqrt{\frac{(\bar{c}\hat{t})^2 - (\rho + \rho')^2}{2\rho\rho'}}, \quad (36b)$$

yields, with $\hat{t} = t - t'$,

$$D(\phi, \phi'; \hat{t}) = -\frac{\bar{c}}{2\pi^2} \frac{\cos(\psi/2)}{\sqrt{\rho\rho'}} \int_0^{\pi/2} \frac{d\gamma}{1 + \cos \psi + b^2 \sin^2 \gamma}, \quad (37)$$

where $D(\phi, \phi'; \hat{t})$ denotes the contribution to the integral in Eq. (21) arising from the $\operatorname{Re} B(\phi, \phi'; i\beta)$ term. The integral in Eq. (37) can be evaluated in closed form,

$$\begin{aligned} D(\phi, \phi'; \hat{t}) &= -\frac{\cos(\psi/2)}{\sqrt{\rho\rho'}} \frac{\bar{c}}{4\pi} \frac{1}{\sqrt{2 \cos^2(\psi/2)}} \frac{1}{\sqrt{1 + \cos \psi + b^2}} \\ &= -\frac{\bar{c}}{4\pi \sqrt{(\bar{c}\hat{t})^2 - R^2(\phi')}} \operatorname{sgn} \cos \frac{\psi}{2}, \end{aligned} \quad (38)$$

where $\operatorname{sgn} x = \pm 1$, $x \gtrless 0$, and $R(\phi')$ is defined in Eq. (10a). Thus, Eq. (21) furnishes the following form for the half-plane Green's function,

$$\begin{aligned} \hat{G}'(\rho, \rho'; t) &= \frac{\bar{c}}{2\pi} U[\pi - |\phi - \phi'|] U\left[\hat{t} - \frac{R(\phi')}{\bar{c}}\right] \frac{1}{\sqrt{(\bar{c}\hat{t})^2 - R^2(\phi')}} \\ &\mp \frac{\bar{c}}{2\pi} U[\pi - (\phi + \phi')] U\left[\hat{t} - \frac{R(-\phi')}{\bar{c}}\right] \frac{1}{\sqrt{(\bar{c}\hat{t})^2 - R^2(-\phi')}} \\ &- \frac{\bar{c}}{4\pi} U\left[\hat{t} - \frac{(\rho + \rho')}{\bar{c}}\right] \left[\frac{\operatorname{sgn}(\pi - |\phi - \phi'|)}{\sqrt{(\bar{c}\hat{t})^2 - R^2(\phi')}} \mp \frac{\operatorname{sgn}(\pi - \phi - \phi')}{\sqrt{(\bar{c}\hat{t})^2 - R^2(-\phi')}} \right], \end{aligned} \quad (39)$$

with $\hat{t} = t - t'$. In view of the symmetry of the half-plane configuration, it has been assumed without loss of generality that $\phi' < \pi$. The various geometric optical regions entering into Eq. (39) are illustrated in Fig. 6.4.2. The result in Eq. (39) demonstrates again how diffraction weakens the singularity that exists across the incident wavefront; the diffracted field is, in fact, finite, except along the geometric-optical boundary lines.

Time-harmonic point-source excitation

The diffraction integral in Eq. (24b) can be reduced to a simpler form involving a finite integration of the Hankel function which replaces the exponential function in Eq. (31a).^{4,5} In the series representation in Eq. (23), put $\mu = m/2$.

Impulsive point-source excitation

The result is given in Eq. (26), with the simplified form from Eq. (35), and with only the $\phi'_n = \phi'$, $\hat{\phi}'_n = -\phi'$ terms included (for $\phi' < \pi$).

Time-harmonic plane-wave excitation

When $\varphi = 2\pi$, the diffraction integral in Eq. (28b) can be reduced to the Fresnel-integral type of function $F(\zeta)$ defined in Eq. (6.3.18).^{1,4} One notes from Eq. (9b) that

$$B(\phi, \phi'; w) = \frac{\cos(w/2)}{2\left(\cos\frac{\phi-\phi'}{2} - \sin\frac{w}{2}\right)}, \quad \varphi = 2\pi, \quad (40)$$

whence the resulting integral in Eq. (28b) can be simplified by the change of variable $\cos w = 1 + is^2$, $-\infty < s < \infty$, i.e.,

$$s = \sqrt{2} e^{i\pi/4} \sin \frac{w}{2}, \quad \frac{dw}{ds} = \sqrt{2} e^{-i\pi/4} \sec \frac{w}{2}. \quad (41)$$

Thus,

$$\begin{aligned} I(\rho, \phi') &= \frac{-i}{2\pi} \int_{i\infty}^{-i\infty} e^{ik\rho \cos w} B(\phi, \phi'; w) dw \\ &= -\frac{i}{8\pi} e^{ik\rho} \int_{-\infty}^{\infty} e^{-k\rho s^2} \frac{ds}{s-b}, \quad b = \sqrt{2} e^{i\pi/4} \cos \frac{\phi-\phi'}{2}, \end{aligned} \quad (42)$$

which can be expressed alternatively in terms of the error-function complement [see Eqs. (4.4.5a) and (4.4.14); the fraction $1/(s-b)$ in the integrand of Eq. (42) can be replaced by $b/(s^2 - b^2)$ because of the symmetrical integration interval]. Hence, for $\phi' < \pi$ but for arbitrary ρ , one finds that the wavefunction in Eq. (33) reduces to

$$\begin{aligned} \bar{u}(\rho, \phi') &= e^{-ik\rho \cos(\phi-\phi')} U(\pi - |\phi - \phi'|) \mp e^{-ik\rho \cos(\phi+\phi')} U(\pi - \phi - \phi') \\ &\quad - e^{ik\rho} \frac{F(\xi_1)}{2} \operatorname{sgn}(\pi - |\phi - \phi'|) \pm e^{ik\rho} \frac{F(\xi_2)}{2} \operatorname{sgn}(\pi - \phi - \phi'), \end{aligned} \quad (43)$$

for $\frac{E}{H}$ modes, where

$$F(\xi) = \frac{2}{\sqrt{\pi}} e^{-i2\xi^2} \int_{(1-i)\xi}^{\infty} e^{-x^2} dx, \quad \xi_{1,2} = \sqrt{k\rho} \left| \cos \frac{\phi \mp \phi'}{2} \right|. \quad (43a)$$

By an asymptotic evalution of the function $F(\xi)$ as in Eq. (6.3.18a), one may derive the results in Eq. (29), with $\varphi = 2\pi$.

A harmonic-series form of the solution is given in Eqs. (16), with $\mu = m/2$.

Impulsive plane-wave excitation

The solution is given by Eq. (30), simplified through use of Eq. (35).

6.6 WEDGE WITH VARIABLE IMPEDANCE WALLS

In an angular transmission representation, the description of the perfectly absorbing and perfectly conducting wedge configurations has given rise, respectively, to the simple boundary conditions in Eqs. (6.4.1) and (6.5.1), imposed on the angular characteristic Green's function $g(\phi, \phi'; \mu)$ in Eq. (6.2.7). More general than either of these is the linear homogeneous boundary condition

$$\frac{dg}{d\phi} = \mp ia_{1,2}g \quad \text{at } \phi = \frac{0}{\varphi}, \quad (1)$$

where a_1 and a_2 are arbitrary constants. The perfectly absorbing wedge result follows from the identification $a_{1,2} = \mu$, whereas in the perfectly conducting case, $a_{1,2} = \infty$ and $a_{1,2} = 0$ for the E -mode and H -mode problems, respectively.[†]

If the one-dimensional characteristic Green's function $g(\phi, \phi'; \mu)$ is to be utilized to synthesize a multidimensional Green's function, it follows that the latter must satisfy on the wedge faces $\phi = 0, \varphi$ boundary conditions of the same type as in Eq.(1). This requirement can be interpreted in terms of a surface impedance Z_s , as will be demonstrated for the time-harmonic line source excitations in Eqs. (6.2.1a) or (6.2.2a). For the electric line current in Eq. (6.2.1a), the electromagnetic fields are derived as in Eq. (6.2.1b) from a scalar Green's function $\bar{G}(\rho, \rho')$ which satisfies the two-dimensional wave equation (6.2.3). The boundary condition

$$\frac{\partial \bar{G}}{\partial \phi} = \mp ia_{1,2}\bar{G} \quad \text{at } \phi = \frac{0}{\varphi}, \quad (2)$$

can thus be rephrased as

$$E_z = \mp Z_{s1,2}H_\rho \quad \text{at } \phi = \frac{0}{\varphi}, \quad (\text{E-mode case}), \quad (3)$$

where

$$Z_{s1,2} = \zeta \frac{k\rho}{a_{1,2}} \quad (3a)$$

are the surface impedances on the wedge faces at $\phi = 0, \varphi$, respectively; ζ is the wave impedance in the unbounded exterior medium, and k is the wavenumber. Alternatively, for the magnetic current excitation in Eq. (6.2.2a), the electromagnetic fields may be derived from the same scalar Green's function, provided that in view of [see Eq. (6.2.2b)]

$$E_\rho = \pm Z_{s1,2}H_z \quad \text{at } \phi = \frac{0}{\varphi}, \quad (\text{H-mode case}), \quad (4)$$

the surface impedances are related to $a_{1,2}$ as follows:

$$Z_{s1,2} = \zeta \frac{a_{1,2}}{k\rho}. \quad (4a)$$

[†] It is recalled that E and H modes distinguish solutions with $H_z \equiv 0$ and $E_z \equiv 0$, respectively. Also, μ denotes a separation parameter and is not to be confused with the same symbol employed elsewhere for the permeability. The time dependence is $\exp(-i\omega t)$.

Thus, to ensure constancy of the parameters $a_{1,2}$ required for separability of the boundary condition in Eq. (2), the surface impedances *increase linearly with ρ* for the *E*-mode problem [Eq. (3a)] but *decrease inversely with ρ* for the *H*-mode problem [Eq. (4a)], with $\operatorname{Re} a_{1,2} > 0$ for a passive surface impedance. It is of interest to observe that in view of Eqs. (2)–(4), diffraction by a constant impedance wedge cannot be solved by the separation of variables procedure and therefore requires more sophisticated mathematical techniques than the variable impedance problems described above.

While the angular characteristic Green's function g satisfying Eqs. (1) and (6.2.7) (with $p \rightarrow \mu$) can readily be constructed for arbitrary values of $a_{1,2}$ [see Eq. (3.4.51)], salient features of the electromagnetic field due to the presence of a variable surface impedance may be demonstrated by prescribing this boundary condition on one surface only. The other wedge face is assumed to be either perfectly absorbing (Sec. 6.6a) or perfectly conducting (Sec. 6.6b).

6.6a One Perfectly Absorbing and One Variable Impedance Wall

Representation emphasizing quasi-optic properties

When the wedge face at $\phi = 0$ has a surface impedance Z_s (*E*-mode problem) or admittance $1/Z_s$ (*H*-mode problem) which increases linearly away from the edge $\rho = 0$, while the wedge face at $\phi = \varphi$ is perfectly absorbing, the relevant angular characteristic Green's function satisfies the differential equation (6.2.7) (with $p \equiv \mu$), the boundary condition (1) at $\phi = 0$, and a “no reflection” condition at $\phi = \varphi$; the latter is equivalent to extending the ϕ domain to $+\infty$ and requiring a radiation condition. The solution is given by [see Eq. (3.4.51), with $\vec{\Gamma} = 0$]

$$g(\phi, \phi'; \mu) = g_\infty(\phi, \phi'; \mu) + \vec{\Gamma}(\mu)g_\infty(\phi, -\phi'; \mu), \quad (5)$$

with

$$g_\infty(\phi, \phi'; \mu) = \frac{e^{\pm i\mu|\phi-\phi'|}}{\mp 2i\mu}, \quad \operatorname{Im} \mu \geqslant 0,$$

where g_∞ in Eq. (6.4.1) is the Green's function for the bilaterally unbounded angular space, while

$$\vec{\Gamma}(\mu) = \frac{\pm \mu - a_1}{\pm \mu + a_1}, \quad \operatorname{Im} \mu \geqslant 0, \quad (5a)$$

is the reflection coefficient at $\phi = 0$ [note that c_1 in Eq. (3.4.53) corresponds to $-a_1$]. This result can be interpreted in terms of the response to the source at ϕ' and a single weighted image at $-\phi'$ on a bilaterally unbounded angular transmission line.

The two-dimensional Green's function corresponding to excitation by a line source as in Fig. 6.3.1 may be obtained by substitution of Eq. (5) into Eq. (6.3.3):

$$\begin{aligned}\bar{G}(\mathbf{p}, \mathbf{p}') &= \bar{G}_{\infty}(\mathbf{p}, \mathbf{p}') \\ &+ \frac{1}{4} \int_0^{i\infty} \mu(1 - e^{i2\mu\pi}) H_{\mu}^{(1)}(k\rho) H_{\mu}^{(1)}(k\rho') \bar{\Gamma}(\mu) g_{\infty}(\phi, -\phi'; \mu) d\mu.\end{aligned}\quad (6)$$

When Eq. (6.3.8), with $A(\phi, \phi'; w)$ taken from Eq. (6.4.2b), is employed for the perfectly absorbing wedge Green's function $\bar{G}_{\infty}(\mathbf{p}, \mathbf{p}')$, this result is valid for arbitrary $|\phi - \phi'|$, but the integral in Eq. (6) converges only for $\phi + \phi' > \pi$ [see discussion following Eq. (6.3.3)]. To obtain a representation valid at all observation angles, we proceed as in Sec. 6.3 and utilize Eq. (6.3.4) to find for the second term on the right-hand side of Eq. (6)⁶:

$$W_1 = \frac{1}{4\pi} \int_{i\infty}^{-i\infty} dw H_0^{(1)}(k\chi) \int_0^{i\infty} \mu e^{i\mu(w-\pi)} (1 - e^{i2\mu\pi}) \bar{\Gamma}(\mu) g_{\infty}(\phi, -\phi'; \mu) d\mu,\quad (7)$$

which, upon use of the identity

$$\bar{\Gamma}(\mu) = \frac{\mu - a_1}{\mu + a_1} = 1 - \frac{2a_1}{\mu + a_1},\quad (8)$$

can be expressed as

$$W_1 = \bar{G}_{\infty}(\mathbf{p}; \mathbf{p}', -\phi') + \int_{i\infty}^{-i\infty} H_0^{(1)}(k\chi) W_2 dw,\quad (9)$$

where

$$W_2 = \frac{-ia_1}{4\pi} \int_0^{i\infty} e^{i\mu(w-\pi)} (1 - e^{i2\mu\pi}) e^{i\mu(\phi+\phi')} \frac{d\mu}{\mu + a_1}\quad (9a)$$

$$= \frac{-ia_1}{4\pi} [N(w + \phi + \phi' - \pi, a_1) - N(w + \phi + \phi' + \pi, a_1)].\quad (9b)$$

N is defined as

$$N(\alpha, a_1) = \int_0^{i\infty} e^{i\mu\alpha} \frac{d\mu}{\mu + a_1} = \int_0^{\infty} \frac{e^{-x\alpha}}{x - ia_1} dx\quad (10a)$$

$$= e^{-i\alpha a_1} E_i(-i\alpha a_1),\quad (10b)$$

where E_i is the exponential integral

$$E_i(y) = \int_y^{\infty} \frac{e^{-x}}{x} dx.\quad (10c)$$

While the integral representation in Eq. (10a) requires $\operatorname{Re} \alpha > 0$ and ia_1 non-positive, the exponential integral formulation in Eq. (10b) is also valid when $\operatorname{Re} \alpha < 0$, since $E_i(y)$ is a regular function of y in the complex y plane cut along the negative real axis; $E_i(y) \sim -1n y$ as $y \rightarrow 0$, so a branch-point singularity is located at $y = 0$. The integral W_2 in Eq. (9b) has branch-point singularities at $w_{b1} = \pi - (\phi + \phi')$ and at $w_{b2} = \pi + (\phi + \phi')$. Therefore, as $\phi + \phi'$ decreases through π , the branch point at w_{b1} moves across the integration path, and the value of W_2 differs from that given in Eq. (9b) by the branch-cut contribution, as shown in Fig. 6.6.1. Thus, for arbitrary values of ϕ, ϕ' one has:

$$\begin{aligned}\bar{G}(\rho, \rho') &= \bar{G}_\infty(\rho, \rho') + \bar{G}_\infty(\rho; \rho', -\phi') \\ &- \frac{i a_1}{4\pi} \int_{i\infty}^{-i\infty} H_0^{(1)}(k\chi) [N(w + \phi + \phi' - \pi, a_1) - N(w + \phi + \phi' + \pi, a_1)] dw \\ &- U(\pi - \phi - \phi') \frac{i a_1}{4\pi} \int_{P_b} H_0^{(1)}(k\chi) N(w + \phi + \phi' - \pi, a_1) dw,\end{aligned}\quad (11)$$

where the representations (6.3.8), with Eq. (6.4.2b), are to be employed for \bar{G}_∞ , and where N is expressed as in Eq. (10b). The first two terms on the right-hand side of Eq. (11) represent the Green's function for a perfectly reflecting surface at $\phi = 0$, while the remaining contributions constitute correction terms

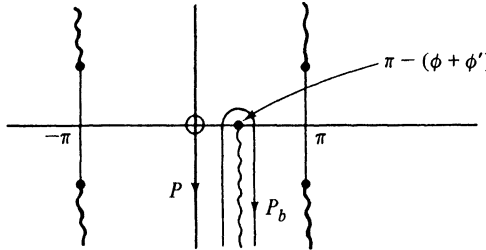


FIG. 6.6.1 Contours of integration in the complex w plane when $\phi + \phi' < \pi$.

that account for the presence of the surface impedance Z_s . The branch cut surrounded by P_b in Fig. 6.6.1 has been chosen so that $\text{Im}(k\chi) > 0$ along P_b (see Fig. 6.3.2). The above solution, derived from an angular transmission formulation, is directly suited to a study of the field behavior when k is large.

Asymptotic evaluation

To effect an asymptotic evaluation of the integrals in Eq. (11) for large values of k , we proceed as in Sec. 6.3 and replace $H_0^{(1)}(k\chi)$ by its asymptotic expression (6.3.12). The first integral has the same form as in Eq. (6.3.8) and yields by comparison with Eq. (6.3.15) the asymptotic result

$$4ia_1[N(\phi + \phi' - \pi, a_1) - N(\phi + \phi' + \pi, a_1)]C(k\rho)C(k\rho'), C(x) = \frac{e^{i(x+\pi/4)}}{2\sqrt{2\pi x}}, \quad (12a)$$

with N defined in Eq. (10b). Since $\exp(ik\chi)$ decays along P_b , the major contribution to the second integral arises from the vicinity of the branch point $w_b = \pi - (\phi + \phi')$. Upon approximating $\chi(w)$ by $R + (\rho\rho'/R)(\cos w - \cos w_b)$, $R \equiv \chi(w_b)$ [see Eq. (6.3.16b)], one finds

$$Q_1 \equiv \frac{i}{4} \int_{P_b} H_0^{(1)}(k\chi) N dw \sim C(kR) e^{-ik(\rho\rho'/R)\cos w_b} \int_{P_b} e^{ik(\rho\rho'/R)\cos w} N dw. \quad (12b)$$

To simplify the integral in Eq. (12b), it is convenient to introduce the change of variable $w = w_b - iz$, whence

$$Q_2 \equiv \int_{P_b} e^{i\alpha \cos w} N(w - w_b, a_1) dw = i \int_{P'_b} e^{i\alpha \cos(w_b - iz)} N(-iz, a_1) dz, \quad (13)$$

where the contour P'_b encloses in the positive sense the branch cut along the positive real z axis. Since the exponential integral possesses the series representation⁷

$$E_1(y) = -y - \ln y - \sum_{n=1}^{\infty} \frac{(-y)^n}{n! n}, \quad y = 0.5772, \quad (14)$$

its multivaluedness is contained in the $\ln y$ term, which alone contributes to the integral over the contour P'_b . Upon recalling that $\ln ze^{i2\pi} = \ln z + i2\pi$, one may reduce Eq. (13) to

$$Q_2 = 2\pi \int_0^\infty e^{i\alpha \cos(w_b - iz) - a_1 z} dz, \quad w_b = \pi - (\phi + \phi') > 0. \quad (15)$$

An approximate evaluation of Q_2 for large positive α can be carried out by approximating $\cos(w_b - iz) \approx \cos w_b + iz \sin w_b$, whence

$$Q_2 \sim \frac{2\pi}{\alpha \sin w_b + a_1} e^{i\alpha \cos w_b} \quad (16)$$

Thus,

$$Q_1 \sim C(kR) \frac{2\pi}{(k\rho\rho'/R) \sin(\phi + \phi') + a_1}, \quad R = \sqrt{\rho^2 + \rho'^2 - 2\rho\rho' \cos(\phi + \phi')}. \quad (17)$$

Upon substituting these results into Eq. (11) and employing Eq. (6.4.6) for the asymptotic representation of \bar{G}_∞ , one obtains⁶

$$\bar{G}(\rho, \rho') \sim \bar{G}^0(\rho, \rho') + \bar{G}^d(\rho, \rho'), \quad (18)$$

where the geometric-optical field is given by

$$\begin{aligned} \bar{G}^0 &= \frac{i}{4} H_0^{(1)}(k|\rho - \rho'|) U(\pi - |\phi - \phi'|) \\ &\quad + C(kR) \bar{\Gamma} \left[\frac{k\rho\rho'}{R} \sin(\phi + \phi') \right] U(\pi - \phi - \phi'), \end{aligned} \quad (18a)$$

with $\bar{\Gamma}(\mu)$ defined in Eq. (5a) and $C(x) = (8\pi x)^{-1/2} \exp(ix + i\pi/4)$. The diffracted field is

$$\begin{aligned} \bar{G}^d &= C(k\rho)C(k\rho') \{ -2A(\phi, \phi'; 0) - 2A(\phi, -\phi'; 0) \\ &\quad + 4ia_1[N(\phi + \phi' - \pi, a_1) - N(\phi + \phi' + \pi, a_1)] \}, \end{aligned} \quad (18b)$$

with

$$A(\phi, \phi'; 0) = \frac{1}{\pi - |\phi - \phi'|} + \frac{1}{\pi + |\phi - \phi'|}, \quad (18c)$$

and N taken from Eq. (10b). When $a_1 = 0$, then $\bar{\Gamma} = 1$, and $a_1 N(\alpha, a_1) \rightarrow 0$, so \bar{G} reduces to

$$\bar{G}(\rho, \rho') = \bar{G}_\infty(\rho; \rho', \phi') + \bar{G}_\infty(\rho; \rho', -\phi'), \quad (19)$$

the correct solution for the perfectly conducting (zero impedance) case corre-

sponding to magnetic current excitation [see Eq. (4a)]. When $a_1 \rightarrow \infty$, then $\tilde{\Gamma} \rightarrow -1$ and⁷

$$E_1(y) \sim \frac{e^{-y}}{y} \sum_{m=0}^{\infty} \frac{m!}{(-y)^m}, \quad |y| \rightarrow \infty, |\arg y| < \frac{3\pi}{2}. \quad (20)$$

Thus,

$$4ia_1[N(\alpha, a_1) - N(\beta, a_1)] = -4 \left[\frac{1}{\alpha} - \frac{1}{\beta} \right] + O\left(\frac{1}{a_1}\right), \quad |a_1| \rightarrow \infty, \quad (21)$$

and \tilde{G} reduces to the expression in Eq. (19), with the plus sign on the right-hand side replaced by minus. The resulting formula accounts correctly for a perfect conductor in the case of electric current excitation [see Eq. (3a)]. The exponential integral in Eq. (10b) permits the detailed calculation of the diffraction effect for any finite surface impedance of the form specified in Eqs. (3a) or (4a). The physical interpretation of the diffracted-wave contribution \tilde{G}^d is as shown in Fig. 6.4.1. It may be noted that the quasi-optic field solution in Eq. (18) does not exhibit explicitly a term that can be identified as a surface wave, the existence of which on the variable impedance boundary is discussed in connection with Eq. (28). In contrast to a surface wave on a constant impedance plane (Sec. 5.7), its contribution in the present instance is contained in the diffraction field function \tilde{G}^d .

When a_1 is very small, the surface impedance changes rapidly from a value of zero at $\rho = 0$ to large values at small but finite distances from the edge [see Eq. (3a)]. Since the last term inside the braces in Eq. (18b) can be neglected in this case, the diffraction field given by the first two terms is the same as for an infinite impedance wedge. This result emphasizes the fact that the diffraction effects are influenced not merely by the surface properties *at* the edge but also in its vicinity, and that the geometric-optical concepts of localized reflection or diffraction can be employed only when the surface properties do not vary rapidly over a distance equal to the local wavelength. The case of slow variation obtains when a_1 is large, and in this instance (as noted above) the diffraction field is essentially the same as for a zero impedance wedge, thereby justifying the use of the local reflection principle.

The field contribution \tilde{G}^o comprises the direct wave and a reflected wave that appears to originate from an image source located at $(\rho', -\phi')$. Hence, the reflected wave reaches the observation point via a ray path leaving the surface at the incident angle δ as shown in Fig. 6.6.2. The reflected-wave amplitude is given by

$$\tilde{\Gamma}[\xi \sin(\phi + \phi')] = \frac{\xi \sin(\phi + \phi') - a_1}{\xi \sin(\phi + \phi') + a_1}, \quad \xi = \frac{k\rho\rho'}{R}. \quad (22)$$

From geometrical optics one expects an incident ray to be reflected at the specular angle, with the reflected-ray amplitude given by the plane-wave reflection coefficient determined from the properties of the surface *at* the point of reflection. For the present case of a variable surface impedance $Z_s(\rho)$, the geometric-

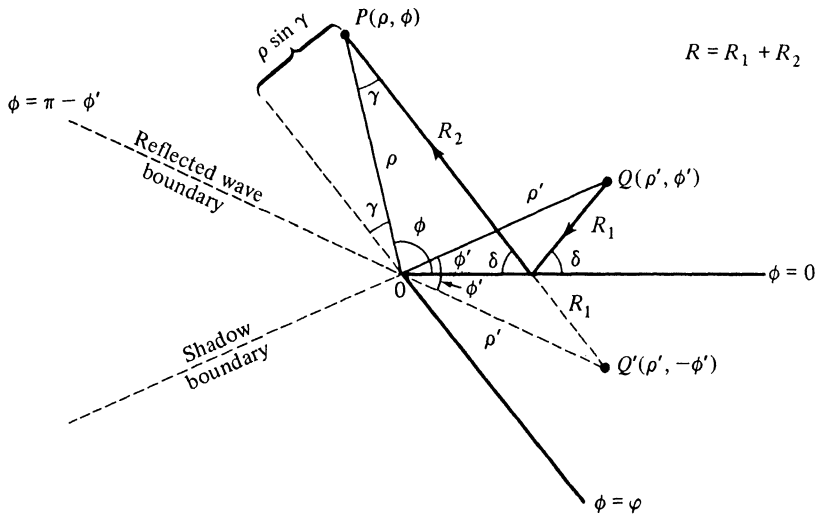


FIG. 6.6.2 Reflected rays and geometric-optical domains.

optical reflection coefficient $\overleftarrow{\Gamma}^o$ at a point $\rho = (x, 0)$ is determined via the expression [see Eqs. (2.4.3), (2.2.15c), and (2.2.15d)]

$$\overleftarrow{\Gamma}^o = \begin{cases} -\frac{Z_s(x) - \zeta \sin \delta}{Z_s(x) + \zeta \sin \delta}, & H\text{-mode case,} \\ \frac{Z_s(x) - \zeta / \sin \delta}{Z_s(x) + \zeta / \sin \delta}, & E\text{-mode case,} \end{cases} \quad (23a)$$

$$\overleftarrow{\Gamma}^o = \begin{cases} \frac{Z_s(x) - \zeta \sin \delta}{Z_s(x) + \zeta \sin \delta}, & H\text{-mode case,} \\ \frac{Z_s(x) - \zeta / \sin \delta}{Z_s(x) + \zeta / \sin \delta}, & E\text{-mode case,} \end{cases} \quad (23b)$$

where δ is the angle of incidence measured from the surface $\phi = 0$, and ζ is the wave impedance in the medium.

To show that $\overleftarrow{\Gamma}$ in Eq. (22) is identical with $\overleftarrow{\Gamma}^o$, we note first that $\overleftarrow{\Gamma}$ does not vary along a reflected ray, i.e.,

$$\frac{k\rho\rho'}{R} \sin(\phi + \phi') = \text{constant along a reflected ray.} \quad (24)$$

This follows from the equation of a reflected ray, $\rho \sin \gamma = \text{const.}$ (see Fig. 6.6.2), and from the law of sines applied to the triangle OPQ' : $\rho' \sin(\phi + \phi') = R \sin \gamma$. From the law of sines applied to the triangle OQS , where S is the point of reflection $R_2 = 0$, one has, furthermore: $R_1 \sin(\pi - \delta) = \rho' \sin \phi'$, so

$$\frac{k\rho\rho'}{R} \sin(\phi + \phi') = k\rho \sin \delta \quad \text{at } \phi = 0. \quad (24a)$$

Thus, Eq. (22) can be rewritten as

$$\overleftarrow{\Gamma} = \frac{kx \sin \delta - a_1}{kx \sin \delta + a_1}, \quad (24b)$$

which reduces via Eqs. (3a) and (4a) to Eqs. (23a) and (23b). Because of the

dependence of $\tilde{\Gamma}$ on x , a group of parallel reflected rays ($\delta = \text{constant}$) does not define a uniform plane-wave front.

Equations (18) are not applicable in the transition regions surrounding the shadow boundary $|\phi - \phi'| = \pi$ and the reflected-wave boundary $(\phi + \phi') = \pi$. Since the dependence on $|\phi - \phi'|$ is contained entirely in the term $\tilde{G}_\infty(\mathbf{p}, \mathbf{p}')$ in Eq. (11), the transition across the shadow boundary is described also in this case by the function \tilde{G}'_∞ in Eq. (6.4.7). This leads to the important conclusion, already verified in Secs. 6.4 and 6.5, that the light-shadow transition behavior is independent of the physical composition of the wedge, and that to a lowest order in the asymptotic representation, the strength of the field on the shadow boundary is one half that of the incident field. The behavior across the reflected-wave boundary does, however, depend on the physical properties of the reflecting surface. Although we do not discuss here the reflected-wave transition function for the variable impedance surface with finite a_1 , the limiting cases $a_1 = 0, \infty$, are covered via the results in Sec. 6.5.

From the similarity of the formal solutions in Eqs. (6) and (6.3.3), it is noted that the procedure described in conjunction with Eq. (6.4.9) can also be employed in the present case to derive higher-order terms in the asymptotic expansion of \tilde{G}^d .⁶ The higher-order coefficients $I_{mn}(\phi, \phi')$ are derivable by differentiation from the lowest-order function $I_{00}(\phi, \phi')$ in Eq. (18b). In a consistent evaluation of \tilde{G} to a higher order in $1/k$ ($k \gg 1$) the branch-cut integral in Eq. (11) must be evaluated more carefully, since diffraction effects in the illuminated region arise not only from the edge but also from local variations of the surface impedance.

Representation emphasizing guided-wave properties: surface wave

In the analysis of radiation in the presence of an infinite plane surface with constant surface impedance Z_s (see Sec. 5.7), it is noted that an electric (magnetic) line current parallel to the boundary will excite a surface wave if Z_s is capacitive (inductive). The guiding properties of the surface become evident in a most direct manner if one chooses a modal formulation in which the transmission axis is parallel to the surface. To explore these properties of the variable impedance surface in the wedge configuration, it is to be expected that a radial transmission representation will prove most fruitful. Such a representation, involving explicitly the radial characteristic Green's function g_ρ in Eq. (3.4.93) with $\tau = k^2$, is given formally in Eq. (6.5.11), and can be derived from the angular transmission formulation (6.3.3) by deforming the integration path around the singularities of $g(\phi, \phi'; \mu)$. As noted in Eq. (3.4.55), g_∞ is represented discontinuously across the positive real μ axis, on which lies the continuous spectrum of eigenvalues associated with the infinitely extended angular domain. Since the initial integration path can be chosen to run along the entire imaginary μ axis [see Eq. (6.3.1)], all other singularities of $g(\phi, \phi'; \mu)$ located in the right half of the complex μ plane contribute to the representation in terms of the angular mode spectrum; hence it is pertinent to examine the analytic prop-

erties of the reflection coefficient $\tilde{\Gamma}(\mu)$ in Eq. (5). Since from Eq. (5a),

$$\tilde{\Gamma}(\mu) = \frac{\mu - a_1}{\mu + a_1} \quad \text{when } \operatorname{Im} \mu > 0, \quad (25a)$$

and

$$\tilde{\Gamma}(\mu) = \frac{-\mu - a_1}{-\mu + a_1} \quad \text{when } \operatorname{Im} \mu < 0, \quad (25b)$$

and $\operatorname{Re} a_1 > 0$ for a passive surface impedance [see Eqs. (3a) and (4a)], one notes that $\tilde{\Gamma}(\mu)$ has no singularities in the first quadrant of the complex μ plane. However, a simple pole singularity exists in the fourth quadrant at

$$\mu_p = a_1, \quad \text{provided that } \operatorname{Im} a_1 < 0. \quad (26)$$

The restriction $\operatorname{Im} a_1 < 0$ implies that $\operatorname{Im} Z_s > 0$ (capacitive) for the electric current excitation and $\operatorname{Im} Z_s < 0$ (inductive) for the magnetic current excitation [note the time dependence $\exp(-i\omega t)$]. Thus, the pole singularity of $\tilde{\Gamma}(\mu)$ contributes what will be identified as a surface wave under conditions analogous to those encountered with a constant impedance surface.

The desired representation is now obtained directly, via Eqs. (3.4.93) (with $\tau = k^2$, $\lambda = \mu^2$), (6.3.1a), and (6.2.8),

$$\bar{G}(\mathbf{p}, \mathbf{p}') = \frac{1}{2} \int_{-i\infty}^{i\infty} \mu J_\mu(k\rho_<) H_\mu^{(1)}(k\rho_>) g(\phi, \phi'; \mu) d\mu, \quad (27)$$

with $g(\phi, \phi'; \mu)$ inserted from Eq. (5). The integration path can be closed by addition of quarter-circles at $|\mu| \rightarrow \infty$ in the first and fourth quadrants because of the decaying behavior of $J_\mu(k\rho_<) H_\mu^{(1)}(k\rho_>)$ therein [see Eqs. (6.A12) and (6.A16)]. Application of Cauchy's theorem transforms Eq. (27) into⁸

$$\bar{G}(\mathbf{p}, \mathbf{p}') = -\pi a_1 e^{-ia_1(\phi+\phi')} J_{a_1}(k\rho_<) H_{a_1}^{(1)}(k\rho_>) U(-\operatorname{Im} a_1) + \bar{G}_1(\mathbf{p}, \mathbf{p}'), \quad (28)$$

where

$$\begin{aligned} \bar{G}_1 &= \frac{i}{4} \int_0^\infty d\mu \left[e^{i\mu(\phi-\phi')} + e^{-i\mu(\phi-\phi')} + \frac{\mu - a_1}{\mu + a_1} e^{i\mu(\phi+\phi')} \right. \\ &\quad \left. + \frac{\mu + a_1}{\mu - a_1} e^{-i\mu(\phi+\phi')} \right] J_\mu(k\rho_<) H_\mu^{(1)}(k\rho_>) \\ &= \frac{i}{4} \int_{-\infty}^\infty d\mu \left[e^{i\mu(\phi-\phi')} + \frac{\mu - a_1}{\mu + a_1} e^{i\mu(\phi+\phi')} \right] J_{|\mu|}(k\rho_<) H_{|\mu|}^{(1)}(k\rho_>). \end{aligned} \quad (28a)$$

While Eq. (27) is subject to the restrictions $|\phi - \phi'| > \pi$, $(\phi + \phi') > \pi$, these conditions can be removed after contour deformation. \bar{G}_1 contains the contribution from the continuous spectrum in the ϕ domain, while the first term in Eq. (28) arises from a discrete spectral component representative of a surface wave.

The surface wave on this variable impedance boundary possesses certain interesting properties that distinguish it from its counterpart on a constant impedance surface. Since $\operatorname{Im} a_1 < 0$, the field decays exponentially away from

the $\phi = 0$ plane along any circular arc centered at the apex. As $\rho \rightarrow \infty$, the Hankel function can be represented by its asymptotic approximation, whence the surface-wave contribution \bar{G}_s varies like $(1/\sqrt{k\rho}) \exp(ik\rho - ia_1\phi)$ [i.e., an outgoing cylindrical wave whose angular intensity decays like $\exp(-|\text{Im } a_1| |\phi|)$]. Thus, energy is radiated into the surrounding medium—a consequence of the non-constancy of the surface impedance. Because its far-field dependence is $O(1/\sqrt{k\rho})$, the surface-wave contribution is not readily distinguished from the ordinary radiation field, which shows the same radial decay [Eq. (18b)]. However, the surface-wave field is orthogonal to the field in the continuous spectrum, as one may verify on multiplying \bar{G}_s by $\exp(-a_1\phi)$ and integrating over ϕ between $\phi = 0$ and $\phi = \infty$. Hence, the surface wave can be excited in pure form by a source distribution that matches its angular variation $\exp(-ia_1\phi)$. This property is of interest in connection with radiation from variable impedance surface-wave antennas.⁹ While the orthogonality statement requires for its exact validity an infinite angular interval, the exponential decay of the surface-wave field permits the effective truncation of the interval at some finite $\phi = \varphi$.

As $\rho \rightarrow 0$, one finds $\bar{G}_s \sim (k\rho)^{a_1} = (k\rho)^{\Re a_1} \exp[i(\text{Im } a_1 \ln k\rho)]$. Thus, $|\bar{G}_s| \rightarrow 0$, and the associated electromagnetic fields satisfy the edge condition in Eq. (1.5.37). The phase is seen to fluctuate violently near the edge.

6.6b Two Variable-Impedance Walls

If the boundary conditions at the wedge faces $\phi = 0$ and $\phi = \varphi$ are specified by a surface impedance of the type indicated in Eqs. (3a) or (4a), the two-dimensional Green's function $\bar{G}(\rho, \rho')$ satisfies the corresponding boundary condition (2). The associated angular characteristic Green's function $g(\phi, \phi'; \mu)$ is given in closed form in Eq. (3.4.51), or in terms of an image representation in Eq. (3.4.57). Substitution of Eq. (3.4.57) into Eq. (6.3.3) yields an integral representation for $\bar{G}(\rho, \rho')$ valid in the geometrical shadow region $|\phi - \phi'| > \pi$. To obtain a representation valid everywhere, it is necessary to treat separately those image contributions that characterize geometrical reflections from the wedge faces (see also Sec. 6.5). If $\varphi > \pi$, only two image terms fall into this category: the image located at $-\phi'$ which has already been treated in Eq. (11), and the image at $2\varphi - \phi'$ for which an analogous representation is employed. The response from the source in the infinitely extended angular region is represented as in Eq. (6.3.8), with Eq. (6.4.2b), and the resulting formulation then applies to all observation points.

In the asymptotic evaluation for large values of k , one obtains a geometric-optical field contribution as in Eq. (18a), with the addition of a similar term to account for possible reflections from the wedge face at $\phi = \varphi$; the physical interpretation is shown in Fig. 6.6.2. The diffracted-wave contribution arising from the true source and from each of the image sources in the infinite angular region has been shown to have the same functional form, as a function of ϕ

and ϕ' , for arbitrary locations of source and observations points [see Eq. (18b)]. An integral representation of the angular diffraction function in the shadow region $|\phi - \phi'| > \pi$ is obtained upon substituting Eq. (3.4.51) (with $j \rightarrow -i$) into Eq. (6.3.3) and following the procedure leading to Eq. (6.4.9), whence⁶

$$\bar{G}^d(\rho, \rho') \sim C(k\rho)C(k\rho')I_{00}(\phi, \phi'), \quad (29)$$

where $C(x) = (8\pi x)^{-1/2} \exp(ix + i\pi/4)$, and

$$I_{00}(\phi, \phi') = -4 \int_0^\infty (e^{-i\mu\pi} - e^{i\mu\pi}) \mu g(\phi, \phi'; \mu) d\mu, \quad |\phi - \phi'| > \pi. \quad (29a)$$

If the integral in Eq. (29a) can be evaluated in closed form, the resulting function $I_{00}(\phi, \phi')$ is valid for all ϕ, ϕ' . Higher-order terms in the asymptotic expansion can be constructed from I_{00} as in Eq. (6.4.9).

A representation emphasizing the guiding properties of the wedge surface can be constructed by considerations analogous to those leading to Eq. (28). Since $g(\phi, \phi'; \mu)$ in Eq. (3.4.51) is an even function of μ , its only singularities in the complex μ plane are poles, whence the angular spectrum is discrete. From the integral representation (27), one may express \bar{G} as a series of residues arising from the poles of g , after closing the contour at infinity in the right half of the complex μ plane. The result is listed below for the special case $a_2 = 0$, $a_1 = i|a_1|$ (i.e., the wedge face at $\phi = \varphi$ is perfectly reflecting while the surface impedance at $\phi = 0$ is purely imaginary). Under these circumstances, the pertinent pole singularities separate into two sets: a discretely infinite number on the positive real μ axis, and a single pole on the negative imaginary μ axis; the latter pole approaches the imaginary axis from the fourth quadrant and is therefore included in the residue evaluation. The result is found to be^{8,10} [see Eqs. (3.4.62)]

$$\begin{aligned} \bar{G}(\rho, \rho') = & \frac{\pi i}{\varphi} \frac{\cosh \eta(\varphi - \phi) \cosh \eta(\varphi - \phi')}{1 + \frac{1}{\varphi|a_1|} \sinh^2 \eta\varphi} J_{-i\eta}(k\rho_-) H_{-i\eta}^{(1)}(k\rho_+) \\ & + \frac{\pi i}{\varphi} \sum_{\xi} \frac{\cos \xi(\varphi - \phi) \cos \xi(\varphi - \phi')}{1 - \frac{1}{\varphi|a_1|} \sin^2 \xi\varphi} J_{\xi}(k\rho_-) H_{\xi}^{(1)}(k\rho_+), \end{aligned} \quad (30)$$

where the eigenvalues ξ and η are the positive solutions of the transcendental equations

$$\cot(\xi\varphi) = -\frac{\xi}{|a_1|}, \quad \coth(\eta\varphi) = \frac{\eta}{|a_1|}. \quad (30a)$$

The series representation in Eq. (30) is rapidly convergent when either the source point or the observation point is located near the apex.

When $|a_1| \rightarrow 0$, then $\eta \rightarrow 0$ and the ξ equation in (30a) reduces to $\sin \xi\varphi = 0$, so $\xi = m\pi/\varphi$, $m = 1, 2, \dots$; moreover, one can show from Eq. (30a) that $\eta^2\varphi/|a_1| \rightarrow 1$, $(1/|a_1|) \sin^2 \xi\varphi \rightarrow 0$. Thus, $\bar{G}(\rho, \rho')$ reduces properly to the expression in Eq. (6.5.13).

The first term in Eq. (30) represents a surface wave in which the field

intensity decays away from the surface $\phi = 0$. This becomes particularly evident when $|a_1|$ is large so that $\eta \approx |a_1|$. The surface-wave contribution then is approximately equal to that in Eq. (28), the interpretation of which was discussed in detail.

6.7 DIFFRACTION BY A CIRCULAR CYLINDER

6.7a Line-source Excitation

The circular cylinder results from the configuration in Fig. 6.1.1 on elimination of the angular boundaries at $\phi = 0, \phi$. For the z -independent problem of excitation by a line source parallel to the cylinder axis, the region exterior to the cylinder may be viewed as a radial waveguide with propagation along the ρ coordinate, or as an angular waveguide with propagation along the ϕ coordinate (see Sec. 3.3c). While both formulations are treated in this section, special attention is given to the angular transmission representation which, as noted in Sec. 6.1, is well suited to the study of high-frequency phenomena. The various geometric optical domains depicted in Fig. 6.7.1 are characterized by different behavior of the high-frequency field. We shall explore in detail the asymptotic form of the field in the illuminated and shadow zones, and interpret the solution in ray-optical terms. Not discussed herein are the more complicated transition phenomena occurring in the shaded regions surrounding the shadow boundaries in Fig. 6.7.1 (see, however, References 11–14; Reference 14(a) has a representative bibliography).

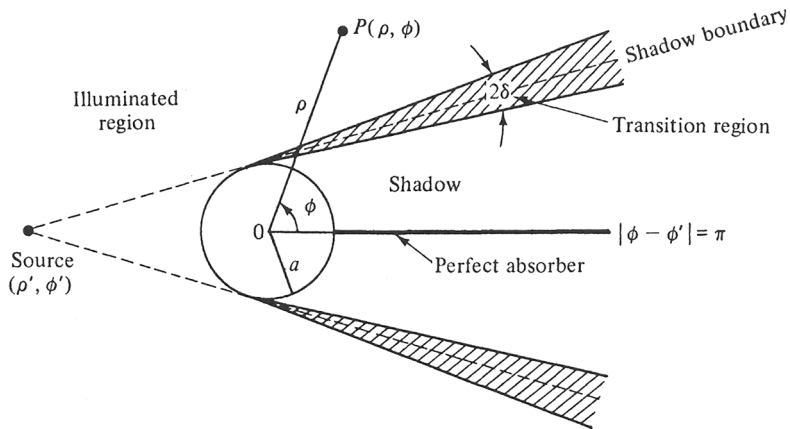


FIG. 6.7.1 Geometric-optical domains in cylinder diffraction problem.

Alternative representations of the formal solution

Diffraction problems in the region exterior to the impenetrable cylinder in Fig. 6.7.1 can be analyzed in the same manner as problems of diffraction by a

wedge. In the angular transmission analysis, the only formal difference stems from the change in the angular waveguide cross section of the wedge from $0 < \rho < \infty$ to $a \leq \rho < \infty$, with appropriate boundary conditions satisfied at $\rho = a$. As for the wedge, the simplest angular transmission problem is one wherein the angular region is infinitely extended; this artificial configuration can be made “physical” by placing at a convenient plane an “angularly matched” surface which absorbs completely all angularly propagating modes. If the surface is located at $|\phi - \phi'| = \pi$ as in Fig. 6.7.1 (i.e., deep in the geometrical shadow), the difference between this auxiliary field solution and the true solution in a periodic ϕ domain (or, equivalently, in a region with a perfectly reflecting termination at $|\phi - \phi'| = \pi$, as in Figs. 3.4.12 and 3.4.13) arises from multiple reflections. In the quasi-optic range $ka \gg 1$, where the cylinder radius is large compared to the wavelength of the incident radiation, the field in the shadow region is small, and reflections from a perturbing surface deep in the shadow have only a small effect. Hence, one expects the infinite angular space solution to yield a good approximation to the diffraction field at high frequencies—a conjecture substantiated by detailed analysis. If the cylinder radius is small compared to the wavelength ($ka \ll 1$), there is no well-defined shadow region, and the angular transmission approach offers no advantage. Instead, a radial transmission analysis is fruitful, with the cylinder representing a reflecting surface for radially propagating waves. We present here primarily the formal analysis, which permits the construction of the desired solution with a minimal effort; when appropriate, reference is made to the technical literature for additional details.

The above-mentioned alternative representations of the solution for the two-dimensional line-source Green's function $\bar{G}(\rho, \rho')$, can be constructed directly from Sec. 3.3c. The Green's function satisfies the equation

$$\left(\frac{1}{\rho} \frac{\partial}{\partial \rho} \rho \frac{\partial}{\partial \rho} + \frac{1}{\rho^2} \frac{\partial^2}{\partial \phi^2} + k^2 \right) \bar{G}(\rho, \rho') = -\frac{\delta(\rho - \rho')}{\rho'} \delta(\phi - \phi') \quad (1)$$

in the domain $a < (\rho, \rho') < \infty$, $0 \leq (\phi, \phi') \leq 2\pi$, subject to a radiation condition at $\rho \rightarrow \infty$, and to the following condition on the cylinder surface:

$$\frac{\partial \bar{G}}{\partial \rho} = -ik\bar{C}\bar{G} \quad \text{at } \rho = a, \quad \bar{C} = \text{constant}. \quad (2)$$

This condition is interpretable in terms of a surface impedance Z_s at $\rho = a$. For excitation by a line source of electric currents (E -mode case), one has, from Eq. (6.2.1b) [for an $\exp(-i\omega t)$ variation],

$$E \equiv E_z = i\omega\mu I\bar{G}, \quad H_\phi = -I \frac{\partial \bar{G}}{\partial \rho}, \quad (3a)$$

whence, at $\rho = a$,

$$E_z = Z'_s H_\phi, \quad Z'_s = \frac{\zeta}{\bar{C}}, \quad \zeta = \left(\frac{\mu}{\epsilon} \right)^{1/2}. \quad (3b)$$

For a magnetic line current (H -mode case), by duality,

$$E_\phi = -Z_s'' H_z, \quad Z_s'' = \zeta \bar{C}. \quad (4)$$

Passivity requirements are met if $\operatorname{Re} \bar{C} \geq 0$. The special case of a perfectly conducting cylinder is obtained when $Z_s \rightarrow 0$, i.e., $\bar{C} \rightarrow 0$ or ∞ for the H - and E -mode cases, respectively.

The radial characteristic Green's function and completeness relation are given in Eqs. (3.4.97) and (3.4.98):

$$g_\rho(\rho, \rho', \lambda) = \frac{\pi i}{2} \left[J_\mu(k\rho_<) + \bar{f}(\mu) H_\mu^{(1)}(k\rho_<) \right] H_\mu^{(1)}(k\rho_>), \quad \mu = \sqrt{\lambda}, \quad (5)$$

where $\bar{f}(\mu)$ is a radial reflection coefficient,

$$\bar{f}(\mu) = -\frac{b(\mu)}{d(\mu)},$$

$$b(\mu) = J'_\mu(ka) + i\bar{C}J_\mu(ka), \quad d(\mu) = H'_\mu^{(1)}(ka) + i\bar{C}H_\mu^{(1)}(ka), \quad (5a)$$

and the prime on J_μ and $H_\mu^{(1)}$ denotes the derivative with respect to the argument. Also,

$$\rho' \delta(\rho - \rho') = -\pi i \sum_{\mu_p} \frac{\mu_p b(\mu_p)}{\left[\frac{\partial}{\partial \mu} d(\mu) \right]_{\mu_p}} H_{\mu_p}^{(1)}(k\rho) H_{\mu_p}^{(1)}(k\rho'), \quad (6)$$

where the μ_p are defined by

$$d(\mu_p) = 0. \quad (6a)$$

For the angular domain, one has, from Eq. (3.4.51c), with the subscript on g_ϕ suppressed,

$$g(\phi, \phi'; \hat{\lambda}) = \begin{cases} \frac{-\cos \hat{\mu}[\pi - |\phi - \phi'|]}{2\hat{\mu} \sin \hat{\mu}\pi}, & \text{Im } \hat{\mu} > 0 \\ 0, & \text{Im } \hat{\mu} \leq 0 \end{cases} \quad (7a)$$

$$g_\infty(\phi, \phi'; \hat{\lambda}) = \sum_{n=-\infty}^{\infty} g_\infty(\phi, 2n\pi + \phi'), \quad (7b)$$

where $\hat{\mu} = \sqrt{\lambda}$ and $g_\infty(\phi, \phi'; \hat{\lambda})$ is the characteristic Green's function for the infinite angular space:

$$g_\infty(\phi, \phi'; \hat{\lambda}) = \frac{e^{i\hat{\mu}|\phi - \phi'|}}{-2i\hat{\mu}}, \quad \text{Im } \hat{\mu} > 0. \quad (7c)$$

The completeness relation is [from Eq. (3.2.50c)]

$$\delta(\phi - \phi') = \frac{1}{2\pi} \sum_{m=-\infty}^{\infty} e^{im(\phi - \phi')}. \quad (8)$$

Alternative modal representations for the two-dimensional Green's function $\bar{G}(\rho, \rho')$ are constructed directly from the z -independent version of Eqs. (3.3.37) and (3.3.38b). In particular, one has the contour-integral representation

$$\bar{G}(\rho, \rho') = -\frac{1}{\pi i} \int_{C_s + C_i} g_\rho(\rho, \rho'; \lambda) g(\phi, \phi'; \lambda) \mu d\mu, \quad (9)$$

where the contours C_3 and C_4 are shown in Fig. 6.7.2. The contour remains open about the pole at $\mu = 0$, whence the principal value of the integral is taken at that point. Since the integrand in Eq. (9) is an odd function of μ , the contour C_4 can be reflected about the origin into the contour C'_3 , and $\int_{C_3+C_4} = \int_{C_3+C'_3}$. In terms of the image representation in Eq. (7b), Eq.(9) becomes

$$\bar{G}(\rho, \rho') = \sum_{n=-\infty}^{\infty} \bar{G}_{\infty}(\rho, \rho'_n), \quad \rho'_n = (\rho', \phi'_n), \quad \phi'_n = \phi' + 2n\pi, \quad (10a)$$

where, in view of Eq. (7c),

$$\bar{G}_{\infty}(\rho, \rho'_n) = \frac{1}{2\pi} \int_{-\infty}^{\infty} g_{\rho}(\rho, \rho'; \lambda) e^{i\mu|\phi - \phi'_n|} d\mu. \quad (10b)$$

Since the integrand in Eq. (10b) has no singularities on the real μ axis, the integration can be taken from $\mu = -\infty$ to $\mu = \infty$. Because g_{ρ} is an even function of μ , replacement of μ by $(-\mu)$ yields the same integrand except for the

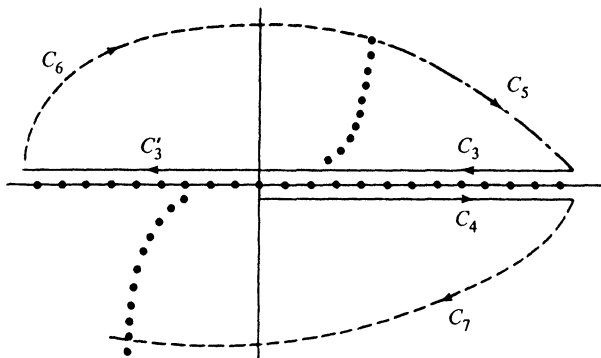


FIG. 6.7.2. Paths of integration and singularities in the complex μ plane.

occurrence of $-|\phi - \phi'|$. Hence, the absolute value is of no consequence and $|\phi - \phi'|$ can be replaced by $\phi - \phi'$. \bar{G}_{∞} and g_{ρ} can therefore be interpreted as Fourier transform pairs in the infinitely extended angular space. The $n = 0$ term in Eq. (10a) represents the Green's function for the configuration in Fig. 6.7.1 and yields the dominant contribution in the quasi-optic range $ka \gg 1$, as shown below. When $n \neq 0$, a rapidly convergent representation for large ka is obtained by closing the integration path by an infinite semicircle in the upper half of the μ plane and evaluating the integral in terms of the residues at the poles of g_{ρ} . Thus, the following representation, rapidly convergent for large ka as shown below, but valid for any cylinder radius, is suitable for all values of $|\phi - \phi'| \leq \pi$:

$$\begin{aligned}\bar{G}(\rho, \rho') &= \frac{1}{2\pi} \int_{-\infty}^{\infty} g_{\rho}(\rho, \rho'; \lambda) e^{i\mu|\phi - \phi'|} d\mu \\ &\quad + \frac{\pi}{2} \sum_{n=-\infty}^{\infty} \sum'_{\mu_n} \frac{b(\mu_p)}{\frac{\partial}{\partial \mu} d(\mu)} H_{\mu_p}^{(1)}(k\rho) H_{\mu_p}^{(1)}(k\rho') e^{i\mu_p|\phi - \phi'_n|},\end{aligned}\quad (11)$$

where $\mu = \sqrt{\lambda}$; the prime on the sum over n denotes omission of the $n = 0$ term, and the sum represents the contribution from the images in the infinite angular space, which restores the required periodicity along the boundary $|\phi - \phi'| = \pi$.

Employing the angular eigenfunctions of Eq. (8), one obtains the radial transmission representation

$$\bar{G}(\rho, \rho') = \frac{i}{4} \sum_{n=-\infty}^{\infty} e^{in(\phi - \phi')} \left[J_n(k\rho_<) - \frac{b(n)}{d(n)} H_n^{(1)}(k\rho_<) \right] H_n^{(1)}(k\rho_>), \quad (12)$$

$$= \frac{i}{4} H_0^{(1)}(k|\rho - \rho'|) + \bar{G}_s(\rho, \rho'), \quad (13a)$$

$$\bar{G}_s(\rho, \rho') = -\frac{i}{4} \sum_{n=-\infty}^{\infty} e^{in(\phi - \phi')} H_n^{(1)}(k\rho) H_n^{(1)}(k\rho') \frac{b(n)}{d(n)}. \quad (13b)$$

Since $b(n)/d(n) \rightarrow 0$ as $a \rightarrow 0$, the contribution from the $J_n(k\rho_<)$ term in the series is recognized as the free-space Green's function \bar{G}_f , whose closed-form result is given in Eq. (5.4.25). The remaining series representation for the scattered field \bar{G}_s converges rapidly when ka is small and can therefore be used for numerical evaluation of the diffraction effects of a *small cylinder*.

The preceding remarks concerning the convergence properties of the image representation in Eq. (11) will now be justified. Although the discussion can be carried out for arbitrary values of the surface impedance Z_s ,¹⁵ we assume for convenience that $\bar{C} = \infty$ in Eq. (5a), so

$$b(\mu) \rightarrow J_{\mu}(ka)i\bar{C}, \quad d(\mu) \rightarrow H_{\mu}^{(1)}(ka)i\bar{C}. \quad (14)$$

Convergence of the integral representation for \bar{G}_{∞} in Eq. (10b) is established upon noting from Eqs. (6.A12) and (6.A16) that g_{ρ} behaves for $\mu \rightarrow \infty$ like

$$g_{\rho} \sim \frac{1}{\mu} \left[\left(\frac{\rho_<}{\rho_>} \right)^{\mu} + \text{const.} \left(\frac{a^2}{\rho \rho'} \right)^{\mu} \right]. \quad (15)$$

Since both $\rho_</\rho_>$ and $a^2/\rho \rho'$ are less than unity, g_{ρ} tends to zero exponentially as $\mu \rightarrow \infty$. [Note: $A^{\mu} = \exp(\mu \ln A)$.] The same applies as $\mu \rightarrow -\infty$, since g_{ρ} is an even function of μ . Equation (15) actually remains valid along an infinite semicircle in the μ plane extending to the right of the lines on which the zeros of $H_{\mu}^{(1)}(ka)$ are located [see Fig. 6.7.2; also curves $C_{1,2}$ in Fig. 6.A1(a)].

If the integration path is closed by the addition of the path segments C_5 and C_6 in Fig. 6.7.2, one assesses the behavior of the integrand in Eq. (10b) on C_5 directly from Eq. (15). Since $\text{Re } \mu > 0$, $\text{Im } \mu > 0$ on C_5 , both g_{ρ} and $\exp(i\mu|\phi - \phi'_n|)$ converge exponentially as $|\mu| \rightarrow \infty$, and there is no contribution to the integral unless $\rho = \rho'$, $\phi = \phi'_n$. The contribution from C_6 is

examined conveniently by introducing a change of variable from μ to $-\mu$, thereby furnishing an integral over the contour C_7 . While the angularly dependent term $\exp(-i\mu|\phi - \phi'_n|)$ still converges exponentially when $\phi \neq \phi'_n$, g_ρ in Eq. (15) converges exponentially when $\operatorname{Re} \mu > 0$, $\rho \neq \rho'$, but diverges over the path segment lying to the left of the negative imaginary μ axis on C_7 . However, if $\mu = |\mu|e^{i\psi}$, and $\psi = -(\pi/2) - \epsilon$, $0 < \epsilon \ll 1$, each term in the integrand of Eq. (10b) has a magnitude characterized by

$$|A^\mu e^{-i\mu\varphi}| = e^{|\mu|[\epsilon + \ln A] - \varphi}, \quad 0 < A < 1, \quad (15a)$$

where, from Eq. (6.A21), $\epsilon \leq \pi[2 \ln(2|\mu|/eka)]^{-1}$ (see Sec. 6.A5 for a discussion of the behavior of μ_p). Hence, if $\varphi \neq 0$, the expression in Eq. (15) decays as $|\mu| \rightarrow \infty$, and there is no contribution to the integral from the path segment C_6 provided that $\phi \neq \phi'_n$. The latter restriction affects only the $n = 0$ term and eliminates observation along the source location angle $\phi = \phi'$.

One notes from the above discussion that, for $\phi \neq \phi'$, the contour deformation can be carried out for all the $\tilde{G}_\infty(\rho, \rho')$ terms, and the resulting integral can be evaluated in terms of the residues at the complex zeros μ_p of $H_\mu^{(1)}(ka)$ in the first quadrant of the μ plane. Hence, one may write an expression for $\tilde{G}(\rho, \rho')$ as in Eq. (11), wherein the integral is omitted and the series over n includes the $n = 0$ term. While the resulting series converges for all $|\phi - \phi'_n| \neq 0$, the μ_p series associated with the $n = 0$ term converges rapidly only when $|\phi - \phi'| > \hat{\phi}$, where the angle $\hat{\phi} = \gamma_1 + \gamma_2$ is as determined in Eq. (18). When $|\phi - \phi'| < \hat{\phi}$, initial terms in the series increase exponentially, and the series is therefore unsuitable for numerical evaluation.

We verify first the convergence of the “residue series” over μ_p for arbitrary n . From Eqs. (6.A22)–(6.A26), as $|\mu_p| \rightarrow \infty$,

$$J_{\mu_p}(ka) \equiv \frac{1}{2} H_{\mu_p}^{(2)}(ka) \sim O\left(\frac{1}{\sqrt{\zeta}}\right), \quad \zeta = |\mu_p|, \dagger \quad (16a)$$

$$\frac{\partial}{\partial \mu} H_\mu^{(1)}(ka) \Big|_{\mu_p} \sim O\left(\frac{\ln(2\zeta/eka)}{\sqrt{\zeta}}\right), \quad (16b)$$

$$H_{\mu_p}^{(1)}(k\rho) \sim O\left\{\frac{1}{\sqrt{\zeta}} \exp\left[\frac{\zeta\pi}{2} \frac{\ln(\rho/a)}{\ln(2\zeta/eka)}\right]\right\}. \quad (16c)$$

While $H_{\mu_p}^{(1)}(k\rho)$, $H_{\mu_p}^{(1)}(k\rho')$ diverge as $\zeta \rightarrow \infty$, the decay of $\exp(-\zeta|\phi - \phi'_n|)$ assures convergence for all n as long as $\phi \neq \phi'_n$ (i.e., $\phi \neq \phi'$). To assess the rapidity of convergence of the residue series, we examine the initial terms in the expansion (for a more detailed discussion of the convergence properties, see Reference 14). Since $H_{\mu_p}^{(2)}(ka)$ and $(\partial/\partial \mu_p)H_{\mu_p}^{(1)}(ka)$ do not have an exponential dependence [see Eqs. (6.A24) and (6.A26)], it suffices to focus attention on the remaining terms in Eq. (11). For large ka , the lowest values of μ_p are $O[ka + \alpha(ka)^{1/3}]$, $\alpha = \text{constant}$, $\operatorname{Im} \alpha > 0$ [see Eq. (6.A35)]; if $k\rho, k\rho' > O[ka + \alpha(ka)^{1/3}]$, the Hankel functions of argument $k\rho, k\rho'$ can be approximated by

[†] Here, ζ should not be confused with the same symbol used elsewhere for wave impedance.

their Debye asymptotic representations in Eq. (6.A1). The exponential dependence of the summand in Eq. (11) is, therefore,

$$\begin{aligned} H_{\mu_p}^{(1)}(k\rho)H_{\mu_p}^{(1)}(k\rho')e^{i\mu_p|\phi-\phi_n|} &\sim \exp\{i[\sqrt{(k\rho)^2 - \mu_p^2} + \sqrt{(k\rho')^2 - \mu_p^2}]\} \\ &\times \exp\left\{i\mu_p\left[|\phi - \phi_n| - \cos^{-1}\frac{\mu_p}{k\rho} - \cos^{-1}\frac{\mu_p}{k\rho'}\right]\right\}. \end{aligned} \quad (17)$$

Since $\mu_p = ka(1 + \Delta)$, with $\text{Im } \Delta > 0$ and increasing for successive terms in the series, one may verify that the exponential decays if

$$|\phi - \phi'_n| > \gamma_1 + \gamma_2, \quad \gamma_1 = \cos^{-1}\frac{a}{\rho'}, \quad \gamma_2 = \cos^{-1}\frac{a}{\rho}. \quad (18)$$

The residue series—physical interpretation

The condition (18) has a simple physical interpretation, as seen from Fig. 6.7.3. For $n = 0$, the condition requires that the source point Q be invisible

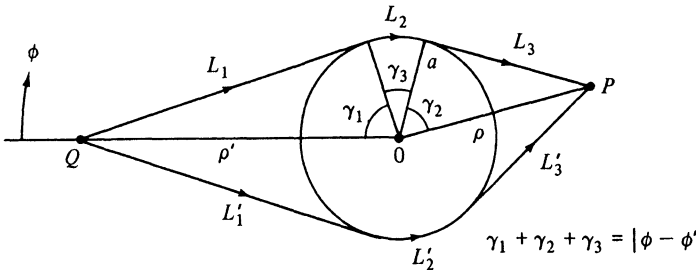


FIG. 6.7.3 Geometrical interpretation of field in shadow region.

from the observation point P (i.e., the observation point lies in the geometrical shadow region behind the cylinder). The decay in Eq. (17) is proportional to $\exp[-(\text{Im } \mu_p)\gamma_3]$, where γ_3 is the angle subtended at the origin by the points of tangency of the lines L_1 and L_3 from the source and observation points to the cylinder surface. Equation (17) can be written as

$$e^{ik(L_1 + L_2 + L_3)} e^{-\chi_p L_2}, \quad \chi_p = \frac{\text{Im } \mu_p}{a}, \quad (19)$$

so each term in the residue series for $n = 0$ may be interpreted as being associated with an incident wave which strikes the cylinder at a glancing angle, travels along the cylinder surface, and sheds energy continually during its progress; due to the leakage of energy, the wave amplitude decays according to the factor $\exp(-\chi_p L_2)$. The associated interpretation in terms of geometrical rays is also evident from Fig. 6.7.3. Because the wave “creeps” along the cylinder surface, it has been termed “creeping wave,”¹⁶ and its ray description “creeping ray.”¹⁷ The creeping rays, launched by a glancing incident ray, represent the diffraction effects and provide the means of guiding energy into the geometrical shadow region. Each μ_p has its own creeping ray; however, because of

the increasing imaginary part of successive μ_n , only the lowest are of importance. Since the creeping-ray amplitude decays exponentially, whereas that on a diffracted ray due to an edge decays algebraically [see Eq. (6.3.15)], the shadow behind a gently curved object is darker than that behind a pointed structure.

Each of the image terms $n \neq 0$ in the series solution (11) is also easily interpreted via the creeping-ray picture. Suppose that $0 < (\phi - \phi') < \pi$. Since $\phi'_n = \phi' + 2n\pi$, one has $|\phi - \phi'_n| = 2|n|\pi + (\phi - \phi')$ or $2n\pi - (\phi - \phi')$ when $n < 0$ and $n > 0$, respectively. Thus, an $n < 0$ image term represents a ray that is launched by the glancing ray L_1 and reaches the observation point P after having encircled the cylinder n times. The $n > 0$ image terms are launched by the alternative glancing ray L'_1 . The $n = 1$ term describes the ray traveling along path $(L'_1 + L'_2 + L'_3)$; in general, the n th term describes a ray that is launched by an incident ray along L'_1 and reaches the observation point P after having encircled the cylinder $(n - 1)$ times. Because of the exponential decay, proportional to the length of travel of a ray on the cylinder surface, only the nearest image terms are of importance. Since $|\phi - \phi'_n| \geq (2|n| - 1)\pi$ for all $|\phi - \phi'| < \pi$ when $n \neq 0$, and $(\gamma_1 + \gamma_2) < \pi$ in Fig. 6.7.3, one notes that the residue-series representation is rapidly convergent and that the image terms in the infinitely extended angular space contribute only to the diffraction effects of the cylinder.

If $|\phi - \phi'| < \gamma_1 + \gamma_2$, the observation point P is located in the illuminated region and the creeping-ray contribution arising from the $n = 0$ term disappears. The residue series corresponding to the $n = 0$ term is no longer rapidly convergent, and it is more appropriate to represent the contribution $\bar{G}_\infty(\mathbf{p}, \mathbf{p}')$ in terms of the integral in Eq. (11). From a saddle-point evaluation (carried out below) it is found that the $\bar{G}_\infty(\mathbf{p}, \mathbf{p}')$ term furnishes in the illuminated region precisely the geometric optical (incident wave and reflected wave) field. In the transition region between the illuminated and shadow regions (Fig. 6.7.1), a more detailed treatment of the integral is required (see remarks below). It is to be emphasized, however, that all geometric-optical, transition, and dominant diffraction effects are contained in the $n = 0$ term; in the illuminated or shadow regions the image terms contribute only the higher-order diffraction effects. For example, if $0 < \phi - \phi' < \gamma_1 + \gamma_2$, the $n = 1$ image term yields the creeping ray launched along L'_1 and emerging along L'_3 in Fig. 6.7.4, while the $n = -1$ image term yields the creeping ray launched along \hat{L}_1 and emerging along \hat{L}_3 .

Equation (11), derived directly via the image concept in an infinitely extended angular domain, may be compared with an alternative representation¹⁶ that utilizes Eq. (9) and also aims at a formulation useful in the illuminated or shadow regions. A residue series for the shadow region can be obtained without difficulty from Eq. (9) by contour deformation and residue evaluation. Equation (9) is not directly suitable, however, for application of the saddle-point method to field evaluation in the illuminated region; a difficulty arises

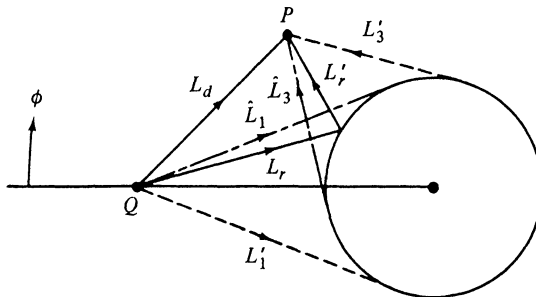


FIG. 6.7.4 Geometrical interpretation of field in illuminated region.

because the resulting saddle points lie on the real μ axis, where the singularities of g at the zeros of $\sin \mu\pi$ introduce rapid fluctuations. To cope with this complication, one may introduce the decomposition

$$\cos \{\mu [\pi - |\phi - \phi'|]\} = e^{\pm i\mu\pi} \cos \mu(\phi - \phi') \mp ie^{i\mu|\phi - \phi'|} \sin \mu\pi, \quad \text{Im } \mu \geq 0, \quad (20)$$

which, when substituted into Eq. (9), permits the contribution from the first term to be evaluated in terms of a rapidly convergent residue series for all $0 < |\phi - \phi'| \leq \pi$. The second term contributes precisely the integral in Eq. (11), whose integrand has no singularities on the real axis and can therefore be evaluated accurately by the saddle-point method, as shown below. The image approach, leading directly to Eq. (11), avoids the necessity for the two separate representations mentioned above.

Illuminated region—geometric-optical field

As noted above, to evaluate the contribution from $\tilde{G}_\infty(\mathbf{p}, \mathbf{p}')$ when the observation point lies in the illuminated region, it is convenient to retain the integral representation in Eq. (11) and to seek an asymptotic evaluation by the saddle-point method. For simplicity, it is assumed again that $\bar{C} = \infty$ [see Eq. (14)], so $\bar{f}(\mu) = -J_\mu(ka)/H_\mu^{(1)}(ka)$ in Eq. (5); the calculation for other values of \bar{C} proceeds in a similar manner. Since ka , $k\rho$, and $k\rho'$ are large quantities, it is suggestive to represent the cylinder functions in the integrand by their Debye asymptotic approximations in Eqs. (6.A1)–(6.A7) and to look for possible stationary points in the resulting exponent. If real saddle points exist, the corresponding asymptotic approximation will yield a field that propagates without exponential decay; admissible complex saddle points lead to attenuating solutions that characterize the fields in the shadow region where the rapidly convergent residue series provides an alternative method of calculation. Real saddle points should therefore occur only when the observation point lies in the illuminated region; this conjecture is confirmed by the analysis.

It is preferable to write the integral in the form¹⁶

$$\tilde{G}_\infty(\mathbf{p}, \mathbf{p}') = \tilde{G}_\infty^{(1)}(\mathbf{p}, \mathbf{p}') + \tilde{G}_\infty^{(2)}(\mathbf{p}, \mathbf{p}'), \quad (21)$$

where

$$\tilde{G}_{\infty}^{(1)} = \frac{i}{8} \int_C e^{i\mu|\phi-\phi'|} H_{\mu}^{(2)}(k\rho_{<}) H_{\mu}^{(1)}(k\rho_{>}) d\mu, \quad (21a)$$

$$\tilde{G}_{\infty}^{(2)} = -\frac{i}{8} \int_C e^{i\mu|\phi-\phi'|} H_{\mu}^{(1)}(k\rho) H_{\mu}^{(1)}(k\rho') \frac{H_{\mu}^{(2)}(ka)}{H_{\mu}^{(1)}(ka)} d\mu, \quad (21b)$$

where the integration path C proceeds as shown in Fig. 6.7.5. As noted pre-

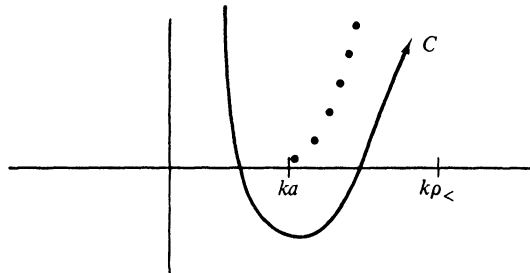


FIG. 6.7.5 Integration path for saddle-point evaluation in the complex μ plane.

viously, this path deformation is permissible and the combined integrand of \tilde{G}_{∞} decays in the upper half of the complex μ plane. Attention is therefore centered on the path segment in the vicinity of the real axis where the Debye approximation for the cylinder functions may be used [Eqs. (6.A1)–(6.A7)]. The resulting expression for $\tilde{G}_{\infty}^{(1)}$ is then as follows:

$$\tilde{G}_{\infty}^{(1)} \sim \frac{i}{4\pi} \int \frac{1}{[k\rho(\sin \beta_1)k\rho'(\sin \beta_2)]^{1/2}} e^{i\psi_1} d\mu, \quad (22)$$

where

$$\psi_1 = \mu|\phi - \phi'| + k\rho_{>}(\sin \beta_1 - \beta_1 \cos \beta_1) - k\rho_{<}(\sin \beta_2 - \beta_2 \cos \beta_2), \quad (22a)$$

$$\beta_1 = \cos^{-1} \frac{\mu}{k\rho_{>}}, \quad \beta_2 = \cos^{-1} \frac{\mu}{k\rho_{<}}, \quad (22b)$$

and the restriction $0 < \operatorname{Re} \beta_{1,2} < \pi$ must be imposed [Eq. (6.A4b)]. The saddle points μ_s of $\psi_1(\mu)$ are determined from $d\psi_1/d\mu = 0$:

$$\cos^{-1} \left(\frac{\mu_s}{k\rho_{<}} \right) - \cos^{-1} \left(\frac{\mu_s}{k\rho_{>}} \right) + |\phi - \phi'| = 0; \quad (23)$$

also, one finds that

$$\left. \frac{d^2\psi_1}{d\mu^2} \right|_{\mu_s} = \frac{1}{k\rho_{>} \sin \beta_{1s}} - \frac{1}{k\rho_{<} \sin \beta_{2s}} < 0, \quad (24)$$

where β_{1s} and β_{2s} denote the values of β_1 and β_2 corresponding to μ_s .

The saddle-point condition (23) admits of the physical interpretation shown in Fig. 6.7.6(a). Since β_{1s} and β_{2s} must be positive in view of the restriction

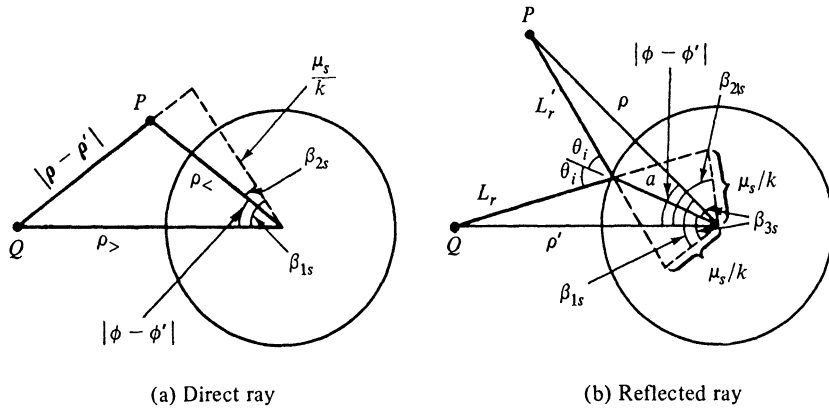


FIG. 6.7.6 Physical interpretation of saddle-point condition.

following Eq. (22b), one observes that a real solution is possible only when $|\phi - \phi'| < \pi/2$. The integration path is readily deformed through the saddle point at $\mu_s = k\rho_< \cos \beta_{2s} = k\rho_> \cos \beta_{1s}$ and leaves the saddle point at a -45° angle [see Eq. (24), which follows from $\beta_{1s} > \beta_{2s}$]; it may be noted that the poles in Fig. 6.7.5 do not occur in the integrand of Eq. (21a). Use of Eq. (4.2.1a) and reference to Fig. 6.7.6(a) then leads directly to the expression

$$\bar{G}_\infty^{(1)} \sim \frac{e^{ik|\rho - \rho'| + i\pi/4}}{2\sqrt{2\pi}\sqrt{k|\rho - \rho'|}}, \quad \text{when } |\phi - \phi'| < \frac{\pi}{2}, \quad (25)$$

which result represents the asymptotic form of the free-space Green's function [see Eqs. (5.4.36) and (5.4.37)]. The integral $\bar{G}_\infty^{(1)}$ therefore furnishes the incident (direct) field in the region $|\phi - \phi'| < \pi/2$ and yields a negligibly small contribution when $|\phi - \phi'| > \pi/2$.

The integral $\bar{G}_\infty^{(2)}$ in Eq. (21b) is treated in the same manner, subject to the recognition that the asymptotic approximation for $H_\mu^{(1,2)}(ka)$ is dependent on whether $\mu < ka$ or $\mu > ka$. In the latter instance, $H_\mu^{(1)}(ka) \sim -H_\mu^{(2)}(ka)$ [see Eqs. (6.A1) and (6.A6)], and the resulting integrand resembles that in Eq. (21a). By proceeding as before, one finds that the saddle-point condition is now given by

$$\beta_{1s} + \beta_{2s} = |\phi - \phi'|, \quad \mu_s = k\rho_> \cos \beta_{1s} = k\rho_< \cos \beta_{2s} > ka, \quad (26)$$

and admits of a graphical interpretation as in Fig. 6.7.6(a) provided that $|\phi - \phi'| > \pi/2$. It is also noted that the restriction $\mu_s/k > a$ defines those rays which connect P and Q without touching the cylinder, thereby restricting the validity of Eq. (26) (for real μ_s) to the illuminated region. The second derivative of the phase function $\psi(\mu_s)$ is now positive, so the path through the saddle point $\mu_s > ka$ proceeds as in the right-hand portion of Fig. 6.7.5. The contribution of this saddle point to $\bar{G}_\infty^{(2)}$ is found to be the same as in Eq. (25), with $|\phi - \phi'| > \pi/2$, so the two results together furnish the incident field in

the entire illuminated region; the analysis actually excludes information along the line $|\phi - \phi'| = \pi/2$, although the solution remains valid there.

When $\mu < ka$, the Debye approximation may be employed for all the Hankel functions in the integrand of Eq. (21b):

$$\tilde{G}_{\infty}^{(2)} \Big|_{\mu < ka} \sim \frac{i}{4\pi} \int \frac{1}{[k\rho(\sin \beta_1)k\rho'(\sin \beta_2)]^{1/2}} e^{i\psi_2} d\mu, \quad (27)$$

where

$$\begin{aligned} \psi_2 &= \mu|\phi - \phi'| + k\rho(\sin \beta_1 - \beta_1 \cos \beta_1) + k\rho'(\sin \beta_2 - \beta_2 \cos \beta_2) \\ &\quad - 2ka(\sin \beta_3 - \beta_3 \cos \beta_3), \\ \mu &= k\rho \cos \beta_1 = k\rho' \cos \beta_2 = ka \cos \beta_3. \end{aligned} \quad (27a)$$

The saddle-point condition $d\psi_2/d\mu = 0$ now reads

$$\beta_{1s} + \beta_{2s} - 2\beta_{3s} = |\phi - \phi'|, \quad (28)$$

and may be interpreted graphically as in Fig. 6.7.6(b). $[d^2\psi_2/d\mu^2]_{\mu_s}$ is found to be negative, so the steepest-descent path traverses the saddle point at $\mu_s < ka$ in the manner shown in the left-hand portion of Fig. 6.7.5. Equation (4.2.1b), together with parameters defined in Fig. 6.7.6(b), then yields the reflected-wave contribution,

$$\tilde{G}_{\infty}^{(2)} \Big|_{\mu_s < ka} \sim \frac{e^{ik(L_r + L'_r) + i\pi/4}}{2\sqrt{2\pi k}} \sqrt{\frac{a \cos \theta_i}{2L_r L'_r + (L_r + L'_r)a \cos \theta_i}}, \quad (29)$$

where L_r and L'_r are the ray trajectories in Fig. 6.7.6(b), θ_i is the angle of incidence, and it has been recognized that

$$\begin{aligned} kL_r &= k\rho' \sin \beta_{2s} - ka \sin \beta_{3s}, & kL'_r &= k\rho \sin \beta_{1s} - ka \sin \beta_{3s}, \\ \sin \beta_{3s} &= \cos \theta_i. \end{aligned} \quad (29a)$$

Equation (29) may be shown to represent exactly the reflected field predicted from geometrical optics, so we verify again the validity of the geometrical-optics method in the range of large k . For finite values of \tilde{C} , Eq. (29) must be multiplied by the reflection coefficient of a plane interface appropriate to a plane wave incident at the angle θ_i .

These simple expressions become invalid when the observation point approaches the light-shadow boundary, in which instance $\mu_s \rightarrow ka$. One observes from Fig. 6.7.5 that this condition corresponds to a coalescence of two saddle points near the sequence of poles, therefore requiring a more sophisticated asymptotic evaluation of the integral. Moreover, it is then no longer possible to approximate $H_{\mu}^{(1,2)}(ka)$ by the Debye formulas which are valid when $|\mu_s - ka| > O[(ka)^{1/3}]$; one requires instead the uniform approximation in terms of Airy functions [Eq. (6.A29)]. Details of the asymptotic field evaluation in this instance may be found in the literature.¹¹⁻¹⁴ However, some simple observations may be made concerning the angular extent of the transition zone separating the illuminated and shadow regions. Since $\mu_s = ka \cos \beta_{3s}$, the condition $|\mu_s - ka| > O[(ka)^{1/3}]$ may be restated as $(1 - \cos \beta_{3s}) = (1 - \sin \theta_i) > O[(ka)^{2/3}]$, or $\theta_i < (\pi/2) - O[(ka)^{-1/3}]$. The geometric-optical formula com-

prising the direct field and the reflected field in Eq. (29) is therefore valid only when $\theta_i = (\pi/2) - \delta$, where δ is an angle of $O[(ka)^{-1/3}]$. Similarly, by examining the exponent in Eq. (19), one finds that the residue series terms in the shadow region decay according to $\exp(-\gamma_3 \operatorname{Im} \mu_p)$, where $\operatorname{Im} \mu_p$ is proportional to $(ka)^{1/3}$. The series therefore converges rapidly only when $\gamma_3 > \delta$ and then permits the physical interpretation of the diffracted field in the shadow in terms of the rays sketched in Fig. 6.7.3.A simple ray-optical description of the field in the illuminated and shadow regions, respectively, applies therefore only exterior to the transition zones shown shaded in Fig. 6.7.1.

6.7b Point-source Excitation

The line-source Green's functions obtained in Sec. 6.7a may be employed directly for the construction of the three-dimensional Green's functions descriptive of the fields excited by a longitudinal electric or magnetic current element exterior to a perfectly conducting cylinder [see Fig. (6.7.7)]. As described in

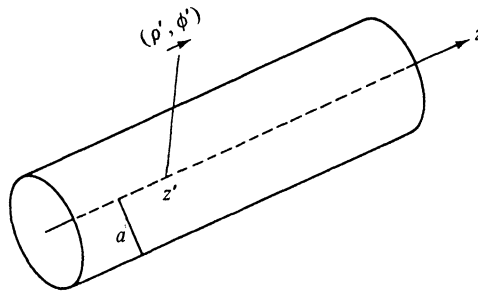


FIG. 6.7.7 Point-source excitation.

Sec. 6.2, one replaces k by $\sqrt{k^2 - \zeta^2}$ in the line source result, and then performs the operation $(1/2\pi) \int_{-\infty}^{\infty} d\zeta \exp[i\zeta(z - z')]$. From these considerations, we construct at once the following alternative representations corresponding to the radial transmission, angular transmission, and general contour integral representations discussed in Sec. 3.3c¹⁴:

$$G(\mathbf{r}, \mathbf{r}') = \left\{ \begin{aligned} & \frac{i}{8\pi} \sum_{n=-\infty}^{\infty} \int_{-\infty}^{\infty} d\zeta e^{in(\phi - \phi')} e^{i\zeta(z - z')} \left[J_n(k_\zeta \rho_<) - \frac{b(n)}{d(n)} H_n^{(1)}(k_\zeta \rho_<) \right] \\ & \times H_n^{(1)}(k_\zeta \rho_>), \end{aligned} \right. \quad (30a)$$

$$G(\mathbf{r}, \mathbf{r}') = \left\{ \begin{aligned} & \frac{1}{4} \sum_{\mu_p} \int_{-\infty}^{\infty} d\zeta \sum_{n=-\infty}^{\infty} e^{i\zeta(z - z')} \frac{b(\mu_p)}{\frac{\partial}{\partial \mu} d(\mu)} H_{\mu_p}^{(1)}(k_\zeta \rho) H_{\mu_p}^{(1)}(k_\zeta \rho') e^{i\mu_p |\phi - \phi'|}, \end{aligned} \right. \quad (30b)$$

$$G(\mathbf{r}, \mathbf{r}') = \left\{ \begin{aligned} & \frac{1}{8\pi} \int_{C_3 + C_4} d\mu \int_{-\infty}^{\infty} d\zeta e^{i\zeta(z - z')} \left[J_\mu(k_\zeta \rho_<) - \frac{b(\mu)}{d(\mu)} H_\mu^{(1)}(k_\zeta \rho_<) \right] \\ & \times H_\mu^{(1)}(k_\zeta \rho_>) \frac{\cos \mu[\pi - |\phi - \phi'|]}{\sin \mu\pi}, \end{aligned} \right. \quad (30c)$$

where $k_\zeta = \sqrt{k^2 - \zeta^2}$, with $\text{Im } k_\zeta \geq 0$, and ϕ'_n is defined in Eq. (10a). Since the cylinder is assumed to be perfectly conducting, one puts $\bar{C} = \infty$ in Eq. (5a) for the E -mode case with respect to z (electric current element) and $\bar{C} = 0$ for the H -mode case (magnetic current element). It is to be emphasized that the replacement $k \rightarrow k_\zeta$ is also to be made in the functions $b(\mu)$ and $d(\mu)$.

Other representations may be derived from the above by deforming the integration path in the complex ζ plane about the branch-point singularities of k_ζ . The results then correspond to a z -transmission formulation, one of which is given by

$$G(\mathbf{r}, \mathbf{r}') = \frac{i}{8\pi} \sum_{n=-\infty}^{\infty} e^{in(\phi-\phi')} \times \int_{-\infty}^{\infty} d\eta \eta \left[J_n(\eta\rho') - \frac{b(n)}{d(n)} H_n^{(1)}(\eta\rho') \right] H_n^{(1)}(\eta\rho) \frac{e^{ik_\eta|z-z'|}}{k_\eta}, \quad (31)$$

where $k_\eta = \sqrt{k^2 - \eta^2}$, with $\text{Im } k_\eta \geq 0$. The derivation is left as an exercise for the reader.

Equation (31) is useful for the derivation of results pertaining to vector point sources with *arbitrary orientation*. We recall from Sec. 2.3c [see also Eqs. (5.2.1)] that the fields may in this case be derived from the potential functions $\mathcal{S}'(\mathbf{r}, \mathbf{r}')$ and $\mathcal{S}''(\mathbf{r}, \mathbf{r}')$, which, in a z -transmission representation, differ from $G'(\mathbf{r}, \mathbf{r}')$ and $G''(\mathbf{r}, \mathbf{r}')$ only through the presence of the factors $1/k_n'^2$ and $1/k_n''^2$, respectively. In the cylindrical waveguide, $k_n' = k_n'' = \eta$ [see Eq. (3.2.46b)], so the formula for \mathcal{S} is obtained by dividing the integrand in Eq. (31) by η^2 . For a proper interpretation of this result, the reader should refer to the remarks following Eq. (5.2.10).

6.8 FIELDS IN SPHERICAL REGIONS

6.8a Introduction

The generic configuration for separable field representations in a spherical coordinate system comprises a combination of spheres, circular cones, and planes as shown in Fig. 6.8.1 (see also Fig. 2.7.1). Although only single spherical and conical surfaces are shown, regions contained between two concentric spheres and two coaxial cones can also be accommodated. Certain physical attributes of fields in the presence of opaque spherical boundaries (e.g., shadowing effects) are analogous to those discussed in Secs. 6.1 and 6.7 for cylindrical scatterers, while other characteristics are strongly affected by the different properties of the cylindrical and spherical coordinates (e.g., scattering by an edge at $\rho = 0$ and by a tip at $r = 0$). The intent in this section is to obtain alternative representations for fields in spherical regions and to contrast them with analogous results for cylindrical regions. Because of the formal similarity of field representations utilizing radially or angularly guided waves in cylindrical and spherical coordinates, alternative modal expansions of fields or their potentials can be written down at once (Sec. 6.8b). To illustrate some

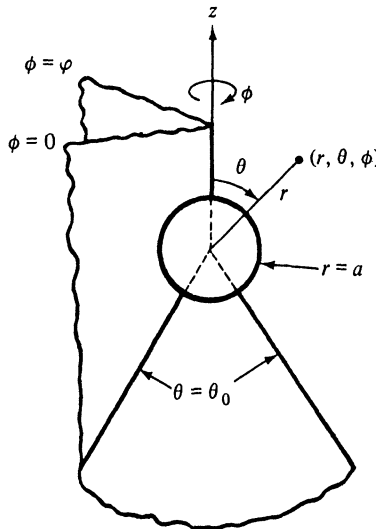


FIG. 6.8.1 Configuration accommodated by a spherical coordinate system.

fundamental differences between scattering in two and three dimensions, field solutions for a perfectly conducting cone are evaluated asymptotically in the high-frequency limit to yield the field diffracted by a conical tip (Sec. 6.8c). For asymptotic results on the thoroughly investigated problem of scattering by a sphere (see Reference 11) and for additional results on the cone, as well as for a representative bibliography, the reader may wish to consult References 18–20.

6.8b Alternative Field Representations

Free space

The fields radiated by arbitrarily prescribed source distributions in an unbounded homogeneous medium may be derived by differentiation from the scalar Green's function $G_f = [4\pi|\mathbf{r} - \mathbf{r}'|]^{-1} \exp[-jk|\mathbf{r} - \mathbf{r}'|]$ [see Eq. (5.4.2b)].[†] A radial transmission representation for G_f follows from Eqs. (2.6.11) with $\zeta Y'_i(r, r') = Z''_i(r, r')/\zeta$ taken from Eq. (2.7.11), and the mode functions inserted from Eqs. (3.4.79a) and (3.2.50):

$$\begin{aligned} G_f(\mathbf{r}, \mathbf{r}') &= \frac{e^{-jk|\mathbf{r}-\mathbf{r}'|}}{4\pi|\mathbf{r}-\mathbf{r}'|} \\ &= \frac{1}{j4\pi krr'} \sum_{m=0}^{\infty} \sum_{n=m}^{\infty} \epsilon_m \frac{(2n+1)(n-m)!}{(n+m)!} \\ &\quad \times \cos m(\phi - \phi') P_n^m(\cos \theta) P_n^m(\cos \theta') j_n(kr_{<}) h_n^{(2)}(kr_{>}), \end{aligned} \quad (1)$$

[†] In this section, the time dependence is $\exp(+j\omega t)$. For $\exp(-i\omega t)$ dependence, replace j by $-i$ and $h_v^{(2)}$ by $h_v^{(1)}$.

where $\epsilon_m = 1$, $m = 0$, and $\epsilon_m = 2$, $m \geq 1$. When the source is located on the z axis, $\theta' = 0$, and since $P_n(1) = 1$, only the $m = 0$ term contributes. Thus,

$$G_f(\mathbf{r}, \mathbf{r}') = \frac{1}{j4\pi krr'} \sum_{n=0}^{\infty} (2n+1) P_n(\cos \theta) j_n(kr_<) h_n^{(2)}(kr_>), \quad \theta' = 0, \quad (2a)$$

and when the source point is at the origin, only the $n = 0$ term remains [see Eq. (2.7.4c)]:

$$G_f(\mathbf{r}, \mathbf{r}') = \frac{1}{j4\pi r} h_0^{(2)}(kr), \quad r' = 0. \quad (2b)$$

The spherical Bessel functions of integral order n may be expressed in terms of a finite number of trigonometric functions:

$$j_0(x) = \sin x, \quad j_1(x) = \frac{\sin x}{x} - \cos x, \quad j_2(x) = \left(\frac{3}{x^2} - 1\right) \sin x - \frac{3}{x} \cos x, \quad (3a)$$

$$n_0(x) = -\cos x, \quad n_1(x) = -\sin x - \frac{\cos x}{x},$$

$$n_2(x) = \left(1 - \frac{3}{x^2}\right) \cos x - \frac{3}{x} \sin x. \quad (3b)$$

Thus, $h_0^{(2)}(x) = j \exp(-jx)$, so Eq. (2b) yields directly the closed-form expression for G_f . One confirms the earlier observation (Sec. 2.7a) that the spherical (radial) transmission-line analysis leads to a rapidly convergent representation for the radiated fields when the sources are confined to a small region about the origin. In particular, a scalar point source at the origin excites only a single spherical mode.

While the fields radiated by an electric or magnetic current element may be calculated by differentiating the closed-form expression for G_f , it is instructive to derive the result directly from the radial transmission representation. If the dipole is chosen to lie on the z axis, the fields are azimuthally symmetrical and Eq. (2a) is applicable. With J_r^0 and M_r^0 denoting the respective dipole strengths, the azimuthal field components, E_ϕ'' for a magnetic and H_ϕ' for an electric dipole, may then be derived from Eqs. (2.6.4) and (2.6.11) as

$$\left. \begin{aligned} & \frac{H_\phi'}{-J_r^0} \\ & \frac{E_\phi''}{M_r^0} \end{aligned} \right\} = \frac{1}{r'} \frac{\partial G}{\partial \theta} = \frac{1}{j4\pi krr'^2} \sum_{n=1}^{\infty} (2n+1) P_n^0(\cos \theta) j_n(kr_<) h_n^{(2)}(kr_>), \quad (4)$$

since $P_n^0 = (d/d\theta)P_n$ and $P_0^0 = 0$. As $r' \rightarrow 0$, only the $n = 1$ term contributes [see Eq. (2.7.4c)] and the result is

$$\left. \frac{1}{r'} \frac{\partial G}{\partial \theta} \right|_{r'=0} = -\frac{k \sin \theta}{j4\pi r} h_1^{(2)}(kr), \quad h_1^{(2)}(kr) = -e^{-jkr} + j \frac{e^{-jkr}}{kr}. \quad (4a)$$

Thus, while the $n = 0$ mode is the lowest mode in the scalar problem, the vector dependence of the source changes this to $n = 1$.

Expressions for \mathcal{S}'/rr' and \mathcal{S}''/rr' in Eqs. (2.6.9) are obtained by including the factor $[n(n + 1)]^{-1}$ in the summand of Eq. (1) and excluding the term $n = 0$.

The sphere

When a source distribution is located exterior to a perfectly conducting sphere, the electromagnetic field may be derived from the scalar functions G' , G'' or $\mathcal{S}', \mathcal{S}''$, whose radial transmission representations are obtained from those in free space on replacing the modal Green's function in Eq. (2.7.11) by those in Eqs. (2.7.12). For example, if the excitation is from a vertical (radial) electric dipole and the coordinate system is oriented so that the source lies on the z axis, then only G' is required for the calculation of the field, and is given via Eqs. (2.7.12), (3.4.67), (3.3.43), (3.4.101), and (2a), in the following alternative forms, with $h_t^{(2)}(ka) = 0$:¹⁸

$$G'(\mathbf{r}, \mathbf{r}') = \begin{cases} G_f(\mathbf{r}, \mathbf{r}') - \frac{1}{j4\pi krr'} \sum_{n=0}^{\infty} (2n+1) P_n(\cos \theta) h_n^{(2)}(kr) h_n^{(2)}(kr') \frac{j_n'(ka)}{h_n^{(2)}(ka)}, & (5a) \\ \frac{1}{4j\pi krr'} \sum_t \frac{(2t+1) j_t'(ka)}{\sin t\pi (\partial/\partial t) h_t^{(2)}(ka)} P_t(-\cos \theta) h_t^{(2)}(kr) h_t^{(2)}(kr') & (5b) \end{cases}$$

with an intermediate contour integral representation also possible [see Eq. (3.3.43c)]. The conversion of Eq. (5a) into Eq. (5b) is known as the Watson transformation;²¹ the original treatment did not, however, utilize the characteristic Green's function concept.

Equation (5a) expresses the Green's function for the sphere as a correction on the free-space result, and is rapidly convergent when ka is small. Alternatively, for large ka , the "residue series" (5b) is suitable for a field calculation in the geometrical shadow region. Since $t = O(ka)$ (see Sec. 6.A5), one may employ the asymptotic approximation (3.4.66b) for the Legendre function provided that $\theta \approx 0, \pi$. The resulting series then has the same form as in the problem of scattering by a circular cylinder (Sec. 6.7a), and the same analysis may be employed to deduce the fields in various geometric-optical domains. The physical interpretation of the behavior of the various field constituents is also directly analogous, due cognizance being given to the three-dimensional, but rotationally symmetric, character of the ray structure in the present instance (see Figs. 6.7.3 and 6.7.4). Simple ray pictures fail along the axis $\theta = 0, \pi$ where $P_t(-\cos \theta)$ cannot be approximated in terms of exponentials; the failure may be explained physically since the creeping rays all intersect along this axis, thereby forming a caustic of the creeping-ray system. As in the cylinder problem, it is convenient to extend the θ domain to $-\infty$ and $+\infty$, and to represent the angular characteristic Green's functions g_θ' and g_θ'' in terms of images in this infinitely extended space. This representation is easily achieved when the Legendre functions may be approximated by their trigonometric forms (i.e., for sufficiently large v), but may also be phrased for arbitrary v by introducing the "traveling-wave" Legendre functions in Eq. (3.4.71).

If the electric current element on the z axis is transverse (for example, $\mathbf{J}^0 = \theta_0 \mathbf{J}^0$, with $\theta' = \phi' = 0$) then the Hertz potentials Π' and Π'' may be derived from \mathcal{S}' and \mathcal{S}'' in Eqs. (2.6.9) as follows:

$$j\omega\epsilon r\Pi'(\mathbf{r}, \mathbf{r}') = \frac{J^0}{r'} \frac{\partial^2}{\partial\theta' \partial r'} \mathcal{S}'(\mathbf{r}, \mathbf{r}'), \quad (6a)$$

$$r\Pi''(\mathbf{r}, \mathbf{r}') = \frac{J^0}{r' \sin\theta'} \frac{\partial}{\partial\phi'} \mathcal{S}''(\mathbf{r}, \mathbf{r}'), \quad (6b)$$

with the limiting operation $\theta', \phi' \rightarrow 0$ to be carried out after the differentiations have been performed. The radial transmission representation for \mathcal{S}'/rr' has the same form as the right-hand side of Eq. (1), provided that one replaces the radial function in Eq. (2.7.11) by that in Eq. (2.7.12b), includes a factor $(n+1)^{-1} \cdot n^{-1}$ in the summand, and excludes the $n=0$ term in the series. In view of the relations listed in Eq. (3.4.79d), only the $m=1$ term remains after the limit $\theta'=0$ has been invoked. Thus,

$$\begin{aligned} j\omega\epsilon r\Pi'(\mathbf{r}, \mathbf{r}') &= \frac{J^0}{r'} \frac{\partial}{\partial r'} \left\{ \frac{-\cos\phi}{j4\pi k} \sum_{n=1}^{\infty} \frac{(2n+1)}{n(n+1)} P_n^1(\cos\theta) \right. \\ &\quad \times \left. \left[j_n(kr_<) - \frac{j'_n(ka)}{h_n^{(2)}(ka)} h_n^{(2)}(kr_<) \right] h_n^{(2)}(kr_>) \right\}, \end{aligned} \quad (7a)$$

and similarly for Π'' ,

$$\begin{aligned} r\Pi''(\mathbf{r}, \mathbf{r}') &= \frac{J^0}{r'} \left\{ \frac{-\sin\phi}{j4\pi k} \sum_{n=1}^{\infty} \frac{(2n+1)}{n(n+1)} P_n^1(\cos\theta) \right. \\ &\quad \times \left. \left[j_n(kr_<) - \frac{j_n(ka)}{h_n^{(2)}(ka)} h_n^{(2)}(kr_<) \right] h_n^{(2)}(kr_>) \right\}, \end{aligned} \quad (7b)$$

which expressions are now inserted into Eq. (2.6.4). As before, the result separates into the free-space field, which may be evaluated in closed form, and a contribution accounting for the effect of the sphere, with the latter rapidly convergent when ka is small.

Alternative representations for the functions inside the braces in Eqs. (7) may again be obtained by utilizing the characteristic Green's functions. By referring to Eq. (3.3.43a) with $q \equiv m = 1$, one may write

$$\mathcal{S}'(\mathbf{r}, \mathbf{r}') = \frac{-\cos(\phi - \phi')}{j2\pi^2} \int_{C_\theta} g_\theta(\theta, \theta'; 1; \lambda_\theta) g'_r(r, r'; \lambda_\theta) \frac{d\lambda_\theta}{\lambda_\theta}, \quad (8)$$

where C_θ surrounds the singularities of $g_\theta = g_\theta^\circ$ [Eq. (3.4.67)] on the positive real axis in the positive sense, but excludes the singularities of g'_r [Eq. (2.7.12b)], and the pole at the origin. This contour may now be deformed about the poles of g'_r , thereby yielding a residue-series representation which converges rapidly in the shadow region of the sphere when $ka \gg 1$. Analogous considerations may be applied to \mathcal{S}'' .

By moving the transverse dipole to infinity along the z axis, one may derive the result for an incident plane wave with electric field $\mathbf{E}_{\text{inc}} = \mathbf{x}_0 \exp(jkz)$. This is achieved by letting $r' \rightarrow \infty$, replacing $h^{(2)}(kr')$ by its asymptotic form,

and setting

$$\frac{-j\omega\mu J^0 e^{-jkr'}}{4\pi r'} = 1.$$

Results for a dielectric sphere may be obtained by inserting the appropriate radial characteristic Green's functions (see Fig. 2.7.4).

The cone

When the scatterer is a perfectly conducting semiinfinite cone as in Fig. 6.8.2, the angular functions in Eqs (3.4.68), (3.4.69), (3.4.80)–(3.4.83), and the radial

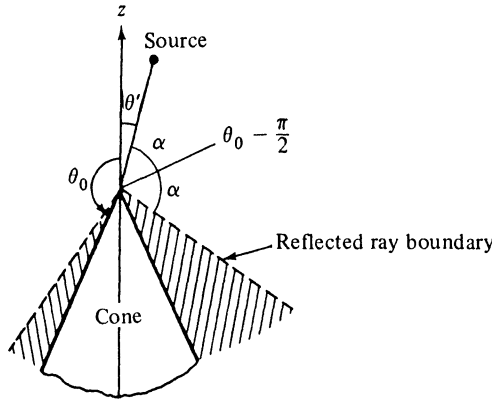


FIG. 6.8.2 Conical obstacle ($\alpha = \theta_0 - \pi/2 - \theta'$).

functions in Eqs (2.7.11), and (3.4.100) are appropriate. The Green's function G' may thus be written in the following alternative forms [see Eqs. (3.3.43)]¹⁹:

$$rr'G'(\mathbf{r}, \mathbf{r}') = \begin{cases} \frac{j}{4k} \sum_{m=0}^{\infty} \epsilon_m \cos m(\phi - \phi') \sum_p (2p + 1) \frac{\Gamma(p + m + 1)}{\Gamma(p - m + 1)} \\ \times \frac{P_p^{-m}(-\cos \theta_0) P_p^{-m}(\cos \theta')}{[\sin(p - m)\pi](\partial/\partial p) P_p^{-m}(\cos \theta_0)} \\ \times j_p(kr_<) h_p^{(2)}(kr_>) P_p^{-m}(\cos \theta), & (9a) \end{cases}$$

$$rr'G_f(\mathbf{r}, \mathbf{r}') = \frac{1}{4\pi^2 k} \sum_{m=0}^{\infty} \epsilon_m \cos m(\phi - \phi') \begin{cases} \oint_{C_\theta} j_\nu(kr_<) h_\nu^{(2)}(kr_>) g_{\theta i}(\theta, \theta'; m^2; \lambda) d\lambda, & (9b) \end{cases}$$

$$rr'G_f(\mathbf{r}, \mathbf{r}') = \frac{1}{16\pi k} \sum_{m=0}^{\infty} \epsilon_m \cos m(\phi - \phi') \int_{-1/2-j\infty}^{-1/2+j\infty} (2\nu + 1) \begin{cases} \frac{\Gamma(\nu + m + 1)}{\Gamma(\nu - m + 1) \sin(\nu - m)\pi} \frac{P_\nu^{-m}(-\cos \theta_0)}{P_\nu^{-m}(\cos \theta_0)} \\ \times h_\nu^{(2)}(kr) h_\nu^{(2)}(kr') P_\nu^{-m}(\cos \theta) P_\nu^{-m}(\cos \theta') dv, & (9c) \end{cases}$$

where $\nu = p$ are the positive zeros of $P_\nu^{-m}(\cos \theta_0)$, $\lambda = \nu(\nu + 1)$ (i.e., $\nu = \sqrt{\lambda + 1/4} - 1/2$), $\epsilon_m = 1$, $m = 0$, and $\epsilon_m = 2$, $m \geq 1$. G_f represents the free-

space Green's function [Eq. (1)] and $g'_{\theta s}$ denotes the second term in Eq. (3.4.68), which expresses the perturbation introduced by the conical surface. The contour C_θ in the complex λ plane, which surrounds the real zeros $\lambda_p = p(p+1)$ of g'_θ in the positive sense, has been deformed about the singularities of g_r (branch point at $\lambda = -1/4$, with branch cut drawn along negative real axis) to achieve the θ -transmission representation in Eq. (9c) [see also Eq. (6.3.3); in the final reduction, we have utilized the fact that $h_v^{(1)} h_v^{(2)}$ and $g'_{\theta s}$ are even functions of $v + 1/2$]. Analogous representations may be written for the H -mode Green's function G'' on replacing $P_v^{-m}(\pm \cos \theta_0)$ by $(d/d\theta_0)P_v^{-m}(\pm \cos \theta_0)$,²² and for \mathcal{S}' and \mathcal{S}'' on including the term $1/p(p+1)$ in Eq. (9a). In the latter instance, the angular transmission representation is found to be²³

$$\mathcal{S}'_s(\mathbf{r}, \mathbf{r}') = Q'(\mathbf{r}, \mathbf{r}') + \bar{\mathcal{S}}'_s(\mathbf{r}, \mathbf{r}'), \quad (10)$$

where $\mathcal{S}'_s \equiv \mathcal{S}' - \mathcal{S}_f$ and

$$Q'(\mathbf{r}, \mathbf{r}') = \frac{1}{4\pi^2 k} \sum_{m=0}^{\infty} \epsilon_m \cos m(\phi - \phi') [2\pi j (\text{Residue at } \lambda = 0)], \quad (10a)$$

$$\bar{\mathcal{S}}'_s(\mathbf{r}, \mathbf{r}') = \frac{-1}{16\pi k} \sum_{m=0}^{\infty} \epsilon_m \cos m(\phi - \phi') \int_{-(1/2)-j\infty}^{-(1/2)+j\infty} \frac{dv}{v(v+1)} [\quad], \quad (10b)$$

[] denoting the integrand in Eq. (9c). The corresponding expression for \mathcal{S}''_s differs only in that $P_v^{-m}(\pm \cos \theta_0)$ is replaced by $(d/d\theta_0)P_v^{-m}(\pm \cos \theta_0)$. One may show via Eqs. (3.4.65) and (3.4.66a) that

$$\begin{aligned} Q' = -Q'' &= \frac{j}{2\pi k} j_0(kr_<) h_0^{(2)}(kr_>) \sum_{m=1}^{\infty} \frac{\cos m(\phi - \phi')}{m} \\ &\times \left[\tan \frac{\theta}{2} \tan \frac{\theta'}{2} \tan^2 \left(\frac{\pi - \theta_0}{2} \right) \right]^m + (m=0) \text{ term}. \end{aligned} \quad (10c)$$

It may also be verified from substitution into Eqs. (2.6.10) that the $m = 0$ term in Eq. (10c) does not contribute to the electromagnetic fields calculated from \mathcal{S}' and \mathcal{S}'' , so it need be of no further concern.

By employing the large- p approximations for the functions in Eq. (9a) [see Eqs. (2.7.4) and (3.4.66)], one may show that the radial transmission representation converges everywhere, but *converges rapidly* only when either the source or the observation point is located near the cone tip (kr or kr' small; see Sec. 6.5c). This formulation is useful to check that the “tip condition” [Eq. (1.5.39)] delimiting the permissible growth of the fields near the tip singularity is satisfied. The series may be employed, for example, for the calculation of the currents induced near the cone tip by an incident plane wave (one replaces $h_p^{(2)}(kr_>)$ by its asymptotic approximation for $r' \rightarrow \infty$, and renormalizes) or for the evaluation of the radiation pattern due to sources placed near the tip, subject however to the availability of the eigenvalues p . When kr and kr' are large, series representations of the type (9a) are inconvenient for calculation since the terms decay in magnitude only when p is larger than $kr_<$. It is then more suitable to employ the integral representation in Eq. (9c) which exhibits the perturbation effect of the cone explicitly. Since the representation theorem involves the

Kontorovich-Lebedev transform, which applies only to a limited class of functions, it is necessary to impose restrictions that assure the convergence of the integral. The considerations are directly analogous to those encountered in the wedge problem [see the discussion following Eq. (6.3.3)], and furnish the conclusion that the contour deformation leading from Eq. (9b) to Eq. (9c) is permissible provided that $\theta + \theta' < 2\theta_0 - \pi$. As in the case of the wedge, the angles θ satisfying this restriction define a region that excludes rays reflected specularly at the cone surface (i.e., the domain $\theta > \theta' + 2\alpha$ in Fig. 6.8.2). In its domain of validity, the second term in Eq. (9c) may therefore be expected to represent the diffraction effect that accounts for the deviation of the high-frequency field from that predicted by geometrical optics.

6.8c The Cone—Diffracted Field at High Frequencies

Asymptotic expansion

In the high-frequency range where kr and kr' are large, the integral in Eq. (9c) may be evaluated asymptotically by the procedure described in Sec. 6.4a, and leads to the following result for $G'_s = G' - G_f$, when $(\theta + \theta') < 2\theta_0 - \pi$:^{23†}

$$G'_s(\mathbf{r}, \mathbf{r}') \sim \frac{i}{4\pi^2 k} \frac{e^{ik(r+r')}}{rr'} \sum_{n=0}^{\infty} \frac{A'_n(\theta, \theta'; \phi, \phi')}{(-2ikr)^n}, \quad (11)$$

where the coefficients A'_n are given by

$$A'_n = \sum_{m=0}^{\infty} \epsilon_m \cos m(\phi - \phi') \int_{-\infty}^{\infty} x e^{ix}(ix, n) g'_{\theta_s} dx, \quad (11a)$$

$$g'_{\theta_s} = \frac{\pi}{2} \frac{K_x^{-m}(\cos \theta) K_x^{-m}(\cos \theta') \Gamma(ix + m + \frac{1}{2})}{(-1)^{m+1} \cosh \pi x \Gamma(ix - m + \frac{1}{2})} \frac{K_x^{-m}(-\cos \theta_0)}{K_x^{-m}(\cos \theta_0)}. \quad (11b)$$

In these equations, the variable $x = -i(v + 1/2)$ has been introduced, as well as Mehler's notation

$$K_x^{\mu}(\cos \theta) \equiv P_{1/2+ix}^{\mu}(\cos \theta) \quad (11c)$$

for the Legendre function of order $ix - \frac{1}{2}$, not to be confused with the modified Bessel function, denoted elsewhere by K_{α} . Also,

$$\begin{aligned} (ix, n) &\equiv \frac{(-1)^n}{n!} (x^2 + \frac{1}{4})(x^2 + \frac{1}{4} + 2) \cdots [x^2 + \frac{1}{4} + n(n-1)] \\ &= \frac{-1}{n} [x^2 + \frac{1}{4} + n(n-1)] (ix, n-1), \quad n = 1, 2, \dots, \end{aligned} \quad (11d)$$

with $(ix, 0) \equiv 1$. While it is straightforward to write an expansion for large but arbitrary kr and kr' as in Sec. 6.4a, Eq. (11) is restricted to $kr' \gg kr$; i.e., the asymptotic series in Eq. (6.4.8a) has been employed for $h_v^{(1)}(kr)$, whereas $h_v^{(1)}(kr')$ has been represented by its leading term [see Eqs. (5.4.6) for passing to the limit of plane-wave incidence]. The dominant contribution,

$$G'_s \sim \frac{ie^{ik(r+r')}}{4\pi^2 krr'} A'_0(\theta, \theta'; \phi, \phi'), \quad (12)$$

†For the high-frequency calculation in this section the time dependence is $\exp(-i\omega t)$.

is, however, correct to $O(1/kr)$ and $O(1/kr')$ regardless of whether $r > r'$ or $r < r'$.

In the analogous expression G''_s for the H -mode case, the last factor in Eq. (11b) involves the derivatives of the Mehler function with respect to θ_0 , and the corresponding expansion coefficients are $A''_n(\theta, \theta'; \phi, \phi')$. Similarly, for the functions \mathcal{S}'_s and \mathcal{S}''_s , the integral in Eq. (10b) may be expanded asymptotically and one finds

$$\mathcal{S}'_s(\mathbf{r}, \mathbf{r}') \sim \frac{-i}{4\pi^2 k} e^{ik(r+r')} \sum_{n=0}^{\infty} \frac{B'_n(\theta, \theta'; \phi, \phi')}{(-i2kr)^n}, \quad (13)$$

where

$$B'_n = \sum_{m=0}^{\infty} \epsilon_m \cos m(\phi - \phi') \int_{-\infty}^{\infty} x e^{ixn} \frac{(ix, n)}{x^2 + \frac{1}{4}} g'_{\theta}, dx. \quad (13a)$$

The analogous result for \mathcal{S}''_s has expansion coefficients B''_n that contain g''_{θ} , instead of g'_{θ} . In view of Eq. (11d) and the differential equation for the Mehler functions,

$$\left[L(\theta) - \frac{m^2}{\sin^2 \theta} - (\frac{1}{4} + x^2) \right] K_x^{-m}(\cos \theta) = 0, \quad L(\theta) = \frac{1}{\sin \theta} \frac{d}{d\theta} \sin \theta \frac{d}{d\theta}, \quad (14)$$

one may verify that

$$C_n = -\frac{1}{n} [r^2 \nabla_r \cdot \nabla + n(n-1)] C_{n-1}, \quad n = 1, 2, \dots, \quad (15a)$$

where C_n stands for any of the coefficients A'_n , A''_n , B'_n , B''_n , and $r^2 \nabla_r \cdot \nabla$ is defined in Eq. (2.6.2). Thus, all the coefficients may be obtained recursively from a knowledge of the $n = 0$ term. Moreover, in view of Eq. (14), the A_n may be derived from the B_n via

$$r^2 \nabla_r \cdot \nabla B_n = A_n, \quad n = 0, 1, 2, \dots. \quad (15b)$$

The field derived from Eq. (12) for a radial electric dipole, or from Eqs. (10) and (13) (and their equivalent for \mathcal{S}'') for an arbitrarily oriented source, has a simple physical interpretation. The phase at the observation point P corresponds to a wave that has traveled from the source to the cone tip along the radius vector \mathbf{r}' and then from the tip to P along the radius vector \mathbf{r} . The dependence on r and r' in Eq. (12) shows that both the incoming and the outgoing waves are spherical waves, that the incoming wave is centered at r' while the scattered wave is centered at the tip, and that the scattered wave has an angular dependence specified by the "diffraction coefficient" A_0 . This process admits of a pictorial representation in terms of diffracted rays as shown in Fig. 6.8.3, the total field comprising free space and diffracted contributions. These observations apply in the region $\theta < \theta_c$ that excludes the geometric-optical rays reflected from the side of the cone. The formulation of the problem in the region $\theta_0 \geq \theta > \theta_c$ is considerably more involved, since the integrals in Eqs. (9c) and (10b) are then no longer convergent. As in the similar analysis of the wedge problem (Secs. 6.3a and 6.5c), it is necessary to subtract the geometrically re-

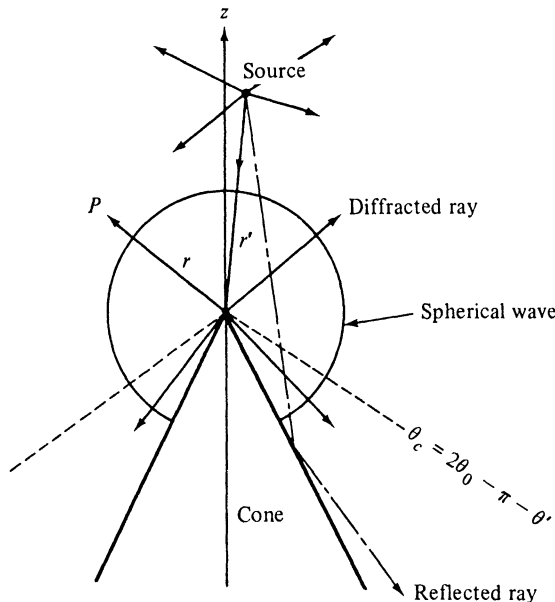


FIG. 6.8.3 Interpretation of high-frequency diffracted field.

flected fields before a convergent integral representation for the remainder can be obtained. Although this procedure is relatively straightforward for the wedge where the plane sides give rise to a reflected field which is of the same type as the incident field, the curved boundary of the cone destroys this simple feature and complicates the analysis. A study of this has been carried out for fields with simple azimuthal behavior^{19,24} [excited by a ring source centered on the axis and phased according to $\exp(im\phi)$], and it is found that the functional form of the diffraction coefficients A'_n, A''_n or B'_n, B''_n is the same throughout the entire region $0 < \theta \leq \theta_0$, although their above-described integral representation is valid only when $\theta < \theta_c$. Thus, if it is possible to evaluate the integral, the resulting function of $\theta, \theta', \phi, \phi'$ is expected to apply everywhere. The extraction of the geometric-optical contribution is facilitated by formulating the angular transmission line problem in terms of images in an infinitely extended θ space as in Eq. (3.4.74). It should be emphasized that the simple characterization of the high-frequency field in terms of contributions from direct, reflected, and diffracted rays is invalid in transition regions bounding the domain of existence of the reflected rays.

Approximation for small cone angles

While the evaluation of the diffraction coefficients must generally be carried out numerically,^{19,25} approximate results may be derived for cones having small apex angles. In this range, $\theta_0 \approx \pi$, and the Legendre functions involving θ_0 may be approximated by elementary forms. Since $F(a, b; c; 0) = 1$, one

finds from Eqs. (3.4.65) that for $\varphi \rightarrow 0$,

$$P_v^{-m}(\cos \varphi) \sim \frac{1}{\Gamma(1+m)} \left(\frac{\varphi}{2}\right)^m, \quad m \geq 0, \quad (16a)$$

$$P_v^{-m}(-\cos \varphi) \sim \frac{\Gamma(m)}{\Gamma(1+m+v)\Gamma(m-v)} \left(\frac{2}{\varphi}\right)^m, \quad m \geq 1, \quad (16b)$$

whereas²⁶

$$P_v(-\cos \varphi) \sim \frac{2 \sin v\pi}{\pi} \ln \frac{\varphi}{2}, \quad (m=0). \quad (16c)$$

Also,

$$\frac{d}{d\varphi} P_v^{-m}(\cos \varphi) \sim \frac{1}{2\Gamma(m)} \left(\frac{\varphi}{2}\right)^{m-1}, \quad m \geq 1, \quad (17a)$$

$$\frac{d}{d\varphi} P_v^{-m}(-\cos \varphi) \sim \frac{-\Gamma(1+m)}{2\Gamma(1+m+v)\Gamma(m-v)} \left(\frac{2}{\varphi}\right)^{m+1}, \quad m \geq 1, \quad (17b)$$

and the expressions for $m = 0$ may be obtained from Eqs. (16a) and (16b) via the formula

$$\frac{d}{d\varphi} P_v(\cos \varphi) = P_v^l(\cos \varphi) = -v(v+1)P_v^{-1}(\cos \varphi). \quad (17c)$$

Thus, as $\theta_0 \rightarrow \pi$,

$$\begin{aligned} \frac{P_v(-\cos \theta_0)}{P_v(\cos \theta_0)} &\sim \frac{\pi \csc v\pi}{2 \ln [(\pi - \theta_0)/2]}, \\ \frac{P_v^{-m}(-\cos \theta_0)}{P_v^{-m}(\cos \theta_0)} &\sim O[(\pi - \theta_0)^{2m}], \quad m \geq 1, \end{aligned} \quad (18a)$$

and

$$\frac{d}{d\theta_0} P_v^{-m}(-\cos \theta_0) \sim \begin{cases} \frac{\Gamma(m-v)\Gamma(1+m+v)}{-\Gamma(m)\Gamma(1+m)} \left(\frac{\pi - \theta_0}{2}\right)^{2m}, & m \geq 1, \\ -\frac{\pi v(v+1)}{\sin v\pi} \left(\frac{\pi - \theta_0}{2}\right)^2, & m = 0. \end{cases} \quad (18b)$$

When the $m = 0$ term contributes to the field, a lowest-order approximation in $\pi - \theta_0$ therefore involves only the $m = 0$ term for the E modes, but the $m = 0$ and $m = 1$ terms for the H modes.

After these approximations have been substituted into Eqs. (11a), (13), and their counterparts for A_n'' , B_n'' , there remain certain integrals that may be evaluated in closed form;^{19,27}

$$I_1 = \int_0^\infty x \frac{\tanh \pi x}{\cosh \pi x} K_x(\cos \theta) K_x(\cos \theta') dx = \frac{1}{\pi(\cos \theta + \cos \theta')}, \quad (19a)$$

$$I_2 = \int_0^\infty x \frac{\tanh \pi x}{\cosh \pi x} K_x^1(\cos \theta) K_x^1(\cos \theta') dx = \frac{2}{\pi} \frac{\sin \theta \sin \theta'}{(\cos \theta + \cos \theta')^3}, \quad (19b)$$

$$I_3 = \int_0^\infty x \frac{\tanh \pi x}{\cosh \pi x} \frac{K_x^1(\cos \theta) K_x^1(\cos \theta')}{(x^2 + 1/4)} dx = \frac{\tan(\theta/2) \tan(\theta'/2)}{\pi(\cos \theta + \cos \theta')}, \quad (19c)$$

$$I_4 = \int_0^\infty x \frac{\tanh \pi x}{\cosh \pi x} (1/4 + x^2) K_x(\cos \theta) K_x(\cos \theta') dx = \frac{2}{\pi} \frac{1 + \cos \theta \cos \theta'}{(\cos \theta + \cos \theta')^3}, \quad (19d)$$

all results being subject to the restriction $\theta + \theta' < \pi$. It is then found that the $n = 0$ diffraction coefficients are given by

$$A'_0(\theta, \theta'; \phi, \phi') \approx \frac{-\pi}{2(\cos \theta + \cos \theta') \ln[(\pi - \theta_0)/2]} [1 + o(1)], \quad (20a)$$

$$A''_0(\theta, \theta'; \phi, \phi') \approx 2\pi \left(\frac{\pi - \theta_0}{2} \right)^2 \left[\frac{1 + \cos \theta \cos \theta' + 2 \sin \theta \sin \theta' \cos(\phi - \phi')}{(\cos \theta + \cos \theta')^3} \right] \times [1 + o(1)], \quad (20b)$$

where $o(1)$ denotes terms which vanish as $\theta_0 \rightarrow \pi$. Thus, one has for the scattered portion of the scalar Green's functions G'_s and G''_s when $\theta_0 \approx \pi$ and $\theta + \theta' < 2\theta_0 - \pi$,²³

$$G'_s(\mathbf{r}, \mathbf{r}') \sim -\frac{ie^{ik(r+r')}}{(4\pi r')kr} \frac{1}{2(\cos \theta + \cos \theta') \ln[(\pi - \theta_0)/2]}, \quad (21a)$$

$$G''_s(\mathbf{r}, \mathbf{r}') \sim \frac{ie^{ik(r+r')}}{(4\pi r')kr} \frac{2}{(\cos \theta + \cos \theta')^3} \times [1 + \cos \theta \cos \theta' + 2 \sin \theta \sin \theta' \cos(\phi - \phi')] \left(\frac{\pi - \theta_0}{2} \right)^2, \quad (21b)$$

which results may be employed for the calculation of the fields due to a radial electric or magnetic dipole. The restriction $\theta + \theta' < 2\theta_0 - \pi$ is retained in view of the observations following Eqs. (10), although the approximation $\theta_0 \approx \pi$ has relaxed the convergence condition to $(\theta + \theta') < \pi$.

When the source is a transverse electric dipole, for example, $\mathbf{J}^0 = \phi^0 J_\phi^0$, the electric field may be determined from Eqs. (2.6.4) and (2.6.9) as follows:

$$\begin{aligned} \frac{r' \mathbf{E}}{J_\phi^0} &= \mathbf{r}_0 \left(\frac{\partial^2}{\partial r^2} + k^2 \right) \frac{1}{\sin \theta'} \frac{\partial^2}{\partial r' \partial \phi'} \frac{\mathcal{S}'}{-i\omega\epsilon} \\ &+ \theta_0 \left(\frac{\partial^2}{r \partial r \partial \theta} \frac{\partial^2}{\sin \theta' \partial r' \partial \phi'} \frac{\mathcal{S}'}{-i\omega\epsilon} - \frac{i\omega\mu}{r \sin \theta} \frac{\partial^2}{\partial \phi \partial \theta'} \mathcal{S}'' \right) \\ &+ \phi_0 \left(\frac{1}{r \sin \theta} \frac{\partial^2}{\partial r \partial \phi} \frac{\partial^2}{\sin \theta' \partial r' \partial \phi'} \frac{\mathcal{S}'}{-i\omega\epsilon} + \frac{i\omega\mu}{r} \frac{\partial^2}{\partial \theta \partial \theta'} \mathcal{S}'' \right). \end{aligned} \quad (22)$$

Since $\partial/\partial\phi'$ appears in all terms involving \mathcal{S}' , the ϕ' -independent $m = 0$ term in Eq. (13) does not contribute. The dominant contribution to \mathcal{S}'_s for a small-angle cone is then found from the $m = 1$ term in the diffraction coefficient B'_0 ,

$$B'_0(\theta, \theta'; \phi, \phi')|_{m=1} \approx -2\pi \left(\frac{\pi - \theta_0}{2} \right)^2 \frac{\tan(\theta/2) \tan(\theta'/2)}{\cos \theta + \cos \theta'} \cos(\phi - \phi'), \quad (23a)$$

whereas to the same order of approximation in $\pi - \theta_0$, both the $m = 0$ and $m = 1$ terms contribute to B''_0 and yield

$$B''_0(\theta, \theta'; \phi, \phi') \approx \pi \left(\frac{\pi - \theta_0}{2} \right)^2 \frac{1}{\cos \theta + \cos \theta'} - B'_0(\theta, \theta'; \phi, \phi')|_{m=1}. \quad (23b)$$

The distant scattered field may now be obtained by substituting Eqs. (23) into Eq. (13) and its counterpart for \mathcal{S}'' and recalling Eq. (10). The result simplifies substantially when the source lies on the axis, so $\theta' = 0$. By moving the dipole to infinity and normalizing as in the paragraph following Eq. (8), one finds for the total electric field in the region $\theta < (2\theta_0 - \pi)$ due to a plane wave incident parallel to the cone axis

$$\mathbf{E} \approx \mathbf{x}_0 e^{-ikz} + (\theta_0 \cos \phi - \phi_0 \sin \phi) \frac{e^{ikr}}{ikr} \left(\frac{\pi - \theta_0}{2} \right)^2 \sec^4 \frac{\theta}{2}, \quad (24)$$

which result is valid in the region $\theta < 2\theta_0 - \pi$. While the exact diffraction coefficient diverges on the reflected wave boundary $\theta = 2\theta_0 - \pi$, the approximate evaluation for $\theta_0 \approx \pi$ has shifted the divergence to $\theta = \pi$. Along the cone axis $\theta = 0$, Eq. (24) reduces to

$$\mathbf{E} \approx \mathbf{x}_0 \left[e^{-ikz} - i \left(\frac{\pi - \theta_0}{2} \right)^2 \frac{e^{ikz}}{kz} \right]. \quad (24a)$$

For arbitrary cone angles in the range $\pi/2 < \theta_0 < \pi$, the integrals in Eqs. (11a), (13a), etc., cannot be evaluated in closed form; numerically computed curves are available and have been presented in References 19 and 25. It is found that the fields calculated from these curves are well approximated by the physical optics expression; moreover, for wide-angle cones $\theta_0 \approx \pi/2$, one may derive approximate closed-form results. These aspects are illustrated in the Problems section at the end of this chapter.

APPENDIX 6A. ASYMPTOTIC FORMULAS FOR $H_v^{(1)}(z)$ AND $H_v^{(2)}(z)$

For many of the problems discussed in the text, it has been necessary to utilize asymptotic expressions for Bessel functions of large complex argument z or order v . The pertinent formulas, listed in this appendix, comprise two different sets: (1) for the range $|v/z| \gg 1$ or $|v/z| \ll 1$, and (2) for the range $|v/z| \approx 1$. Expressions for (1) were derived by Debye²⁸; those for (2) are due primarily to Langer²⁹ and Olver³⁰ (see also Reference 31).

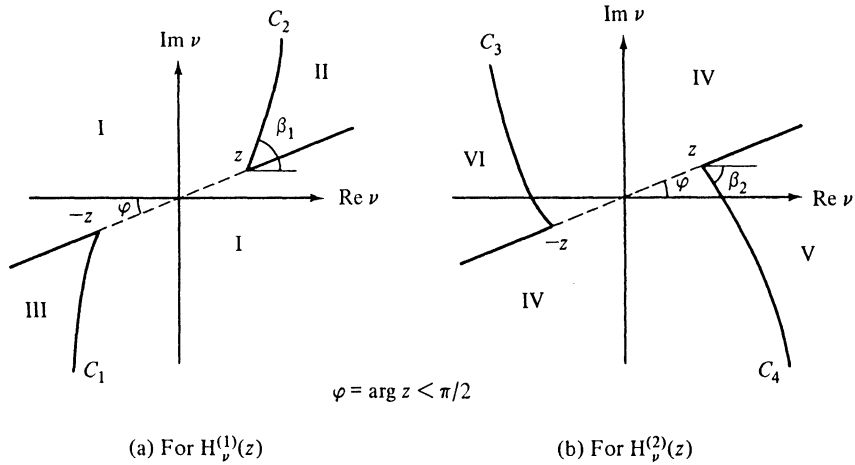
6A.1 Large, Unequal Order and Argument

If the argument and order are not approximately equal [more precisely, if $|v - z| > O(|v|^{1/3})$], three different asymptotic representations for $H_v^{(1),2}(z)$ suffice to cover the entire complex plane divided as in Fig. 6A.1.

For $H_v^{(1)}(z)$, one has

Region I

$$H_v^{(1)}(z) \sim \sqrt{\frac{2}{\pi^2 z \sin \gamma}} e^{-i\pi/4} e^{iz(\sin \gamma - \gamma \cos \gamma)} \sum_{n=0}^{\infty} \frac{A_n \Gamma[n + (1/2)] e^{-i\pi n/2}}{[(z \sin \gamma)/2]^n}. \quad (A1)$$

FIG. 6A.1 Various regions in the complex ν plane.*Region II*

$$H_v^{(1)}(z) \sim -\sqrt{\frac{2}{\pi^2 z \sin \gamma}} e^{i\pi/4} e^{-iz(\sin \gamma - \gamma \cos \gamma)} \sum_{n=0}^{\infty} \frac{A_n \Gamma[(n + 1/2)] e^{i\pi n/2}}{[(z \sin \gamma)/2]^n}. \quad (\text{A2})$$

Region III

$$H_v^{(1)}(z) \sim -\sqrt{\frac{2}{\pi^2 z \sin \gamma}} e^{i\pi/4} e^{-iz[\sin \gamma + (2\pi - \gamma) \cos \gamma]} \sum_{n=0}^{\infty} \frac{A_n \Gamma[n + (1/2)] e^{i\pi n/2}}{[(z \sin \gamma)/2]^n}. \quad (\text{A3})$$

In these formulas, $\Gamma(x)$ is the gamma function, with

$$\cos \gamma = \frac{\nu}{z}, \quad |\arg z| < \pi/2, \quad (\text{A4a})$$

and γ is restricted so that

$$0 < \operatorname{Re} \gamma < \pi. \quad (\text{A4b})$$

The first few of the expansion coefficients A_n are

$$A_0 = 1, \quad A_1 = \frac{1}{8} + \frac{5}{24} \cot^2 \gamma, \quad A_2 = \frac{3}{128} + \frac{77}{576} \cot^2 \gamma + \frac{385}{3456} \cot^4 \gamma. \quad (\text{A4c})$$

For $H_v^{(2)}(z)$, one has

Region IV

$$H_v^{(2)}(z) \sim \sqrt{\frac{2}{\pi^2 z \sin \gamma}} e^{i\pi/4} e^{-iz(\sin \gamma - \gamma \cos \gamma)} \sum_{n=0}^{\infty} \frac{A_n e^{i\pi n/2} \Gamma[n + (1/2)]}{[(z \sin \gamma)/2]^n}. \quad (\text{A5})$$

Region V

$$H_v^{(2)}(z) \sim -\sqrt{\frac{2}{\pi^2 z \sin \gamma}} e^{-i\pi/4} e^{iz(\sin \gamma - \gamma \cos \gamma)} \sum_{n=0}^{\infty} \frac{A_n \Gamma[n + (1/2)] e^{-i\pi n/2}}{[(z \sin \gamma)/2]^n}. \quad (\text{A6})$$

Region VI

$$H_v^{(2)}(z) \sim -\sqrt{\frac{2}{\pi^2 z \sin \gamma}} e^{-i\pi/4} e^{iz[\sin \gamma + (2\pi - \gamma) \cos \gamma]} \sum_{n=0}^{\infty} \frac{A_n \Gamma[n + (1/2)] e^{-inn/2}}{[(z \sin \gamma)/2]^n}. \quad (\text{A7})$$

Equations (A4) apply here as well. The zeros of $H_v^{(1)}(z)$ for large v, z lie on the curves C_1 and C_2 which form a partial boundary of regions III and II, respectively. To obtain an expression for $H_v^{(1)}(z)$ near or on C_1 , one adds Eqs. (A1) and (A3), while the sum of Eqs. (A1) and (A2) is appropriate for a representation of $H_v^{(1)}(z)$ near or on C_2 . This addition is required since in the above formulas, in which the exponential terms assume large magnitude, a further contribution of exponentially small magnitude has been omitted. Near C_1 or C_2 , however, the magnitude of the exponential terms approaches unity, and both contributions must be taken into account. Similar considerations apply to the representation of $H_v^{(2)}(z)$ in the vicinity of the contours C_3 and C_4 in Fig. 6.A.1(b). The slope of $C_{1,2}$ at $v = \mp z$ is defined by the angle $\beta_1 = (\pi + \arg z)/3$, while the corresponding angle for $C_{3,4}$ is $\beta_2 = (\pi - \arg z)/3$ [see Eq. (A35)]. As $|v| \rightarrow \infty$ along the curves, both $|\operatorname{Re} v|$ and $|\operatorname{Im} v|$ increase but the growth of $|\operatorname{Im} v|$ is more rapid than that of $|\operatorname{Re} v|$, whence $|\arg v| \rightarrow \pi/2$ [see Eqs. (A21) and the discussion following Eq. (A44) for the behavior along C_2].

On the line $\arg(v/z) = 0$, $|v| > |z|$, formulas (A1) and (A6) apply for $H_v^{(1)}$ and $H_v^{(2)}$, respectively, with $\gamma = i\delta$, $\delta > 0$. On the line $|\arg(v/z)| = \pi$, $|v| > |z|$, the appropriate formulas are (3) and (5), with $\gamma = \pi + i\delta$, $\delta > 0$.

Formulas for

$$J_v(z) = \frac{1}{2}[H_v^{(1)}(z) + H_v^{(2)}(z)] \quad (\text{A8})$$

can be obtained by addition from the above, except in those cases when $H_v^{(1)}(z) \sim -H_v^{(2)}(z)$, in which instance the Bessel function has a behavior characterized by an exponentially small contribution. Thus, when v and z are large and positive and $v > z$, $J_v(z)$ is represented asymptotically by the real function

$$J_v(z) \sim \frac{1}{2}S(-i\delta), \quad \delta > 0, \quad (\text{A9})$$

where $S(\gamma)$ denotes the expression on the right-hand side of Eq. (A1).

6A.2 Large Argument

When z is large and $|z| \gg |v|$ (i.e. $\gamma \rightarrow \pi/2$), formulas (1) and (5) can be replaced by the simpler expressions

$$H_v^{(1)}(z) \sim \sqrt{\frac{2}{\pi z}} e^{i(z-v\pi/2-\pi/4)} \sum_{n=0}^{\infty} \frac{(v, n)}{(-2iz)^n}, \quad -\pi < \arg z < 2\pi, \quad (\text{A10a})$$

$$H_v^{(2)}(z) \sim \sqrt{\frac{2}{\pi z}} e^{-i(z-v\pi/2-\pi/4)} \sum_{n=0}^{\infty} \frac{(v, n)}{(2iz)^n}, \quad -2\pi < \arg z < \pi, \quad (\text{A10b})$$

where

$$(v, n) \equiv \frac{[4v^2 - 1^2][4v^2 - 3^2] \cdots [4v^2 - (2n-1)^2]}{2^{2n} n!}, \quad (v, 0) \equiv 1. \quad (\text{A10c})$$

A formula for $J_v(z)$ is obtained from Eq. (A8).

6A.3 Large Order

When v is large and $|v| \gg |z|$, the results in Sec. A1 may likewise be simplified; $\cos \gamma$ is now very large and can be approximated by its dominant exponential. Suppose that $\gamma = i\xi$, $\operatorname{Re} \xi > 0$, so that $2v/z = 2 \cos \gamma \approx \exp(\xi) \approx -2i \sin \gamma$. Then, from the $n = 0$ term in Eq. (A1),

$$H_v^{(1)}(z) \sim \sqrt{\frac{2}{\pi z(iv/z)}} e^{-iv/4} e^{-v+v\xi} = -i\sqrt{\frac{2}{\pi v}} \left(\frac{2v}{ez}\right)^v. \quad (\text{A11})$$

Since $\gamma = i \ln(2v/z) = i \ln|2v/z| - \arg(v/z)$, one notes from Eq. (A4b) that the validity of Eq. (A11) is restricted to that portion of region I in Fig. A1(a), in which $-\pi < \arg(v/z) < 0$. Expressions appropriate to other portions of the complex v plane, obtained in a similar manner, are summarized below, and apply in the range $|\arg(v/z)| < \pi$:

$$\left(e^{i(\pm 1-1)\pi/4}\sqrt{\frac{2}{\pi v}}\left(\frac{2v}{ez}\right)^{\mp v}, \quad \arg\left(\frac{v}{z}\right) \geq 0,\right. \quad \text{in region I,} \quad (\text{A12a})$$

$$H_v^{(1)}(z) \sim \begin{cases} -i\sqrt{\frac{2}{\pi v}}\left(\frac{2v}{ez}\right)^v, & \text{in region II,} \\ -\sqrt{\frac{2}{\pi v}}e^{-iv}\left(\frac{2v}{ez}\right)^{-v}, & \text{in region III.} \end{cases} \quad (\text{A12b})$$

$$\left(e^{i(\pm 1+1)\pi/4}\sqrt{\frac{2}{\pi v}}\left(\frac{2v}{ez}\right)^{\pm v}, \quad \arg\left(\frac{v}{z}\right) \geq 0,\right. \quad \text{in region IV,} \quad (\text{A13a})$$

$$H_v^{(2)}(z) \sim \begin{cases} i\sqrt{\frac{2}{\pi v}}\left(\frac{2v}{ez}\right)^v, & \text{in region V,} \\ -\sqrt{\frac{2}{\pi v}}e^{iv}\left(\frac{2v}{ez}\right)^{-v}, & \text{in region VI.} \end{cases} \quad (\text{A13b})$$

$$\left(-\sqrt{\frac{2}{\pi v}}e^{iv}\left(\frac{2v}{ez}\right)^{-v}, \quad \text{in region VI.} \right) \quad (\text{A13c})$$

These formulas are continuous across the lines $\arg(v/z) = 0$ and $|\arg(v/z)| = \pi$, and may therefore be employed also on these boundaries. The continuity across the line $\arg(v/z) = 0$ is evident. To show the equality of Eqs. (A12a) and (A12c) on the line $\arg(v/z) = \pm\pi$, it is noted that the values of v in regions I and III are related there via $v_I = v_{III}e^{\pm i\pi}$. Similar considerations apply to Eqs. (A13a) and (A13c). The factors $(2v/ez)^{\pm v}$ approach unit magnitude near the curves C_2 and C_4 , while $|(2ve^{\pm i\pi}/ez)^v| \rightarrow 1$ near the curves $C_{1,3}$. In the vicinity of any of these contours, the pertinent expressions for $H_v^{(1),(2)}$ are given by the formulas valid on either side.

The asymptotic formula for the Bessel function is obtained directly from the power-series expansion

$$J_v(z) = \sum_{n=0}^{\infty} \frac{(-1)^n (z/2)^{v+2n}}{n! \Gamma(v+n+1)}, \quad (\text{A14})$$

upon substitution of the large-argument expression for the gamma function,

$$\Gamma(v+\alpha) \sim \sqrt{\frac{2\pi}{v}} \left(\frac{v}{e}\right)^v v^\alpha, \quad |v| \rightarrow \infty, \quad |\arg v| < \pi, \quad \alpha > 0. \quad (\text{A15})$$

Thus,

$$J_\nu(z) \sim \frac{1}{\sqrt{2\pi\nu}} \left(\frac{2\nu}{ez}\right)^{-\nu}, \quad |\arg \nu| < \pi. \quad (\text{A16})$$

Equations (A12) and (A13) could also have been derived from Eq. (A16) and the formula

$$H_\nu^{(1,2)}(z) = \frac{J_{-\nu}(z) - e^{\mp i\nu\pi} J_\nu(z)}{\pm i \sin \nu\pi}. \quad (\text{A17})$$

To assess the magnitude of the factor $(2\nu/ez)^{\pm\nu}$, we let

$$\nu = \zeta e^{i\psi}, \quad \zeta = |\nu| \rightarrow \infty, \quad (\text{A18a})$$

to obtain

$$\left| \left(\frac{2\nu}{ez} \right)^{\pm\nu} \right| = \exp \left\{ \pm \zeta \left[\cos \psi \ln \frac{2\zeta}{e|z|} - \sin \psi (\psi - \arg z) \right] \right\}. \quad (\text{A18b})$$

This term grows faster than exponentially whenever $\pm \cos \psi > 0$, decays whenever $\pm \cos \psi < 0$, and assumes unit magnitude only when $|\psi| \rightarrow \pi/2$ [see Eq. (A21)]. Hence, the Hankel functions grow faster than exponentially as $|\nu| \rightarrow \infty$ everywhere except when $|\psi| \rightarrow \pi/2$. In the latter range (i.e., near the curves $C_{1,2,3,4}$) the simple expressions in Eqs. (A12) and (A13) must be modified as mentioned above, and a study of the resulting formulas reveals that for $|\nu| \rightarrow \infty$, $H_\nu^{(1)}(z)$ is small in the region between the curves C_1 and C_4 but large outside this region, while $H_\nu^{(2)}(z)$ is small in the region between the curves C_2 and C_3 but large outside this region. $J_\nu(z)$ in Eq. (A16) decays to the right of the curves C_2 and C_4 but increases elsewhere. On the imaginary axis, for z positive real,

$$H_\nu^{(1)}(z), J_\nu(z) \sim O[\zeta^{-1/2} e^{\zeta\pi/2}]; \quad H_\nu^{(2)}(z) \sim O[\zeta^{-1/2} e^{-\zeta\pi/2}], \quad \psi = \frac{\pi}{2}, \quad (\text{A19a})$$

$$H_\nu^{(1)}(z) \sim O[\zeta^{-1/2} e^{-\zeta\pi/2}]; \quad H_\nu^{(2)}(z), J_\nu(z) \sim O[\zeta^{-1/2} e^{\zeta\pi/2}], \quad \psi = -\frac{\pi}{2}. \quad (\text{A19b})$$

Because of its bearing on the cylinder diffraction problem in the text, we now consider behavior of $H_\nu^{(1,2)}(z)$, $(\partial/\partial z)H_\nu^{(1)}(z)$, $(\partial/\partial v)H_\nu^{(1)}(z)$, and $J_\nu(z)$ on the curve C_2 , as well as that of $H_\nu^{(1)}(y)$, $y \neq z$. In the vicinity of C_2 , the asymptotic approximation of $H_\nu^{(1)}(z)$ comprises the sum of Eqs.(A12a) and (A12b):

$$H_\nu^{(1)}(z) \sim \sqrt{\frac{2}{\pi\nu}} \left[\left(\frac{2\nu}{ez} \right)^{-\nu} - i \left(\frac{2\nu}{ez} \right)^\nu \right]. \quad (\text{A20})$$

Each term inside the brackets takes on unit magnitude when

$$\psi = \frac{\pi}{2} - \delta, \quad \delta \cong \frac{\pi}{2 \ln(2\zeta/ez)} \quad \text{or} \quad \zeta = \frac{ez}{2} e^{\pi/2\delta}, \quad (\text{A21})$$

where z is assumed to be positive real for convenience. Equation (A21) actually defines the distant portions of the curve C_2 on which the zeros of $H_\nu^{(1)}(z)$ are located since Eq. (A20) can vanish only when each of the exponential terms

has the same magnitude. One observes from a comparison of Eqs. (A19) and (A21) that all functions vary extremely rapidly as $|\psi| \rightarrow \pi/2$.

Since the distant zeros of $H_v^{(1)}(y)$, y positive and unequal to z , also have $|\psi| \rightarrow \pi/2$, the representation of $H_v^{(1)}(y)$ near C_2 likewise comprises the two terms in Eq.(A20). On C_2 ,

$$\delta \ln \frac{2\zeta}{ey} = \delta \ln \left(\frac{z}{y} e^{\pi/2\delta} \right) = \frac{\pi \ln(z/y)}{2 \ln(2\zeta/ez)} + \frac{\pi}{2}. \quad (\text{A22a})$$

so

$$\left| \left(\frac{2\psi}{ey} \right)^{\pm v} \right| = \exp \left[\pm \frac{\zeta \pi}{2} \frac{\ln(z/y)}{\ln(2\zeta/ez)} \right]. \quad (\text{A22b})$$

Thus, one or the other of the terms in Eq. (A20) (with z replaced by y) dominates when $z > y$ or $z < y$, respectively, and one finds for any positive y ,

$$|H_v^{(1)}(y)| \sim \sqrt{\frac{2}{\pi\zeta}} \exp \left[\frac{\zeta\pi}{2} \frac{|\ln(z/y)|}{\ln(2\zeta/ez)} \right] \text{ on } C_2, \quad \text{as } \zeta \rightarrow \infty. \quad (\text{A23})$$

Upon differentiating Eq. (A20) with respect to v , noting that $|(2\psi/ez)^{\pm v}|$ is $O(1)$ on C_2 and that the terms in the brackets of Eq. (A20) must cancel at the zeros of $H_v^{(1)}(z)$, one finds that

$$\frac{\partial}{\partial v} H_v^{(1)}(z) \sim O \left(\frac{\ln(2\zeta/ez)}{\sqrt{\zeta}} \right), \quad (\text{A24})$$

along C_2 and at the zeros of $H_v^{(1)}(z)$. Similarly,

$$\frac{\partial}{\partial z} H_v^{(1)}(z) \sim O(\sqrt{\zeta}), \quad (\text{A25})$$

and, also,

$$J_v(z) \sim O \left(\frac{1}{\sqrt{\zeta}} \right), \quad H_v^{(2)}(z) \sim O \left(\frac{1}{\sqrt{\zeta}} \right), \quad \zeta \rightarrow \infty, \quad (\text{A26})$$

along C_2 and at the zeros of $H_v^{(1)}(z)$.

Since

$$H_{-v}^{(1,2)}(z) = e^{\pm iv\pi} H_v^{(1,2)}(z), \quad (\text{A27})$$

the zeros of $H_v^{(1,2)}(z)$ are disposed symmetrically with respect to the origin in the complex v plane as indicated by the curves C_1 , C_2 and C_3 , C_4 . One may also verify that the locus of the zeros of $(d/dz)H_v^{(1)}(z)$ behaves in a manner similar to $C_{1,2}$ as $v \rightarrow \infty$.

6A.4 Large and Almost Equal Order and Argument

When $v \approx z$, then $\gamma \rightarrow 0$ in the Debye expansions in Eqs. (A1)–(A7) and the resulting expressions become invalid. In this range the Hankel functions can be approximated by Airy functions that provide the means of passing smoothly from the region $|v - z| > O(|v|^{1/3})$, wherein the Debye formulas are valid, to the region $|v - z| \leq O(|v|^{1/3})$. The expressions below have been obtained by Olver.³⁰

If an arbitrary complex number τ is defined by the relation

$$z = v + \tau v^{1/3}, \quad (\text{A28})$$

then $H_v^{(1,2)}(z)$ has the asymptotic expansion as $v \rightarrow \infty$,

$$\begin{aligned} H_v^{(1,2)}(z) &\sim \frac{2^{1/3}}{v^{1/3}} [\text{Ai}(-2^{1/3}\tau) \mp i \text{Bi}(-2^{1/3}\tau)] \sum_{n=0}^{\infty} \frac{A_n(\tau)}{v^{2n/3}} \\ &+ \frac{2^{1/3}}{v^{1/3}} [\text{Ai}'(-2^{1/3}\tau) \mp i \text{Bi}'(-2^{1/3}\tau)] \sum_{n=0}^{\infty} \frac{B_n(\tau)}{v^{2n/3}}, \end{aligned} \quad (\text{A29})$$

where the first few coefficients are

$$\begin{aligned} A_0 &= 1, \quad A_1 = -\frac{\tau}{5}, \quad A_2 = -\frac{9}{100}\tau^5 + \frac{3}{35}\tau^2, \\ B_0 &= 0, \quad B_1 = \frac{3}{10}\tau^2, \quad B_2 = -\frac{17}{3}\tau^3 + \frac{1}{70}. \end{aligned} \quad (\text{A29a})$$

The expansion for $H_v^{(1)}(z)$ is valid when $-\pi/2 < \arg v < 3\pi/2$, while that for $H_v^{(2)}(z)$ applies when $-3\pi/2 < \arg v < \pi/2$. For values of v outside these ranges, one may employ Eq. (A27). $\text{Ai}(x)$, $\text{Bi}(x)$ and $\text{Ai}'(x)$, $\text{Bi}'(x)$, denote the Airy functions and their x derivatives, respectively (see Chapter 4, Appendix B). To identify the $n = 0$ term in Eq. (A29) with the similar result in Eq. (4.5.33), one observes from Eq. (4.5.35a) that η in these equations is given approximately by

$$\eta \approx 2^{1/3}\tau z^{-2/3}, \quad z \approx v. \quad (\text{A30})$$

Expressions for the derivatives $(d/dz)H_v^{(1,2)}(z) \equiv H_v'^{(1,2)}(z)$ are obtained by differentiation of the asymptotic series for $H_v^{(1,2)}(z)$. The Airy functions and their zeros are tabulated in Reference 32.

6A.5 The Zeros of $H_v^{(1)}(z)$, $H_v'^{(1)}(z)$, and Related Results

From the results in the preceding section, it is noted that the zeros of $H_v^{(1,2)}(z)$ or $H_v'^{(1,2)}(z)$ when $v \approx z$, $|z|$ large, are given in first approximation by the zeros of the appropriate Airy function combinations or their derivatives.

Since the Airy differential equation

$$\left(\frac{d^2}{d\sigma^2} + \sigma \right) \text{Ai}(-\sigma) \text{Bi}(-\sigma) = 0 \quad (\text{A31})$$

is also solved by $\sqrt{\sigma} Z_{1/3}(\frac{2}{3}\sigma^{3/2})$, where $Z_{1/3}(x)$ is any Bessel function of order $\frac{1}{3}$ and argument x , one finds from a comparison of the large- σ asymptotic solution for the function $A_1(-\sigma)$ [see Eqs. (4.2.51)] and the Hankel function of order $1/3$ that

$$\begin{aligned} A_1(-\sigma) \equiv \text{Ai}(-\sigma) - i \text{Bi}(-\sigma) &= e^{i\pi/6} \sqrt{\frac{\sigma}{3}} H_{1/3}^{(1)}(\frac{2}{3}\sigma^{3/2}) \\ &= -2e^{-i2\pi/3} \text{Ai}(-\sigma e^{-i2\pi/3}). \end{aligned} \quad (\text{A32})$$

Although it is more convenient to deal directly with the Airy function formu-

lation [see Eqs. (A39)], many investigations in the literature have utilized the $\frac{1}{3}$ -order Bessel functions; for this reason, both treatments are included. Upon introducing the change of variable

$$\frac{2}{3}\sigma^{3/2} = \xi e^{-i\pi}, \quad (\text{A33})$$

and employing Eq. (A17), one may show that the zeros $\tilde{\xi}_p$ of $H_{1/3}^{(1)}(\xi e^{-i\pi})$ are identical with those of the equation

$$J_{-1/3}(\tilde{\xi}_p) + J_{1/3}(\tilde{\xi}_p) = 0, \quad (\text{A34})$$

which are real. With $\sigma = 2^{1/3}\tau$, $\tau = (z - v)v^{-1/3}$, and z fixed, the zeros $\pm\xi_p$ of $H_v^{(1)}(z)$ are given via Eqs. (A29), (A33), and (A34) by

$$\xi_p \sim z + 2^{-1/3}(\frac{3}{2}\tilde{\xi}_p)^{2/3}e^{i\pi/3}z^{1/3}, \quad H_{\xi_p}^{(1)}(z) = 0, \quad \tilde{\xi}_p > 0. \quad (\text{A35})$$

To a first approximation, the zeros of $H_v^{(1)}(z)$ coincide with those of $A'_i(-2^{1/3}\tau) \equiv A'_i(-\sigma)$, which, in view of the formula

$$\frac{d}{d\xi} [\xi^\mu H_\mu^{(1)}(\xi e^{-i\pi})] = \xi^\mu H_{\mu-1}^{(1)}(\xi e^{-i\pi}) \quad (\text{A36})$$

applied to $\mu = \frac{1}{3}$, and Eqs. (A17), (A32), and (A33), can be seen to be derivable from the purely real zeros $\tilde{\eta}_p$ of the equation

$$J_{2/3}(\tilde{\eta}_p) - J_{-2/3}(\tilde{\eta}_p) = 0. \quad (\text{A37})$$

If $\pm\eta_p$ denotes the zeros of $H_v^{(1)}(z)$ in the complex v plane, then

$$\eta_p \sim z + 2^{-1/3}(\frac{3}{2}\tilde{\eta}_p)^{2/3}e^{i\pi/3}z^{1/3}, \quad H'_{\eta_p}^{(1)}(z) = 0, \quad \tilde{\eta}_p > 0. \quad (\text{A38})$$

If z is positive real, the zeros of $H_v^{(2)}(z)$ and $H_v^{(2)}(z)$ are given by the complex conjugates of ξ_p and η_p , respectively.

The zeros ξ_p and $\tilde{\eta}_p$ can also be expressed as zeros of the Airy function $\text{Ai}(-\alpha)$ or of its derivative. From Eqs. (4.2.32) and (4.2.34) one may verify that

$$A_1(-\alpha e^{-i2\pi/3}) = -2e^{i2\pi/3} \text{Ai}(-\alpha), \quad \alpha = (\frac{3}{2}\xi)^{2/3}, \quad (\text{A39a})$$

$$A_2(-\alpha e^{-i2\pi/3}) = e^{i2\pi/3}A_1(-\alpha), \quad A_{2,1}(x) \equiv \text{Ai}(x) \pm i \text{Bi}(x), \quad (\text{A39b})$$

whence the $\tilde{\xi}_p$ also satisfy the equation

$$\text{Ai}(-\bar{\alpha}_p) = 0, \quad \bar{\alpha}_p = (\frac{3}{2}\tilde{\xi}_p)^{2/3}, \quad (\text{A40})$$

while for the $\tilde{\eta}_p$,

$$\text{Ai}'(-\bar{\beta}_p) = 0, \quad \bar{\beta}_p = (\frac{3}{2}\tilde{\eta}_p)^{2/3}. \quad (\text{A41})$$

$\bar{\alpha}_p$ and $\bar{\beta}_p$ are tabulated in reference 32. The first few zeros are

$$\begin{aligned} \bar{\alpha}_1 &= 2.3381, & \bar{\alpha}_2 &= 4.0879, & \bar{\alpha}_3 &= 5.5205, \\ \bar{\beta}_1 &= 1.0188, & \bar{\beta}_2 &= 3.2482, & \bar{\beta}_3 &= 4.8201. \end{aligned} \quad (\text{A41a})$$

One also verifies from Eqs. (A29) that

$$\frac{\partial H_v^{(1,2)}(z)}{\partial v} \sim -H_v^{(1,2)}(z) \sim \left(\frac{2}{v}\right)^{2/3} A'_i(-2^{1/3}\tau), \quad (\text{A42a})$$

$$\frac{\partial H_v^{(1,2)}(z)}{\partial v} \sim -\frac{d^2 H_v^{(1,2)}(z)}{dz^2} = \left(1 - \frac{v^2}{z^2}\right) H_v^{(1,2)}(z) + \frac{1}{z} H_v'^{(1,2)}(z), \quad (\text{A42b})$$

with the last equality resulting from the Bessel differential equation.

The preceding expressions are the lowest-order asymptotic approximations and can be improved by developing the pertinent quantities in asymptotic series involving inverse powers of z . Such expansions have been obtained by a number of investigators; including the second terms in the expansions, one finds^{14,33}

$$\xi_p \sim z + \left(\frac{z}{2}\right)^{1/3} \left[t_p + \left(\frac{2}{z}\right)^{2/3} \frac{t_p^2}{60} + \dots \right], \quad t_p = \bar{\alpha}_p e^{i\pi/3}, \quad (\text{A43a})$$

$$\left[\frac{1}{\partial H_v^{(1)}(z)/\partial v}\right]_{v=\xi_p} \sim \frac{1}{2} \left(\frac{z}{2}\right)^{2/3} \frac{e^{-i\pi/3}}{\text{Ai}'(-\bar{\alpha}_p)} \left[1 + \left(\frac{2}{z}\right)^{2/3} \frac{t_p}{10} + \dots \right], \quad (\text{A43b})$$

$$\eta_p \sim z + \left(\frac{z}{2}\right)^{1/3} \left[q_p + \left(\frac{2}{z}\right)^{2/3} \frac{q_p^2}{60} \left(1 + \frac{8}{3\bar{\eta}_p^2}\right) + \dots \right], \quad q_p = \bar{\beta}_p e^{i\pi/3}, \quad (\text{A44a})$$

$$\left[\frac{1}{\partial H_v'^{(1)}(z)/\partial v}\right]_{v=\eta_p} \sim \frac{1}{[1 - (\eta_p/z)^2] H_{\eta_p}^{(1)}(z)} \left[1 + \frac{1}{6} q_p \left(\frac{2}{z}\right)^{2/3} + \dots \right], \quad (\text{A44b})$$

where for the first few values of p ,

$$\begin{aligned} \text{Ai}(-\bar{\beta}_1) &= +0.5356, & \text{Ai}(-\bar{\beta}_2) &= -0.4190, & \text{Ai}(-\bar{\beta}_3) &= +0.3804, \\ \text{Ai}'(-\bar{\alpha}_1) &= +0.7012, & \text{Ai}'(-\bar{\alpha}_2) &= -0.8031, & \text{Ai}'(-\bar{\alpha}_3) &= +0.8652. \end{aligned} \quad (\text{A44c})$$

The preceding discussion has dealt with the zeros of $H_v^{(1,2)}(z)$ and $H_v'^{(1,2)}(z)$ in the complex v plane when the large parameter z is specified and $v \approx z$. It can be shown, however, that the magnitude of the zeros is always greater than z , so ξ_p and η_p in Eqs. (A35) and (A38) do indeed constitute the first zeros of $H_v^{(1)}(z)$ and $H_v'^{(1)}(z)$, respectively. These zeros lie on a straight line which, for real z , departs into the first quadrant at an angle of 60° from the point $v = z$ (see Fig. 6.A.1). They are of the first order and infinite in number, but their value as $|\xi_p| \rightarrow \infty$ or $|\eta_p| \rightarrow \infty$ is no longer given by the equations above; instead, they are derived from the representations in Eqs. (A12), which are appropriate to the range $|v| \rightarrow \infty$. One finds that $\arg \eta_p \rightarrow \pi/2$ [see Eq. (A21)], whence, as indicated in Fig. 6A.1, the locus of zeros bends toward the vertical direction as $|\eta_p| \rightarrow \infty$.³⁴

APPENDIX 6B.

MISCELLANEOUS FORMULAS INVOLVING CYLINDER FUNCTIONS

The product of two modified Hankel functions of imaginary argument can be represented as³

$$K_{iv}(a) K_{iv}(b) = \frac{1}{2} \int_{-\infty}^{\infty} K_0(\sqrt{a^2 + b^2 + 2ab \cosh x}) e^{ixv} dx, \quad v \text{ real}, \quad (\text{B1})$$

where a and b are assumed to be positive and the square root is positive. Because of the asymptotic behavior of $K_0(|y|) \sim |y|^{-1/2} \exp(-|y|)$, $|y| \rightarrow \infty$, the integrand decays faster than exponentially as $|x| \rightarrow \infty$. The integral remains convergent when a and b are imaginary since $|H_0^{(1)}(\sqrt{\alpha + \beta} \cosh x)| \sim \exp(-|x|/4)$ as $|x| \rightarrow \infty$, with α, β real. Upon employing the formula

$$K_{\nu}(-i\xi) \equiv \frac{\pi i}{2} e^{-\nu\pi/2} H_{\nu}^{(1)}(\xi), \quad (B2)$$

one obtains, from Eq. (B1),

$$H_{\nu\nu}^{(1)}(\xi) H_{\nu\nu}^{(1)}(\eta) = \frac{1}{\pi i} \int_{-\infty}^{\infty} H_0^{(1)}(\sqrt{\xi^2 + \eta^2 + 2\xi\eta \cosh x}) e^{(ix+\pi)\nu} dx, \quad (B3)$$

where ξ and η and the square root are assumed positive.

The Hankel function of arbitrary order μ and argument x can be represented by the Sommerfeld integral,

$$H_{\mu}^{(1)}(x) = \frac{1}{\pi} \int_{i\infty-\epsilon}^{-i\infty+\epsilon} e^{ix \cos w} e^{i\mu(w-\pi/2)} dw, \quad (B4)$$

with ϵ chosen so that the integral converges. For positive real x and arbitrary μ , one has $0 < \epsilon < \pi$. If μ is imaginary, one may verify that

$$\lim_{a \rightarrow \infty} \int_{ia}^{ia-\epsilon} e^{ix \cos w + i\mu(w-\pi/2)} dw = 0, \quad (B5)$$

so the integration path may be deformed into the imaginary axis. Thus, for real ν and positive x ,

$$H_{\nu\nu}^{(1)}(x) = \frac{1}{\pi} \int_{i\infty}^{-i\infty} e^{ix \cos w} e^{-\nu(w-\pi/2)} dw. \quad (B6)$$

P R O B L E M S

1. Show that the high-frequency asymptotic solution for the time-harmonic point source Green's function for a wedge, comprising the geometric optical contribution in Eq. (6.3.30a) and the diffracted contribution in Eq. (6.3.30b), can be constructed from the corresponding plane wave results in Eqs. (6.3.28a) and (6.3.28b) on application of the ray optical method discussed in Sec. 1.7d.
2. Derive the time-harmonic electromagnetic fields described by the scalar line source Green's functions for a perfectly conducting wedge [see Eqs. (6.5.12) and (6.5.13)] and show that the fields satisfy the edge condition of Eq. (1.5.37). Repeat the calculation for the fields excited by an axial electric or magnetic dipole source [see Eq. (6.5.23)].
3. Expand the time-dependent point source Green's functions for a perfectly conducting wedge, as given in Eq. (6.5.26), in powers of $(t - t') - (L/c)$, where $t = t' + L/c$ denotes the time of arrival of the wavefronts and L is an appropriate distance parameter, to obtain series of the form (1.7.81). Show that on use in Eq. (1.7.80) of the leading expansion coefficients, one may construct the time-harmonic high-frequency asymptotic result in Eqs. (6.5.24a) and (6.5.25a).

4. Use the procedure detailed in connection with Eq. (6.4.9) to derive higher order terms in the asymptotic expansion of the diffracted part of the Green's function for a wedge with a linearly varying surface impedance [see Eqs. (6.6.6) and (6.6.18b)].

5. A distribution of magnetic currents

$$\mathbf{M}(\rho) = \mathbf{z}_0 M_0 e^{i\xi\rho} e^{-i\omega t}, \quad l_1 < \rho < l_2, \quad (1)$$

with $M_0 = \text{constant}$, is located on the $\phi = 0$ face of a perfectly conducting wedge and simulates radiation from an array of axial line sources progressively phased in the ρ direction; the second wedge face is located at $\phi = \varphi$. The radiated magnetic field $H = H_z$ is parallel to the edge (z axis) and is given by :

$$H_z(\rho) = ik \sqrt{\frac{\epsilon}{\mu}} \int_{l_1}^{l_2} [\bar{G}''(\rho, \rho') M(\rho')]_{\phi'=0} d\rho', \quad (2)$$

where $\bar{G}''(\rho, \rho')$ is the H -mode Green's function in Sec. 6.5c, whose asymptotic form for large ρ is given in Eqs. (6.5.19) and (6.5.20). Show that for $\rho \rightarrow \infty$, $kl_1 \gg 1$, and $\varphi > \pi$, the magnetic field in Eq. (2) is given for arbitrary ϕ by :

$$H_z(\rho) \sim i k l_1 \sqrt{\frac{\epsilon}{\mu}} M_0 \frac{e^{i(k\rho + (\pi/4))}}{\sqrt{2\pi k\rho}} [A(\xi, k, \phi) + B(\xi, k, \phi) + C(\xi, k, \phi)], \quad (3)$$

where

$$\begin{aligned} A(\xi, k, \phi) &= \frac{e^{i2(\gamma_2^2 - \delta_2^2)} - e^{i2(\gamma_1^2 - \delta_1^2)}}{i2(\gamma_1^2 - \delta_1^2)} U(\pi - \phi) \\ &= e^{i(\xi - k \cos \phi)(l_1 + l)} \frac{2 \sin [(\xi - k \cos \phi)l]}{(\xi - k \cos \phi)l} U(\pi - \phi), \quad 2l = l_2 - l_1, \end{aligned} \quad (3a)$$

$$\begin{aligned} B(\xi, k, \phi) &= \frac{i\pi}{2\varphi} \sin \frac{\pi^2}{\varphi} \frac{1}{[\cos(\pi^2/\varphi) - \cos(\pi\phi/\varphi)]} \frac{1}{\gamma_1 \sqrt{kl_1}} \\ &\times [e^{i2\gamma_1^2} F(\gamma_1) - e^{i2\gamma_2^2} F(\gamma_2)], \end{aligned} \quad (3b)$$

$$\begin{aligned} C(\xi, k, \phi) &= \text{sgn}(\pi - \phi) \frac{i}{4(\gamma_1^2 - \delta_1^2)} \left\{ e^{i2\gamma_2^2} \left[F(\delta_2) - \frac{\gamma_2}{\delta_2} F(\gamma_2) \right] \right. \\ &\left. - e^{i2\gamma_1^2} \left[F(\delta_1) - \frac{\gamma_1}{\delta_1} F(\gamma_1) \right] \right\}, \end{aligned} \quad (3c)$$

$$\begin{aligned} \gamma_{1,2} &= \sqrt{\left(\frac{k+\xi}{2}\right)l_{1,2}}, \quad \delta_{1,2} = \sqrt{kl_{1,2}} \left| \cos \frac{\phi}{2} \right|, \\ \gamma_2^2 - \delta_2^2 &= \frac{l_2}{2} (\xi - k \cos \phi) = \frac{l_2}{l_1} (\gamma_1^2 - \delta_1^2), \\ F(y) &= \frac{2}{\sqrt{\pi}} e^{-iy^2} \int_{(1-i)y}^{\infty} e^{-x^2} dx. \end{aligned} \quad (3d)$$

Show that $A(\xi, k, \phi)$ represents the angular pattern function when the source distribution is contained in an infinite plane, that the effect of the edge outside the transition region $\phi \approx \pi$ is given by $B(\xi, k, \phi)$, and that the entire expression (3) is required to yield the field behavior in the transition domain. More precisely, note that the exterior of the transition region is defined by $\delta_1 \gg 1$ and

that since C is $O(\delta_1^{-2})$, it can be neglected in this range. Verify the evaluation of the following integrals, required for calculation of the result in Eq. (3) :

$$I_1 = \int_a^b \frac{e^{i\alpha\rho}}{\sqrt{\rho}} d\rho = e^{i\pi/4} \sqrt{\frac{\pi}{\alpha}} \left[e^{i\alpha a} F\left(\sqrt{\frac{\alpha a}{2}}\right) - e^{i\alpha b} F\left(\sqrt{\frac{\alpha b}{2}}\right) \right]. \quad (4)$$

$$I_2 = \int_a^b d\rho e^{i\alpha\rho} F(\beta\sqrt{\rho}) = I'_2 + I''_2, \quad (5)$$

where

$$I'_2 = \frac{2}{\sqrt{\pi}} \int_a^b d\rho e^{i\gamma\rho} \int_{(1-i)\beta\sqrt{b}}^{\infty} dx e^{-x^2} = \frac{e^{iyb} - e^{ya}}{i\gamma} \frac{2}{\sqrt{\pi}} S(\beta\sqrt{b}), \quad (5a)$$

$$I''_2 = \frac{2}{\sqrt{\pi}} \int_a^b d\rho e^{i\gamma\rho} \int_{(1-i)\beta\sqrt{\rho}}^{(1-i)\beta\sqrt{b}} dx e^{-x^2}, \quad (5b)$$

with

$$S(y) = \int_{(1-i)y}^{\infty} dx e^{-x^2}, \quad \gamma = \alpha - 2\beta^2. \quad (6)$$

For the evaluation of I''_2 , interchange the order of integration and obtain :

$$\begin{aligned} I''_2 &= \frac{2}{\sqrt{\pi}} \int_{(1-i)\beta\sqrt{a}}^{(1-i)\beta\sqrt{b}} dx e^{-x^2} \int_a^{(ix^2/2\beta^2)} d\rho e^{i\gamma\rho} \\ &= -\frac{2}{\sqrt{\pi}} \frac{1}{i\gamma} e^{iy\alpha} [S(\beta\sqrt{a}) - S(\beta\sqrt{b})] \\ &\quad + \frac{2}{\sqrt{\pi}} \frac{1}{i\gamma\sqrt{\delta}} [S(\beta\sqrt{\delta a}) - S(\beta\sqrt{\delta b})], \quad \delta = 1 + \frac{\gamma}{2\beta^2} = \frac{\alpha}{2\beta^2}, \end{aligned} \quad (7)$$

whence

$$I_2 = \frac{1}{i\gamma} \left\{ e^{i\alpha b} \left[F(\beta\sqrt{b}) - \frac{1}{\sqrt{\delta}} F\left(\sqrt{\frac{\alpha b}{2}}\right) \right] - e^{i\alpha a} \left[F(\beta\sqrt{a}) - \frac{1}{\sqrt{\delta}} F\left(\sqrt{\frac{\alpha a}{2}}\right) \right] \right\} \quad (8)$$

6. A perfectly conducting half-plane occupying the region $y < 0$ in the $z = 0$ plane is illuminated by a plane wave incident at an angle θ_0 with respect to the z axis (Fig. P6.1). The incident wave is polarized so that its electric vector is parallel to the edge whence, due to translational symmetry along x , the total electric field E has only an x component.

- (a) Show that on use of Eq. (5.4.26a) and the equivalence theorem leading to Eq. (1.5.33), the secondary field E_s produced by the induced currents on the half-plane can be expressed for a time-dependence $\exp(-i\omega t)$ as

$$E_s(\hat{\mathbf{p}}) = -\frac{\omega\mu}{4} \int_{-\infty}^0 H_0^{(1)}(k|\hat{\mathbf{p}} - \hat{\mathbf{p}}'|) J(y') dy', \quad \hat{\mathbf{p}} = (y, z) \quad (9)$$

where the x -directed currents $J(y')$ flow on both sides of the screen. Show that the requirement $E = 0$ on the screen, where

$$E = E_i + E_s, \quad E_i = e^{ik(z \cos \theta_0 + y \sin \theta_0)}, \quad (10)$$

is the total electric field, also satisfies the edge condition (1.5.37), and derive on substitution of Eq. (9) an integral equation for the induced currents $J(y)$ (see also Problem 11 of Chapter 1). While the integral equation can be solved by

the Wiener-Hopf technique,[†] utilize the physical optics approximation for the evaluation of the scattered field, and assume that the induced currents are the same as for an infinite plane at $z = 0$. Thus, on the illuminated side $z = -0$,

$$J(y) \approx 2H_{y1}|_{z=0} = \frac{2k \cos \theta_0}{\mu \omega} e^{iky \sin \theta_0}, \quad (11)$$

while on the dark side $z = +0$, one takes $J(y) \approx 0$. For k large, and observation points $\hat{\mathbf{p}}$ sufficiently far from the screen, use the asymptotic form for $H_0^{(1)}$ [see Eq. (5.3.13b)] to show that

$$E_s \approx -\frac{\sqrt{k} \cos \theta_0 e^{-i\pi/4}}{\sqrt{2\pi}} \int_{-\infty}^0 \frac{\exp \{ik[|\hat{\mathbf{p}} - \hat{\mathbf{p}}'| + y' \sin \theta_0]\}}{|\hat{\mathbf{p}} - \hat{\mathbf{p}}'|^{1/2}} dy'. \quad (12)$$

- (b) Evaluate the integral in Eq. (12) by the saddle-point method. Show that there is a saddle point y'_s located at

$$y'_s = y - |z| \tan \theta_0 \quad (13)$$

Interpret the saddle-point condition as shown in Fig. P6.1 and relate to the

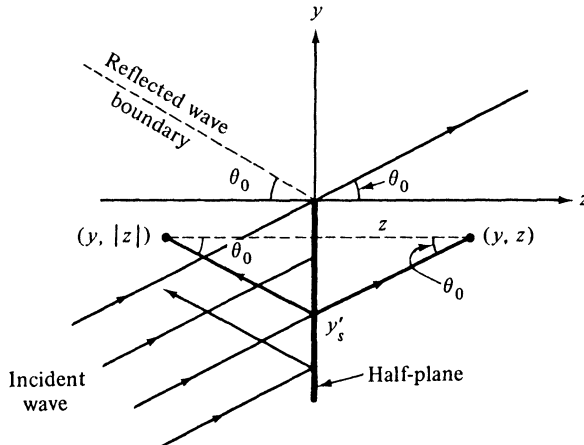
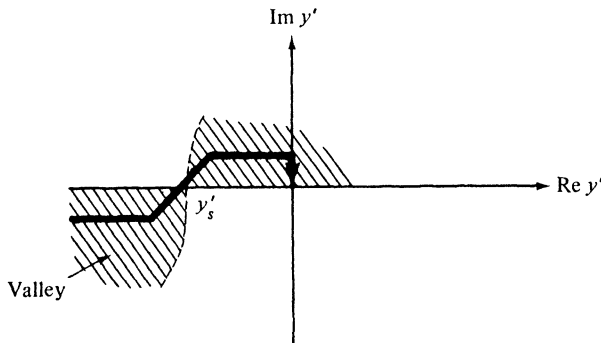


FIG. P6.1 Physical configuration and interpretation of saddle point condition.

geometric optical properties of the field; note in particular the role played by $|z|$ in Eq. (13) (the induced current distribution radiates symmetrically). Verify that the integration path can be deformed through the saddle point as shown in Fig. P6.2, provided that $-\infty < y'_s < 0$. Use the asymptotic formula in Eq. (4.2.20) to obtain the approximate value of the integral in Eq. (12), comprising contributions from the saddle point, when relevant, and from the endpoint $y' = 0$. Show that the saddle-point contribution E_{s1} is given by

$$E_{s1} \sim -e^{ik(|z| \cos \theta_0 + y \sin \theta_0)} \left[1 + O\left(\frac{1}{k}\right) \right], \quad (14a)$$

[†]B. Noble, *Methods Based on the Wiener-Hopf Technique for the Solution of Partial Differential Equations*, Pergamon Press, New York (1958), Chapter 2.

FIG. P6.2 Deformed integration path in y' -plane.

while the endpoint contribution E_{s2} is

$$E_{s2} \sim \frac{-\cos \theta_0}{\sin \theta - \sin \theta_0} \frac{e^{i[k\hat{\rho} + (\pi/4)]}}{\sqrt{2\pi k \hat{\rho}}} \left[1 + O\left(\frac{1}{k}\right) \right], \quad \sin \theta = \frac{y}{\hat{\rho}} = \frac{y}{\sqrt{y^2 + z^2}} \quad (14b)$$

Add the incident field E_i to the secondary field $E_{s1} + E_{s2}$ and interpret the result in ray-optical terms. Comment particularly on the role of the saddle point y'_s and the endpoint $y' = 0$ in selecting those portions of the induced current distribution that are principally responsible for establishing the field at a given observation point (y, z) . Compare with the ray-optical construction in Fig. 1.7.8, with $n_1 = n_2$ [the factor $\exp(ik_0 n R_8)/R_8$ in Eq. (1.7.64d) should be set equal to unity for an incident plane wave]. When $y'_s \rightarrow 0$, improve the asymptotic evaluation by use of the uniform approximation in Sec. 4.6a.

(c) Compare the results of part (b) with the asymptotic approximation of the exact solution [Eq. (6.5.29), with $\varphi = 2\pi$]. Comment on why the geometric-optical portion of the field in part (b) is given correctly whereas the diffracted portion is not. Show from the exact field solution in Eq. (6.5.43) that the induced currents are given exactly by :

$$J(y') = \frac{k}{\omega \mu} \left\{ 2 \cos \theta_0 e^{iky' \sin \theta_0} + 2 \sqrt{\frac{2}{-\pi k y'}} e^{-i[ky' - \pi/4]} \cdot \sin \frac{\phi'}{2} [1 - 2\sqrt{2} \xi e^{-i[2\xi^2 + (\pi/4)]} Q[(1-i)\xi]] \right\} \quad (15)$$

where $Q[(1-i)\xi] \equiv S(\xi)$ in Eq. (6) and

$$\xi = \sqrt{-ky'} \cos \frac{\phi'}{2}, \quad \phi' = \frac{\pi}{2} - \theta_0. \quad (15a)$$

The first term in Eq. (15) is the physical optics approximation in Eq. (11); the second represents a rigorous correction and contains the contributions from the illuminated and the dark sides of the half-plane. Show that the correction is appreciable only near the edge [see Fig. 4.4.3(a)], and relate this observation to the validity, or not, of the results in Eqs. (14a) and (14b).

(d) Obtain an improved expression for the diffracted field E_{s2} by substituting Eq. (15) into Eq. (9) and using the asymptotic approximation for the Hankel

function as before. Note that the endpoint contribution due to the physical optics term in Eq. (15) yields Eq. (14). Show that the correction E'_s to E_s arising from the first term inside the large square brackets in Eq. (15) is given by

$$E'_s \sim \frac{-e^{[ik\hat{\beta} + (\pi/4)]}}{\sqrt{2\pi k \hat{\beta}}} \frac{\sqrt{2} \sin(\phi'/2)}{\sqrt{1 + \sin \theta}}, \quad \sqrt{2} \sin \frac{\phi'}{2} = \sqrt{1 - \sin \theta_0}, \quad (16)$$

where it has been noted that $|\hat{\mathbf{p}} - \hat{\mathbf{p}}'| = \hat{\rho} - y' \sin \theta + O(y'^2)$ near $y' = 0$, whence the calculation involves evaluation of the integral

$$I_1 = \int_{-\infty}^0 \frac{e^{-ik(1+\sin\theta)y'}}{\sqrt{-y'}} dy' = \sqrt{\frac{\pi}{-ik(1+\sin\theta)}}. \quad (16a)$$

Note that calculation of the correction E''_s due to the last term in the large square brackets in Eq. (15) requires consideration of the integral

$$I_2 = \int_0^\infty \exp[-ik(1+\sin\theta)y' - i2\xi^2] Q dy' = \int_0^\infty \exp[ik(\sin\theta_0 - \sin\theta)y'] Q dy' \quad (17a)$$

$$= \frac{1}{ik(\sin\theta_0 - \sin\theta)} \int_0^\infty Q \frac{d}{dy'} \exp[ik(\sin\theta_0 - \sin\theta)y'] dy'. \quad (17b)$$

Use integration by parts, and $Q(0) = \sqrt{\pi}/2$, $dQ/d\xi = -(1-i)\exp(2i\xi^2)$, to obtain

$$I_2 = \frac{1}{ik(\sin\theta_0 - \sin\theta)} \left\{ \frac{\sqrt{\pi}}{2} - \frac{e^{-i\pi/4}\sqrt{k}}{\sqrt{2}} \cos \frac{\phi'}{2} \int_0^\infty \frac{e^{-ik(1+\sin\theta)y'}}{\sqrt{-y'}} dy' \right\}, \quad (17c)$$

and evaluate via Eq. (16a). Show that the resulting contribution E''_s is obtained as

$$E''_s \sim \frac{-e^{i[k\hat{\beta} + (\pi/4)]}}{\sqrt{2\pi k \hat{\beta}}} \frac{\cos\theta_0}{(\sin\theta_0 - \sin\theta)} \left[1 - \frac{\sqrt{1 + \sin\theta_0}}{\sqrt{1 + \sin\theta}} \right]. \quad (18)$$

The total diffracted field E_{s2} is comprised of the sum of E'_s , E''_s , and the physical optics formula in Eq. (14b). Show that the resulting expression agrees with the exact formula in Eq. (6.5.29), with $\varphi = 2\pi$.

7. (a) A perfectly conducting wedge formed of the two intersecting half-planes $\phi = 0$ and $\phi = \varphi$ is a “separable” configuration in either a cylindrical or spherical coordinate system. When the wedge is excited by a current element that lies on a straight line passing through the apex at point A , show that the analysis is simplified in spherical coordinates since the element is then radial with respect to an origin chosen at A . [Note that fields due to radial current elements can be derived from a single spherical potential function as in Eqs. (2.6.11).] Discuss how this simplification may be utilized for non-axially oriented tangential magnetic current elements located on one of the wedge faces, and for excitation by small slot radiators represented by such elements.
- (b) Using spherical coordinates, show that the H mode Green’s function $G''(\mathbf{r}, \mathbf{r}')$ is given in a radial transmission representation by [$\exp(-i\omega t)$ dependence]:

$$G''(\mathbf{r}, \mathbf{r}') = \frac{i}{2k\varphi rr'} \sum_{m=0}^{\infty} \epsilon_m \cos p\phi \cos p\phi' f_p(r, r'; \theta, \theta') \quad (19a)$$

where

$$f_p(r, r'; \theta, \theta') = \sum_{n=0}^{\infty} [2(n+p) + 1] \frac{\Gamma(n+2p+1)}{n!} P_{n+p}^{-p}(\cos \theta) \\ \cdot P_{n+p}^{-p}(\cos \theta') j_{n+p}(kr_<) h_{n+p}^{(1)}(kr_>); \quad (19b)$$

$p = (m\pi/\varphi)$, $\epsilon_0 = 1$, and $\epsilon_m = 2$, $m \geq 1$. Use this Green's function to derive the fields radiated by a magnetic current element located on one of the wedge faces. The orientation of the element is arbitrary as long as it is not parallel to the edge. Show that the edge condition is satisfied [see Eq. (1.5.39)]. Repeat for the E -mode Green's function $G'(\mathbf{r}, \mathbf{r}')$.

(c) Derive from Eqs. (19) the result for a plane wave of unit amplitude incident from (θ', ϕ') (Let $r' \rightarrow \infty$, use the asymptotic form for $h_{n+p}^{(1)}(kr')$, and replace $[\exp(ikr')]/4\pi r'$ by unity);

$$u''(\mathbf{r}; \theta', \phi') = \frac{2\pi}{\varphi} \sum_{m=0}^{\infty} \epsilon_m \cos p\phi \cos p\phi' e^{-ip\pi/2} \bar{f}_p(r, \theta; \theta') \quad (20a)$$

where

$$\bar{f}_p(r, \theta; \theta') = \sum_{n=0}^{\infty} [2(n+p) + 1] \frac{\Gamma(n+2p+1)}{n!(kr)} P_{n+p}^{-p}(\cos \theta) \\ \cdot P_{n+p}^{-p}(\cos \theta') j_{n+p}(kr) e^{-in\pi/2}. \quad (20b)$$

By using an analysis in cylindrical coordinates, show that u'' is also given by [see Eqs. (6.5.16b) and (6.2.18)]:

$$u''(\mathbf{r}; \theta', \phi') = \frac{2\pi}{\varphi} e^{-ikr \cos \theta \cos \theta'} \sum_{m=0}^{\infty} \epsilon_m \cos p\phi \cos p\phi' e^{-ip\pi/2} J_p(kr \sin \theta \sin \theta'). \quad (21)$$

Compare Eqs. (20) and (21) to deduce the addition theorem

$$J_p(kr \sin \theta \sin \theta') e^{-ikr \cos \theta \cos \theta'} = \bar{f}_p(r, \theta; \theta'). \quad (22)$$

8. Consider the series

$$S = \sum_{p=1}^{\infty} f(v_p), \quad (23)$$

where the index v_p is assumed to be given by the simple zeros of a certain transcendental function $g(v)$; i.e.,

$$g(v_p) = 0, \quad p = 1, 2, 3, \dots. \quad (24)$$

For example, if $v_p = 1, 2, 3, \dots$, the appropriate function is $g(v) = \sin \pi v$. Assume that $f(v)$ and $g(v)$ are analytic functions almost everywhere in the complex v plane.

(a) Show that S can be expressed in terms of the contour integral

$$S = \frac{1}{2\pi i} \int_C f(v) \frac{dg(v)/dv}{g(v)} dv, \quad (25)$$

where C is a contour which encloses in the positive sense the zeros v_p , $p = 1, 2, \dots$, of $g(v)$, but no other singularities of the integrand.

(b) Apply Eqs. (23) and (25) to the cylinder Green's function representation in Eq. (6.7.12) and derive a contour integral representation. Show that the integrand so obtained does not decay as $v \rightarrow \infty$ in the complex plane, thereby preventing path deformations leading to an alternative representation. Modify the integrand

by adding a function $\psi(v)$ which has no singularities inside C (i.e., it does not alter the value of S) but is so chosen that the resulting integrand decays at infinity. Carrying out a path deformation about the singularities of $f(v)$, derive the residue series representation in Eq. (6.7.11). Compare this approach with the one in the text utilizing the characteristic Green's functions. Which is more direct? (The above-described procedure is usually referred to as the *Watson transformation*, after G. N. Watson[†] who used this technique in connection with the problem of diffraction by a sphere.)

9. Derive the three-dimensional cylinder Green's function in Eq. (6.7.31) directly by treating the configuration in Fig. 6.7.7 as a uniform waveguide along z , with the transverse mode functions given in Eqs. (3.4.99).
10. Multiply Eqs. (6.7.30a) and (6.7.31) by $\exp(im\phi')$, $m = \text{integer}$, and integrate over ϕ' , to derive alternative representations for the Green's function for a cylinder excited by a ring source with radius $\rho' > a$ and having a phase variation $\exp(im\phi)$. Referring to Sec. 5.9c, compare the result with the two-dimensional Green's function for the variable medium described in Eq. (5.9.1) [see Eq. (5.9.9), etc.].
11. In the configuration in Fig. 6.7.7, assume that either the source point or the observation point is located far from the cylinder surface.
(a) Evaluate the integral in Eq. (6.7.30a) asymptotically by the method of saddle points to derive the E -mode result (for $k\rho_> \sin \theta_> \gg 1$ and an $e^{-i\omega t}$ dependence):

$$G'(\mathbf{r}, \mathbf{r}') \sim \frac{e^{ikr_>}}{4\pi r_>} \sum_{n=0}^{\infty} \epsilon_n \cos n(\phi - \phi') e^{-inn/2} e^{-ikz_< \cos \theta_>} \\ \cdot [J_n(kr_< \sin \theta \sin \theta') - \frac{J_n(ka \sin \theta_>)}{H_n^{(1)}(ka \sin \theta_>)} H_n^{(1)}(kr_< \sin \theta \sin \theta')], \quad (26)$$

where $z_>, r_>, \theta_>$ stand for z, r, θ when $\rho > \rho'$, and for z', r', θ' when $\rho < \rho'$. The converse holds for $z_<, r_<, \theta_<, r, \theta$ are spherical polar coordinates defined as follows: $r_> \cos \theta_> = z_>, r_> \sin \theta_> = \rho_>$, etc., and $\epsilon_n = 1, n = 0, \epsilon_n = 2, n \neq 0$. Derive an analogous expression for the H -mode Green's function $G''(\mathbf{r}, \mathbf{r}')$. Evaluate the electromagnetic field components when the source is a longitudinal electric or magnetic dipole [see Eqs. (5.2.1)].

(b) By moving the source to infinity, specialize Eq. (26) to the case of plane-wave incidence and show that if the incident field is derived from the wave function

$$u'_{\text{inc}} = \exp[-ikr \sin \theta \sin \theta' \cos(\phi - \phi') - ikr \cos \theta \cos \theta'], \quad (27)$$

the corresponding expression for the total wave function is $u' = u'_{\text{inc}} + u'_s$, where

$$u'_s = -e^{-ikr \cos \theta \cos \theta'} \sum_{n=0}^{\infty} \epsilon_n \cos n(\phi - \phi'') e^{-inn/2} \frac{J_n(ka \sin \theta'')}{H_n^{(1)}(ka \sin \theta')} \\ \cdot H_n^{(1)}(kr \sin \theta \sin \theta''). \quad (28)$$

Derive the corresponding result for the H -mode wave function $u''(\mathbf{r}, \mathbf{r}')$. By a

[†]G. N. Watson, "Diffraction of electric waves by the earth," *Proc. Roy. Soc. (London)*, A95 (1919), pp. 83-99. See also H. Bremmer, *Terrestrial Radio Waves*, Elsevier Publishing Co., New York (1949), Chapter. 3.

suitable superposition of E - and H -mode constituents, derive the fields due to an arbitrarily polarized incident plane wave.

(c) Specialize the H -mode analogue of Eq. (26) to the case where the source is located on the cylinder and show that the H -mode radiated far field may be derived from

$$G''(\mathbf{r}, \mathbf{r}') = \frac{e^{ikr}}{4\pi r} \frac{2ie^{-ikz' \cos \theta}}{\pi ka \sin \theta} \sum_{n=0}^{\infty} \epsilon_n \cos n(\phi - \phi') \frac{e^{-inn/2}}{H_n^{(1)}(ka \sin \theta)}. \quad (29)$$

Use this result to derive expressions for the fields radiated by an axial slot in the cylinder, assuming that the electric field in the slot has only an E_ϕ component which is specified (this excitation is equivalent to a distribution of axial magnetic currents $\mathbf{M} = \mathbf{E}_\phi \times \mathbf{p}_0$ on the smooth cylinder surface).

12. Repeat Problem 11, starting from the representation for $G(\mathbf{r}, \mathbf{r}')$ in Eq. (6.7.30b). Show that an alternative expression for $G''(\mathbf{r}, \mathbf{r}')$ in Eq. (29) is

$$G''(\mathbf{r}, \mathbf{r}') \sim \frac{e^{ikr}}{4r} e^{-ikz' \cos \theta} \cdot \sum_{\mu_p} \frac{H_{\mu_p}^{(1)}(ka \sin \theta) H_{\mu_p}^{(2)}(ka \sin \theta) \cos [\mu_p(\pi - |\phi - \phi'|)] e^{-i\mu_p \pi/2}}{(\partial/\partial \mu) H_{\mu}^{(1)}(ka \sin \theta)|_{\mu_p} \sin \mu_p \pi}, \quad (30)$$

where $H_{\mu_p}^{(1)}(ka \sin \theta) = 0$. Discuss the convergence properties of this series. Show that for $ka \sin \theta \gg 1$, the series converges rapidly in the shadow region $|\phi - \phi'| > \pi/2$; give a simplified form of the summand in this instance. Show that the field in the shadow region may be interpreted as arising from a creeping ray that leaves the source point along a helical trajectory on the cylinder surface and then departs tangentially toward the distant observation point P (see Fig. P6.3).

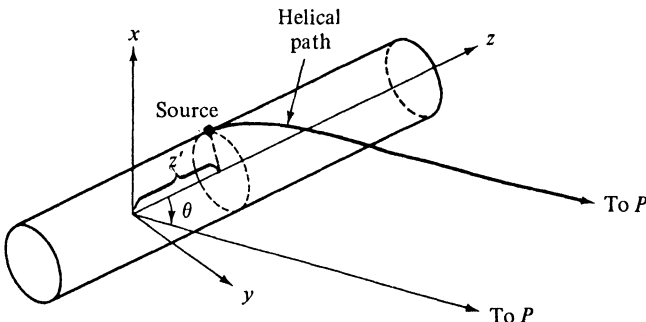


FIG. P6.3 Creeping rays on a cylinder (oblique propagation).

13. It was shown that for line-source excitation, the residue series in Eq. (6.7.11) resulting from the angular transmission analysis converges provided that $\phi \neq \phi'$ [include the integral in Eq. (6.7.11) as the $n = 0$ term in the sum; see remarks preceding Eq. (6.7.16)]. Derive the result for plane-wave incidence by letting $\rho' \rightarrow \infty$, thereby replacing $H_{\mu_p}^{(1)}(k\rho')$ by its asymptotic form [see Eq. (5.3.13)]. Show that the resulting series now converges only in the shadow region.
14. A line source of magnetic currents is located at (ρ', ϕ') in a cylindrical coordi-

nate system centered at the apex of a perfectly conducting wedge. The wedge faces are described by the half-planes $\phi = 0$ and $\phi = \varphi$. From Eqs. (6.3.3) and (6.5.2b), the magnetic field H_z is proportional to the scalar Green's function ($e^{-i\omega t}$ dependence)

$$\tilde{G}(\rho, \rho') = \frac{1}{2} P \int_{-i\infty}^{i\infty} \mu J_\mu(k\rho') H_\mu^{(1)}(k\rho) g_\phi(\phi, \phi'; \mu) d\mu, \quad (31)$$

where ρ and ρ' may be interchanged,

$$g_\phi(\phi, \phi'; \mu) = -\frac{\cos \mu\phi_- \cos \mu(\varphi - \phi_+)}{\mu \sin \mu\varphi}, \quad (31a)$$

and "P" denotes that the principal value of the integral is taken at $\mu = 0$.

(a) Assume that an aperture of infinite length parallel to the edge is located on the wedge face $\phi = 0$, and that the electric field in the aperture has only a component E_ρ which is specified. Utilizing Eq. (31), derive an expression for the magnetic field in the shadow region. (Note that the aperture field is given equivalently in terms of a magnetic current distribution $\mathbf{M} = \mathbf{E} \times \phi_0$ on the unperforated wedge.)

(b) If the aperture occupies the entire wedge face and the electric field is assumed to have the progressive phase dependence

$$E_\rho = e^{i\xi\rho}, \quad \text{Im } \xi \geq 0, \quad (32)$$

use the formulas†

$$\int_0^\infty H_\mu^{(1)}(k\rho) e^{i\xi\rho'} d\rho' = \frac{2e^{-i\mu\pi/2} \sin \mu[(\pi/2) - \gamma]}{k \cos \gamma \sin \mu\pi}, \quad |\text{Re } \mu| < 1, \quad (33a)$$

$$\int_0^\infty J_\mu(k\rho) e^{i\xi\rho'} d\rho' = \frac{e^{i\mu\gamma}}{k \cos \gamma}, \quad \text{Re } \mu > -1, \quad (33b)$$

with $\gamma = \sin^{-1}(\xi/k)$, to show that the magnetic field H_z is now proportional to

$$S(\rho) = \frac{-1}{k \cos \gamma} P \int_{-i\infty}^{i\infty} J_\mu(k\rho) \frac{e^{-i\mu\pi/2} \sin \mu[(\pi/2) - \gamma] \cos \mu(\varphi - \phi)}{\sin \mu\pi \sin \mu\varphi} d\mu \quad (34a)$$

$$= -\frac{1}{2k \cos \gamma} P \int_{-i\infty}^{i\infty} H_\mu^{(1)}(k\rho) \frac{e^{i\mu\gamma} \cos \mu(\varphi - \phi)}{\sin \mu\varphi} d\mu. \quad (34b)$$

Show that these integrals converge in the region $\phi > (\pi/2) - \text{Re } \gamma$ so that Eqs. (34) are valid in this extended domain. For real γ , interpret this region as the geometric-optical shadow region for the source distribution in Eq. (32) extending over a semi-infinite interval (cf. Problem 28 of Chapter 1 for the radiation characteristics of a progressively phased sheet current).

(c) Show that the integral in Eq. (34a) may be evaluated in terms of the residues at the poles of the integrand in the right half of the μ plane, leading to the result‡, §

†W. Magnus and F. Oberhettinger, *Formulas and Theorems for the Special Functions of Mathematical Physics*, Chelsea Pub. Co., New York (1954), pp. 131, 133.

‡G. D. Malyuzinec, "Radiation of sound by vibrating boundaries of an arbitrary wedge," *Acoustical Journal (USSR)*, **1** (1955), p. 144.

§L. B. Felsen, "Radiation from source distributions covering one face of a perfectly conducting wedge," *IEEE Trans. on Antennas and Propagation AP-12* (1964), p. 653.

$$S(\rho) = \frac{\pi i}{2k\varphi} J_0(k\rho) + \frac{\pi i}{k\varphi} \sum_{n=1}^{\infty} \cos n\phi J_n(k\rho) \frac{e^{-ivn/2}}{\cos(v\pi/2)} - \frac{2}{k} \sum_{n=1}^{\infty} \frac{\cos(2n-1)(\varphi-\phi)}{\sin(2n-1)\varphi} J_{2n-1}(k\rho), \quad v = \frac{n\pi}{\varphi}. \quad (35)$$

This formula is useful for the calculation of the field near the origin.

(d) By using the integral representation (5.4.36c) for $H_\mu^{(1)}(k\rho)$ and following the procedure leading to Eq. (6.3.8), show that Eq. (34b) can be transformed into (for $\varphi > \pi$)

$$S(\rho) = \frac{i}{k \cos \gamma} e^{ik\rho \cos[(\pi/2) - \gamma - \phi]} U\left[\frac{\pi}{2} - \gamma - \phi\right] + \frac{1}{2\varphi k \cos \gamma} \int_{i\infty}^{-i\infty} e^{ik\rho \cos w} \frac{\sin[(\pi/\varphi)(w + \gamma - \pi/2)]}{\cos[(\pi/\varphi)(w + \gamma - \pi/2)] - \cos(\pi\phi/\varphi)} dw, \quad (36)$$

where $U(x)$ is the Heaviside unit function. This result is valid for all angles in the interval $0 < \phi < \varphi$. Identify the first term as the geometric-optical field and the second as the diffraction field. Calculate the radiation field by evaluating the diffraction integral asymptotically for large values of $k\rho$ and for all values of ϕ . Interpret the asymptotic field formula in ray-optical terms.

15. This problem deals with alternative representations for the z -independent two-dimensional Green's functions and for the three-dimensional Green's functions $G'(\mathbf{r}, \mathbf{r}')$, $G''(\mathbf{r}, \mathbf{r}')$, $\mathcal{S}'(\mathbf{r}, \mathbf{r}')$, $\mathcal{S}''(\mathbf{r}, \mathbf{r}')$ for the (perfectly conducting) tipped wedge configuration shown in Fig. 6.1.1.
- (a) Since the radial characteristic Green's function in Eq. (3.4.97) consists of two parts, one of which represents the result in the absence of the cylindrical boundary while the other accounts for the presence of the boundary, show that the total Green's functions obtained by the radial transmission formulation may be separated as follows: the Green's function for the untipped wedge plus a correction term due to the cylinder. Show that this representation is useful when the cylinder radius is small.
 - (b) Repeat the preceding considerations for the angular transmission formulation by resorting to the image superposition in the infinite angular space (see Eq. (6.7.10), modified in accord with Eq. (3.4.57)). Show that the resulting representation comprises the Green's function for the cylinder configuration in Fig. 6.7.1, plus correction terms due to the presence of the wedge faces at $\phi = 0$, φ . Show that this representation is useful when the cylinder radius is large and both wedge faces are invisible from the source. Derive an asymptotic approximation for the fields, following the procedure in Sec. 6.7.
 - (c) When the cylinder radius is large and one of the wedge faces is visible from the source, show from an asymptotic evaluation by the saddle-point method that the dominant contribution to the scattered field in the illuminated region may be interpreted as corresponding to geometric-optical rays arising from reflection at the cylinder only, from reflection at the wedge face only, and from multiple reflections as shown in Fig. P6.4. Construct the field amplitude and phase along a multiply reflected ray directly from geometrical optics and compare with the asymptotic solution.
 - (d) Repeat the analysis in (c) when both wedge faces are visible from the source.

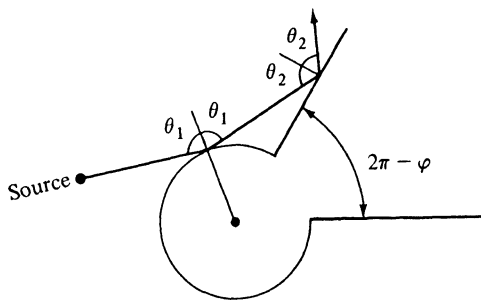


FIG. P6.4 Multiply reflected rays on a cylindrically tipped wedge.

16. A cone defined by the surface $\theta = \theta_0$ is tipped by a sphere at $r = a$, all surfaces being perfectly conducting. Derive alternative representations for the Green's functions for this configuration. In particular, obtain a radial transmission formulation wherein the cone Green's function appears explicitly, with the effect of the sphere occurring as a perturbation, and an angular transmission formulation wherein the sphere Green's function appears explicitly, with the conical portions of the surface contained as a perturbation. Discuss the convergence properties of these representations (see also Problem 15 for the analogous configuration in cylindrical geometry) and show that the radial transmission result is convenient for small spherical tips and arbitrary cones while the angular transmission result is useful for large tips and narrow angle cones.
17. A cylinder with radius a is excited by a line source of magnetic currents of unit strength directed parallel to the cylinder axis at a location $\phi = \phi'$, $p = p' > a$. The boundary conditions on the cylinder are specified in terms of the angularly dependent surface impedance

$$\bar{Z}(\phi) = -\frac{E_\phi}{H_z} = Z\sqrt{\frac{\mu}{\epsilon}}[1 + \alpha \cos p(\phi - \phi_0)] \quad \text{at } \rho = a. \quad (37)$$

Z denotes a normalized reference impedance, $\sqrt{\mu/\epsilon}$ is the impedance of free space, α is a real constant descriptive of the modulation amplitude, $p = 2\pi a/L$ is an integer, with L denoting the spatial period of the impedance modulation, and ϕ_0 is a phase reference. For a passive structure, it is required that $\text{Re } \bar{Z} \geq 0$, and an $\exp(-i\omega t)$ dependence is implied.

(a) Show that the only component of magnetic field is given by $H_z = i\omega\epsilon\bar{G}$ where the scalar Green's function $\bar{G}(\mathbf{p}, \mathbf{p}')$ satisfies the inhomogeneous wave equation

$$(\nabla^2 + k^2)\bar{G}(\mathbf{p}, \mathbf{p}') = -\delta(\mathbf{p} - \mathbf{p}'), \quad (38)$$

subject to

$$\frac{\partial \bar{G}}{\partial \rho} = -ikZ[1 + \alpha \cos p(\phi - \phi_0)]\bar{G} \quad \text{at } \rho = a, \quad (38a)$$

and a radiation condition at $\rho \rightarrow \infty$. By assuming a representation in terms of angular eigenfunctions,

$$\bar{G}(\rho, \rho') = \frac{1}{2\pi} \sum_{n=-\infty}^{\infty} e^{-in(\phi - \phi')} h(\rho, \rho'; n) \quad (39)$$

$$h(\rho, \rho'; n) = \frac{\pi i}{2} [J_n(k\rho_<) + A(n)H_n^{(1)}(k\rho_<)]H_n^{(1)}(k\rho_>), \quad (39a)$$

show that this series represents the formal solution provided that the coefficients $A(n)$ satisfy the inhomogeneous second-order difference equation†

$$\frac{iZ\alpha}{2} [c_1(n, p)A(n+p) + c_1(n, -p)A(n-p)] + d(n)A(n) = c_2(n), \quad (40)$$

where

$$c_1(n, p) = e^{ip(\phi' - \phi_0)} \frac{H_{n+p}^{(1)}(ka)H_{n+p}^{(1)}(kp')}{H_n^{(1)}(kp')} \quad (40a)$$

$$d(n) = H_n^{(1)}(ka) + iZH_n^{(1)}(ka), \quad (40b)$$

$$\begin{aligned} c_2(n) = & -b(n) - \frac{iZ\alpha}{2} \left[\frac{J_{n+p}(ka)H_{n+p}^{(1)}(kp')}{H_n^{(1)}(kp')} e^{ip(\phi' - \phi_0)} \right. \\ & \left. + \frac{J_{n-p}(ka)H_{n-p}^{(1)}(kp')}{H_n^{(1)}(kp')} e^{-ip(\phi' - \phi_0)} \right] \end{aligned} \quad (40c)$$

$$b(n) = J'_n(ka) + iZJ_n(ka). \quad (40d)$$

(b) To solve Eq. (40), assume that $A(n)$ has the power series expansion

$$A(n) = \sum_{m=0}^{\infty} f(n, m)\alpha^m, \quad (41)$$

where α is a small parameter. Show that

$$f(n, 0) = -\frac{b(n)}{d(n)}, \quad (41a)$$

$$f(n, 1) = \frac{Z/(\pi ka)}{d(n)H_n^{(1)}(kp')} \left[\frac{e^{ip(\phi' - \phi_0)} H_{n+p}^{(1)}(kp')}{d(n+p)} + \frac{e^{-ip(\phi' - \phi_0)} H_{n-p}^{(1)}(kp')}{d(n-p)} \right], \quad (41b)$$

and that the coefficients $f(n, m)$, $m \geq 2$, may be derived recursively from a knowledge of $f(n \pm p, m-1)$.

(c) To $O(\alpha)$, derive an alternative expression for $\bar{G}(\rho, \rho')$ analogous to the one in Eq. (6.7.11). Discuss its convergence properties. Simplify the resulting formulas by passing to the limit of plane-wave incidence ($\rho' \rightarrow \infty$). Show that the dominant characteristics of the high frequency field ($ka \gg 1$) are determined for plane wave incidence by the integrals

$$\bar{G}(\rho, \rho') = \bar{G}_0(\rho, \rho') + \alpha \bar{G}_1(\rho, \rho') + O(\alpha^2), \quad (42)$$

where

$$\bar{G}_0 = \int_{-\infty}^{\infty} e^{i\mu|\phi - \phi'| - i\mu\pi/2} \left[J_\mu(k\rho) - \frac{b(\mu)}{d(\mu)} H_\mu^{(1)}(k\rho) \right] d\mu \quad (42a)$$

pertains to the constant impedance cylinder, and

†L. B. Felsen and C. J. Marcinkowski, "Diffraction by a cylinder with a variable surface impedance," *Proc. Roy. Soc. (London)*, A267(1962), pp. 329-350.

$$\tilde{G}_1 = \hat{G}_1(p) + \hat{G}_1(-p), \quad (42b)$$

$$\hat{G}_1(p) = \frac{Z}{\pi ka} e^{ip[\phi' - \phi_0 - (\pi/2)]} \int_{-\infty}^{\infty} \frac{e^{i\mu(\phi' - \phi - (\pi/2))} H_{\mu}^{(1)}(k\rho)}{d(\mu)d(\mu + p)} d\mu. \quad (42c)$$

18. This problem is concerned with the asymptotic evaluation and physical interpretation of the Green's function for a cylinder with periodically varying surface impedance.

(a) From a saddle-point evaluation of the integrals in Eqs. (42a) and (42c), show that the field in the illuminated region of the cylinder is given by the asymptotic approximation:[†]

$$\tilde{G} = e^{-ik\rho \cos(\phi - \phi')} + \tilde{G}_r, \quad (43)$$

$$\begin{aligned} \tilde{G}_r \sim & A_0(0)\Gamma_0 D(0)e^{iks} \\ & + \alpha[A_0(p)\Gamma_1(p)D(p)e^{iks(p)} + A_0(-p)\Gamma_1(-pD(-p)e^{iks(-p)})] + O(\alpha^2), \end{aligned} \quad (44)$$

where for $n = 0, \pm 1$,

$$A_0(np) = e^{-ika \cos[\theta_i(np)]}, \quad (44a)$$

$$D(np) = \frac{1}{\sqrt{1 + [s(np)]/[r(np)]}}, \quad r(np) = a \frac{\cos[\theta_r(np)]}{1 + [d\theta_r(np)/d\theta_i(np)]}, \quad (44b)$$

$$\Gamma_0 = \frac{\cos \theta_i - Z}{\cos \theta_i + Z}; \quad \Gamma_1(p) = \frac{-Z \cos \theta_i(p) e^{ip(\phi' \pm \theta_i)}}{\{Z + \cos[\theta_i(p)]\}\{Z + \cos[\theta_r(p)]\}}, \quad \theta_n \geq 0. \quad (44c)$$

The relation between $\theta_i(np)$ and $\theta_r(np)$ is given by the "grating law"

$$\sin[\theta_r(np)] = \sin[\theta_i(np)] \pm \frac{np}{ka}, \quad \theta_n \geq 0. \quad (44d)$$

The parameters θ_i , θ_r , and s denote the angles of incidence, reflection, and the distance along a reflected ray from the cylinder surface to the observation point, respectively, as shown in Fig. P6.5; depending on the incident ray in question, one defines $\theta_n = \pm \theta_i$. Interpret the first term in Eq. (44) as a specularly reflected ray ($\theta_r = \theta_i$) on a cylinder with constant surface impedance Z [cf. Eq. (6.7.29), with $L_r \rightarrow \infty$ and subsequent normalization to plane-wave incidence], and the second and third terms as first-order reflected "grating rays." Show that the divergence coefficient $D(np)$ follows from a conservation-of-energy argument applied to an incident- and reflected-ray tube for the general case where the angles of incidence and reflection are not equal (cf. Problems 30 and 32 of Chapter 1). Discuss the symmetry properties of the field in Eq. (44) for $\phi' = \phi_0$ and $\phi' \neq \phi_0$. Discuss the behavior of the reflected grating rays and delimit their domains of existence relative to the cylindrical boundary.

(b) When the surface impedance varies slowly [$(p/ka) \ll 1$], show that the three reflected rays corresponding to $n = 0, \pm 1$ in Eq. (44d) have only slightly different trajectories which intersect at the observation point P and originate from three closely adjacent points on the cylinder surface, two of these being equidistant from the specular reflection point. Show that the contribution from the

[†]C. J. Marcinkowski and L. B. Felsen, "On the geometrical optics of curved surfaces with periodic impedance properties," *J. Res. NBS*, **66D** (1962), pp. 699-705.

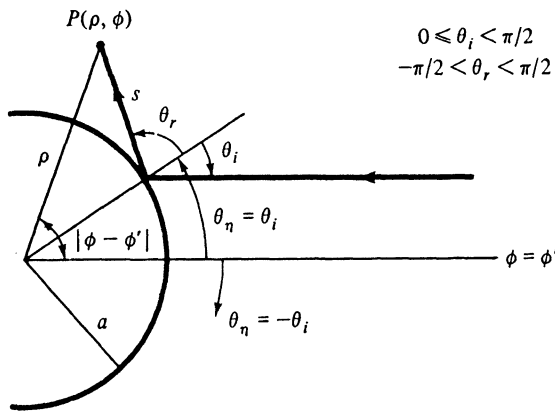


FIG. P6.5 Ray structure for a cylinder with variable surface impedance.

three reflected rays may be combined into a single specularly reflected ray as in the first term in Eq. (44) provided that Γ_0 is replaced by the *local reflection coefficient* Γ'_0 at the point of reflection $\hat{\phi}$:

$$\Gamma'_0 = \frac{\cos \theta_i - \bar{Z}(\hat{\phi})/\sqrt{\mu/\epsilon}}{\cos \theta_i + \bar{Z}(\hat{\phi})/\sqrt{\mu/\epsilon}}, \quad (44e)$$

with $\bar{Z}(\phi)$ given in Eq. (37). Interpret this result as validating the simple geometric-optical construction of the field in terms of the local parameters on the surface near the reflection point [cf. Eqs. (6.6.23)].

19. A line source of electric current is located exterior to a perfectly conducting cylinder whose surface is described by the equation $\rho = a + b \cos p\phi$, where p is an integer.[†] If b is a small parameter, show that the solution to this problem can be obtained as a special case of the one in Problem 17.
20. Starting from the relations in Eq. (6.8.16), and from[‡]

$$\begin{aligned} \frac{d}{d\theta_0} P_v^{-q}(\cos \theta_0) &= \cos(v - q)\pi \frac{d}{d\theta_0} P_v^{-q}(-\cos \theta_0) \\ &+ \frac{\sin(v - q)\pi}{\sin q\pi} \left[\cos v\pi \frac{d}{d\theta_0} P_v^{-q}(-\cos \theta_0) - \frac{\Gamma(v - q + 1)}{\Gamma(v + q + 1)} \frac{d}{d\theta_0} P_v^q(-\cos \theta_0) \right], \end{aligned} \quad (45)$$

show that when $\theta_0 \approx \pi$, the solutions of $(d/d\theta_0)P_p^{-q}(\cos \theta_0) = 0$ are given approximately by:

$$p \approx q + k - \frac{\Gamma(2q + n + 1)}{\Gamma(1 + q)\Gamma(1 + n)\Gamma(q)} \left(\frac{\pi - \theta_0}{2} \right)^{2q}, \quad (46)$$

where $n = 0, 1, 2, \dots$ and $\Gamma(x)$ is the gamma function.

[†]P. C. Clemmow and V. H. Weston, "Diffraction of a plane wave by an almost circular cylinder," *Proc. Roy. Soc. (London)*, A264 (1961), p. 246.

[‡]E. W. Hobson, *The Theory of Spherical and Ellipsoidal Harmonics*, Cambridge Univ. Press (1931), p. 407.

Repeat to obtain the solutions of $P_p^{-q}(\cos \theta_0) = 0$.

When $\theta_0 \approx \pi/2$, obtain approximate values of the zeros from the asymptotic formula in Eq. (3.4.66b).

21. Construct the H -mode Green's function $G''(\mathbf{r}, \mathbf{r}')$ for a perfectly conducting semiinfinite cone in a representation corresponding to Eq. (6.8.9a), and pass to the special case of axial plane-wave back-scattering ($r' \rightarrow \infty$ with subsequent normalization, and $\theta, \theta' \rightarrow 0$) [use an $\exp(-i\omega t)$ dependence]. Replace the function $j_p(kr)$ by its Sommerfeld integral

$$j_p(kr) = \frac{1}{2\pi} \sqrt{\frac{\pi kr}{2}} \int_{\hat{P}} \exp\{ikr \cos w + i[p + (1/2)][w - (\pi/2)]\} dw, \quad (47)$$

where \hat{P} is the path shown in Fig. P6.6. Interchange the order of summation

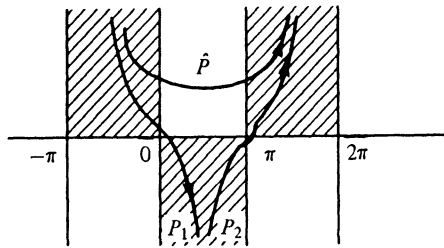


FIG. P6.6 Integration paths.

and integration (justify this) to obtain the representation†

$$G'' = e^{i\pi/4} \sqrt{\frac{\pi}{2kz}} \int_{\hat{P}} e^{ikz \cos w} T(w) dw, \quad (48)$$

where

$$\begin{aligned} T(w) &= \frac{1}{2\pi} \csc^2 \frac{\theta_0}{2} e^{i(w-\pi)/2} \\ &- \sum_p \frac{(d/d\theta_0) P_p(-\cos \theta_0)[p + (1/2)]}{(\sin p\pi)(\partial^2/\partial p \partial \theta_0) P_p(\cos \theta_0)} e^{i(p + (1/2))(w-\pi)}, \end{aligned} \quad (48a)$$

and $(d/d\theta_0) P_p(\cos \theta_0) = 0$,

For an approximate evaluation when $\theta_0 \approx \pi/2$, use the asymptotic formula (3.4.66b) to determine the zeros p and also to replace the Legendre functions, to show that

$$T(w) \approx \frac{1}{\theta_0} \sum_{n=0}^{\infty} \left(p + \frac{1}{2} \right) e^{i(p + (1/2))(w-\pi)}, \quad p \approx \left(n + \frac{1}{4} \right) \frac{\pi}{\theta_0} - \frac{1}{2}, \quad (49)$$

and write for this geometric series its closed form exhibiting double poles at $w = \pi$ and $w = \pi - 2\theta_0$. Upon substituting the closed-form expression for $T(w)$ into Eq. (48), show that the contour can be deformed into the steepest-descent paths P_1 and P_2 through the saddle points at $w = 0$ and $w = \pi$, respectively. From an asymptotic evaluation for large kr (see Sec. 4.2d), show that

†L. B. Felsen, "Back-scattering from wide-angle and narrow-angle cones," *J. Applied Physics* **26** (1955), p. 138.

$$G'' \sim e^{-ikz} - \frac{1}{2} \sqrt{\frac{\pi}{2}} e^{i(kz + \pi/4)} \frac{dF}{d\xi}, \quad \xi \text{ small}, \quad (50a)$$

$$\sim e^{-ikz} + \frac{i}{4[\theta_0 - (\pi/2)]^2} \frac{e^{ikz}}{kz}, \quad \xi \text{ large}, \quad (50b)$$

where $\xi = \sqrt{kz} |\cos \theta_0|$, $\theta_0 \approx \pi/2$, and $F(\xi) = (2/\sqrt{\pi}) e^{-iz\xi^2} \int_{(1-i)\xi}^{\infty} e^{-y^2} dy$.

22. Repeat the calculation in Problem 21 for an x -directed electric current element on the z axis which is then moved to infinity. Show that the total electric field on the z axis is given by

$$E_x \sim e^{-ikz} + \frac{1}{2} \sqrt{\frac{\pi}{2}} e^{i(kz + \pi/4)} \frac{dF}{d\xi}, \quad (51)$$

where ξ and $F(\xi)$ are defined in Problem 21.

23. The discussion in Problems 21 and 22 has dealt with the case $\theta_0 = (\pi/2) + \delta$, where δ is small and positive. How must the result in Eqs. (50) be modified when $\delta < 0$? [Note the location of the poles of $T(w)$.] Explain in terms of ray focusing along the cone axis.
24. A uniform plane wave with electric field $E = \exp(-ikz)$ is incident along the axis of a perfectly conducting semiinfinite cone described by the equation $\theta = \theta_0 > \pi/2$. Approximate the induced current distribution on the cone by the physical optics value $\mathbf{J} = 2\mathbf{H}_{\text{inc}} \times \mathbf{\hat{\theta}_0}$, where \mathbf{H}_{inc} is the incident magnetic field and $\mathbf{\hat{\theta}_0}$ is the normal unit vector directed into the cone surface. Calculate the electric field E_s due to this induced current distribution at a distant observation point on the z axis and show that it yields

$$E_s \sim -\frac{ie^{ikz}}{4kz} \tan^2(\pi - \theta_0). \quad (52)$$

Since the result agrees well with that obtained by a more accurate calculation when $\theta_0 \approx \pi/2$ (see Problems 20 and 21) or $\theta_0 \approx \pi$ [see Eq. (6.8.24a)], is the use of the physical optics approximation justified in the present instance? Explain, paying attention to the presence of the cone tip.

25. A semiinfinite cone is attached to a semiinfinite plane in the manner shown in Fig. P6.7, and all surfaces are assumed to be perfectly conducting. This configuration is excited by a ring source centered on the z axis. If the intensity variation along the ring source is proportional to $\sin(\phi/2)$, show that the E mode Green's function $G'(\mathbf{r}, \mathbf{r}')$ is given by :

$$G'(\mathbf{r}, \mathbf{r}') = \sqrt{\frac{r' \sin \theta'}{r \sin \theta}} \sin \frac{\phi}{2} \bar{G}'(\mathbf{p}, \mathbf{p}'), \quad \mathbf{p} = (r, \theta), \quad (53)$$

where $\bar{G}'(\mathbf{p}, \mathbf{p}')$ is the two-dimensional wedge Green's function in Eqs. (6.5.12) or (6.5.18), with (r, θ) interpreted as cylindrical coordinates and the wedge faces situated at $\theta = 0, \theta_0$.

(Note : $P_v^{-1/2}(\cos \theta) = \{\sqrt{2} \sin[(v + 1/2)\theta]\}/\{[v + (1/2)]\sqrt{\pi \sin \theta}\}.$)

26. (a) Employ the formulas [see Part (b) and Problem 5 of Chapter 4]

$$\lim_{\substack{v \rightarrow \infty \\ \theta \rightarrow 0}} v^q P_v^{-q}(\cos \theta) = J_q(v\theta), \quad (54a)$$

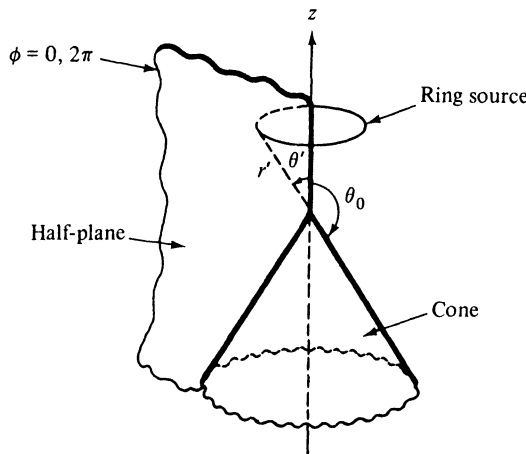


FIG. P6.7 Cone-tipped half-plane.

and

$$\lim_{\substack{v \rightarrow \infty \\ \theta \rightarrow 0}} \frac{v^q P_v^{-q}(-\cos \theta)}{\sin v\pi} \Big|_{\arg v \geq 0} = \mp ie^{\pm iq\pi} H_q^{(1,2)}(v\theta) \quad (54b)$$

in Eq. (3.4.71) to show that

$$\lim_{\substack{|\xi| \rightarrow \infty \\ \theta \rightarrow 0}} E_q^{(1,2)}(\xi, \theta) = \xi^{-q} H_q^{(1,2)}(\xi\theta), \quad \arg \xi \neq 0. \quad (54c)$$

Combine this result with Eqs. (3.4.72) to obtain an asymptotic approximation valid for small and large values of θ :

$$E_q^{(1,2)}(\xi, \theta) \sim \xi^{-q} \sqrt{\frac{\theta}{\sin \theta}} H_q^{(1,2)}(\xi\theta), \quad |\xi| \rightarrow \infty. \quad (55)$$

(b) Use Eqs. (54a), (6.A17), and the formula

$$P_v^{-q}(-\cos \theta) = \frac{\sin v\pi}{\sin q\pi} P_v^{-q}(\cos \theta) - \frac{\sin(v-q)\pi}{\sin q\pi} \frac{\Gamma(v-q+1)}{\Gamma(v+q+1)} P_v^q(\cos \theta), \quad (56)$$

to derive Eq. (54b).

27. When the cone angle $\theta_0 \approx \pi$ and source and observation points are located far from the tip and near the cone surface, a conical obstacle appears locally like the surface of a cylinder (see Fig. P6.8). Show that in order to explore the transition from the scattering problem for the cone to that for the circular cylinder, one may imagine the origin to be pulled to infinity, with some selected point, say P , serving as a fulcrum. Define the following limiting quantities:

$$\lim_{\substack{r \rightarrow \infty \\ \theta \rightarrow \pi}} r(\pi - \theta) = \rho = \lim_{\substack{r' \rightarrow \infty \\ \theta \rightarrow \pi}} r'(\pi - \theta) \quad (57)$$

and similarly for ρ' (with $\theta \rightarrow \theta'$). Show that the radius a of the resulting cylinder is obtained by letting θ or θ' equal θ_0 , and $(r_> - r_<) \rightarrow |z - z'| = |\bar{z} - \bar{z}'|$, where \bar{z} is measured from a new origin located near $\rho = 0$ or $\rho' = 0$ on the z axis.

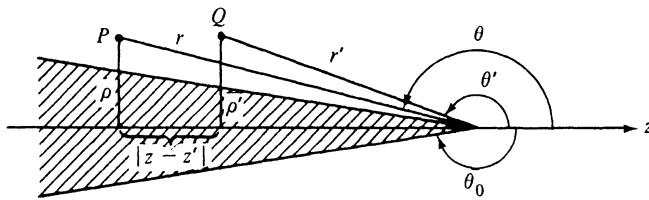


FIG. P6.8 Transition from cone to cylinder.

Show that in consequence of the above transition, the radial characteristic Green's function in Eq. (2.7.11) is replaced by that in Eq. (2.7.10) [with the switch to an $\exp(-i\omega t)$ dependence],

$$g_r \rightarrow \frac{i}{2k} h_v^{(2)}(kr_<)h_v^{(1)}(kr_>), \quad (58)$$

since no reflections occur from the distant cone tip (assume a slightly dissipative medium). Since this modified g_r is an even function of $v + (1/2)$, as is g_θ' in Eq. (3.4.68), show that the lower portion of the integration path in Eq. (6.8.9b) (with g_θ' inserted instead of $g_{\theta s}$, and the G_f term omitted) may be reflected into the third quadrant of the complex v plane, whence the resulting contour integral representation involves a path passing above the entire real v -axis.

Use the asymptotic formulas for the cylinder functions (Sec. 6.A1) to show that

$$g_r \rightarrow \frac{i}{2} \frac{\exp(i\sqrt{k^2 - \xi^2}|z - z'|)}{\sqrt{k^2 - \xi^2}}, \quad \text{Im } \sqrt{k^2 - \xi^2} > 0, \quad (59)$$

where $\xi = t/a$, and the change of variable

$$t = \frac{v + (1/2)}{\alpha}, \quad \alpha = \csc \theta_0, \quad \theta_0 \rightarrow \pi, \quad (59a)$$

has been introduced. Also show via Eqs. (54) and (57), etc., that

$$g_\theta'[\theta, \theta'; m^2; v(v + 1)] \rightarrow \frac{i\pi}{2} \left[J_m(\xi\rho_<)H_m^{(1)}(\xi\rho_>) - H_m^{(1)}(\xi\rho)H_m^{(1)}(\xi\rho') \frac{J_m(\xi a)}{H_m^{(1)}(\xi a)} \right], \\ \text{Im } \xi > 0, \quad (60)$$

and derive a similar result for the H mode case, g_θ'' . Compare with the cylinder Green's function in Eq. (6.7.30a).

28. Show that the electromagnetic fields derived from the scalar functions in Eqs. (6.8.9) and (6.8.10) satisfy the "tip condition" as $r \rightarrow 0$ [see Eq. (1.5.39)].

REFERENCES

- SOMMERFELD, A., "Mathematische Theorie der Diffraktion," *Math. Ann.* **47** (1896). See also Chapter 20, Vol. 2 in P. FRANK und R. V. MISES, *Die Differential- und Integralgleichungen der Mechanik und Physik*, Braunschweig, Germany: Vieweg and Son, 1961.

2. BOWMAN, J. J., T. B. A. SENIOR, and P. L. E. USLENGHI (Eds.), *Electromagnetic and Acoustic Scattering by Simple Shapes*, Chapter 6. Amsterdam: North Holland Publishing Co., 1969. Further references may be found here.
3. OBERHETTINGER, F., "On the diffraction and reflection of waves and pulses by wedges and corners," *J. Res. (NBS)* **61** (1958), pp. 343-365.
4. BOWMANN, J. J., et al., *Electromagnetic and Acoustic Scattering by Simple Shapes*, Chapter 8. Amsterdam: North Holland Publishing Co., 1969.
5. McDONALD, H. M., "A class of diffraction problems," *Proc. London Math. Soc.* **14** (1915), pp. 410-427.
6. FELSEN, L. B., "High-frequency diffraction by a wedge with a linearly varying surface impedance," *Appl. Sci. Res.* **B9** (1961), pp. 170-188.
7. ERDELYI, A., et al., *Higher Transcendental Functions*, Bateman Manuscript Project, Vol. 2, pp. 143-147. New York: McGraw-Hill, 1953.
8. FELSEN, L. B., "Electromagnetic properties of wedge and cone surfaces with a linearly varying surface impedance," *IRE Trans. on Antennas and Propagation*, AP-7 (1959), pp. S231-S243.
9. FELSEN, L. B., "Radiation from a tapered surface wave antenna," *IRE Trans. on Antennas and Propagation*, AP-8 (1960), pp. 577-586.
10. TALANOV, V. I., "On surface electromagnetic waves in systems with non-uniform impedance," *Radiofisika (Russian)* **2** (1959), pp. 132-133.
11. FOCK, V. A., *Electromagnetic Diffraction and Propagation Problems*, Chapters 2, 9, 13. New York: Pergamon Press, 1965.
12. KING, R. W. P. and T. T. WU, *The Scattering and Diffraction of Waves*. Cambridge, Mass.: Harvard University Press, 1959.
13. JONES, D. S., *The Theory of Electromagnetism*, Secs. 8.6-8.8. New York: Macmillan, 1964.
- 14(a). BOWMAN, J. J., et al., *Electromagnetic and Acoustic Scattering by Simple Shapes*, Secs. I.2.13.5-I.2.13.6 and Chapter 2. Amsterdam: North Holland Publishing Co., 1969.
- 14(b). WAIT, J. R. *Electromagnetic Radiation from Cylindrical Structures*. New York: Pergamon Press, 1959.
15. WAIT, J. R., "Pattern of an antenna on a curved lossy surface," *IRE Trans. on Antennas and Propagation*, AP-6 (1958), pp. 348-359.
16. FRANZ, W., *Theorie der Beugung Elektromagnetischer Wellen*, Secs. 11-16. Berlin: Springer, 1957.
17. KELLER, J. B., "Diffraction by a convex cylinder," *IRE Trans. on Antennas and Propagation*, AP-4 (1956), pp. 312-321.
18. BOWMAN, J. J., et al., *Electromagnetic and Acoustic Scattering by Simple Shapes*, Chapter 10. Amsterdam: North Holland Publishing Co., 1969.
19. BOWMAN, J. J., et al., *Electromagnetic and Acoustic Scattering by Simple Shapes*, Chapter 18. Amsterdam: North Holland Publishing Co., 1969.

20. RUCK, G. T., D. E. BARRICK, W. D. Stuart, and C. K. Krichbaum, *Radar Cross Section Handbook*, Chapters 3 and 6. New York: Plenum Press, 1970.
21. WATSON, G. N., "The diffraction of electric waves by the earth," *Proc. Roy. Soc. (London)*, A95 (1918), pp. 83-99.
22. CARSLAW, H. S., "Scattering of sound waves by a cone," *Math. Ann.* 75 (1914), p. 133.
23. FELSEN, L. B., "Plane wave scattering by small angle cones," *IRE Trans. on Antennas and Propagation* AP-5 (1957), p. 404. Also, "Asymptotic expansions of the diffracted wave for a semi-infinite cone," *IRE Trans. on Antennas and Propagation*, AP-5, 1957, p. 121, and "Alternative field representations in regions bounded by spheres, cones and planes," *IRE Trans. on Antennas and Propagation*, AP-5, 1957, p. 109.
24. FELSEN, L. B., "Radiation from ring sources in the presence of a semi-infinite cone," *IRE Trans. on Antennas and Propagation* AP-7 (1959), p. 168.
25. GORYANOV, A. S., "Diffraction of a plane electromagnetic wave propagated along the axis of a cone," *Radio Engrg. and Electronics* (English translation from Russian) 6 (1961), pp. 47-57.
26. HOBSON, E. W., *The Theory of Spherical and Ellipsoidal Harmonics*, p. 225. Cambridge, England: Cambridge University Press, 1931.
27. FELSEN, L. B., "Some definite integrals involving conical functions," *J. Math. Phys.* 35 (1956), p. 127.
28. DEBYE, P., "Näherungsformeln für Zylinderfunktionen für grosse Werte des Arguments und unbeschränkt veränderliche Werte des Index," *Math. Ann.* 67 (1909), pp. 535-558.
29. LANGER, R. E., "On the asymptotic solutions of ordinary differential equations with application to Bessel functions of large order," *Trans. Amer. Math. Soc.* 33 (1931), pp. 23-64.
30. OLVER, F. W. J., "Some new asymptotic expansions for Bessel functions of large orders," *Proc. Camb. Phil. Soc.* 48 (1952), pp. 414-427.
31. WATSON, G. N., *A Treatise on the Theory of Bessel Functions*, Sec. 8.61. Cambridge, England: Cambridge University Press, 1944.
32. MILLER, J. C. P., *The Airy Integral*, Cambridge, England: Cambridge University Press, 1946.
33. FRANZ, W. and R. GALLE, "Semiasymptotische Reihen für die Beugung einer ebenen Welle am Zylinder," *Z. f. Naturforschung* 10a (1955), pp. 374-378.
34. MAGNUS, W. and L. KOTIN, "The zeros of the Hankel function as a function of its order," *Numerische Mathematik* 2 (1960), pp. 228-244. See also J. B. KELLER, S. I. RUBINOW, and M. GOLDSTEIN, "Zeros of Hankel functions and poles of scattering amplitudes," *J. of Math. Phys.* 4, No. 6 (June 1963).